LASER EXCITED ATOMIC FLUORESCENCE IN A MINIATURE GLOW DISCHARGE ATOM RESERVOIR

By

CHERYL LYNN DAVIS

A DISSERTATION PRESENTED TO THE GRADUATE SCHOOL
OF THE UNIVERSITY OF FLORIDA IN PARTIAL FULFILLMENT
OF THE REQUIREMENTS FOR THE DEGREE OF
DOCTOR OF PHILOSOPHY

UNIVERSITY OF FLORIDA

1994

To James for his encouragement and understanding

ACKNOWLEDGEMENTS

Although this dissertation is presented as the endeavor of a single individual, several people made considerable contributions, and this project was very much a team effort. I would like to thank Drs. Mikhail Bolshov and Nicolò Omenetto for their helpful discussions concerning my experimental results. Dr. Bolshov devoted much of his valuable time to the derivation of the theoretical model of my system, and it was greatly appreciated. Dr. Benjamin Smith deserves special recognition for his unending patience and creative suggestions, and of course, this work would not have been possible without the guidance of Dr. James Winefordner. It was an honor to be a member of his research group.

Lastly, I wish to thank James Stephenson. Without his emotional support and cherished friendship, this work would likely not have been completed. His faith in me never diminished. Words cannot express how much he has meant to me over the last three years, for he was by my side throughout, if only in spirit.

TABLE OF CONTENTS

Abstract of Dissertation Presented to the Graduate School
of the University of Florida in Partial Fulfillment of the
Requirements for the Degree of Doctor of Philosophy

LASER EXCITED ATOMIC FLUORESCENCE IN A
MINIATURE GLOW DISCHARGE ATOM RESERVOIR

By

Cheryl Lynn Davis

December 1994

Chairperson: James D. Winefordner
Major Department: Chemistry

In the last few decades, the need for ultratrace analysis has received considerable attention. One technique that has proven capable of trace analysis is laser excited atomic fluorescence spectrometry (LEAFS). The work presented herein involves the design and evaluation of a miniature glow discharge atom reservoir for LEAFS.

The glow discharge is theoretically the ideal atom source for LEAFS because atoms are produced non-thermally in an inert, low pressure environment. Matrix interferences and quenching of the fluorescence are as a result minimized. It was hoped that the reduced volume of the miniature reservoir would cause an increase in the atom densities, leading to low absolute detection limits.

In this technique, a nanoliter-sized volume of an aqueous solution was deposited onto the nickel cathode of the glow discharge. The cathode was then placed into the discharge chamber, and following evacuation of the reservoir, the pressure was set to the

desired operating value with argon fill gas. A current between 10 to 80 mA was applied to the cathode, producing an atom cloud representative of the analyte. This cloud was probed by the laser, and the fluorescence was measured.

The figures of merit for the measurement of lead (Pb), europium (Eu), yttrium (Y) and thulium (Tm) were determined. Limits of detection of 0.6 pg, 5 ng, 3 ng and 60 pg were obtained for Pb, Eu, Y and Tm, respectively, based on peak detection. These values were improved when gated peak integration of the fluorescence profiles was employed. Detection limits of 2 fg, 9 fg, 100 fg and 0.03 fg were obtained for Pb, Eu, Y and Tm, respectively, under those conditions.

It was concluded that the redeposition of the analyte on the surface of the cathode led to the improvement in the detection limits. Atoms were sputtered and excited several times during a measurement. The sensitivity of this technique rivals other ultratrace analytical methods due to this trapping of the atoms, leading to the possibility of single atom detection.

CHAPTER 1
INTRODUCTION

The emphasis of a great deal of the recent efforts in analytical chemistry has been the identification and quantitation of trace constituents found in a sample with trace elements being those present in amounts lower than 0.01% (100 μg/g) (1, 2). The goal of achieving increasingly lower limits of detection is often a common one in the development of an analytical method. Indeed, one widely discussed topic has been the possibility of single atom detection, the ultimate goal of chemical analysis.

Although single atom detection is widely debated, techniques capable of trace analysis have been firmly established and include such atomic spectrometric techniques as atomic absorption (2, 3), atomic fluorescence with electrothermal atomization (4, 5) and atomic emission with the combination of inductively coupled plasma (2, 3, 6) and mass spectrometry (4, 7). The focus of elemental analysis has now begun to shift towards microtrace analysis and ultratrace analysis with microtrace analysis being the determination of a trace component in a sample weighing between 10^{-4} to 10^{-2} g and ultratrace analysis similarly involving samples weighing less than 10^{-4} g (1).

The Importance of Ultratrace Sensitivity

Ultratrace analysis can be a particularly challenging task, for manipulation of such small samples without contamination can be difficult. The obvious question naturally arises as to whether there is actually a need for ultratrace sensitivity. The answer to that

question, according to Dr. Gunter Tölg, is an unequivocal "yes" (8). Techniques capable of ultratrace analysis are in fact warranted. The electronic and semiconductor industry and the biomedical industry most notably require such stringent sensitivity (4, 8).

In material sciences, the distribution of elements in grain boundaries and on surfaces down to trace levels assumes an ever increasing importance. There are many unsolved problems in the characterization of particles, dust or small amounts of sediments (8). Moreover, the analysis of metal dopant impurities at ultratrace levels is essential in the semiconductor industry, for the dopants' potential electrical activity is directly related to their purity (4).

In biological systems, there is a growing interest in the distribution of elemental components in tissues, even in single cells or cell membranes. Such common elements as aluminum (Al), vanadium (V) and chromium (Cr) are found in blood serum at concentrations below the ng/g (10^{-9} g/g) range with rarer elements falling in the fg/g range (10^{-15} g/g) (8). The determination of an element at the concentration of 1 ng/g in an individual cell weighing 1 μg, for example, would require an absolute detection limit of 1 fg.

Researchers are finding that elements that were once considered to be toxic to biological systems, particularly to humans, at all concentrations are actually essential for life at trace levels. Notable examples include selenium (Se), cobalt (Co), zinc (Zn), copper (Cu), nickel (Ni), fluorine (F), V and iron (Fe) (2). There is now data to suggest that the well-known toxic elements arsenic (As), cadmium (Cd) and lead (Pb) may be essential at very low levels. In fact, it has been hypothesized that all elements will be

eventually found to be essential for human life at some concentration. Improved detection limits and new ultratrace analytical techniques are necessary for the quantitation of these components.

Volumes of such precious samples as human renal, ocular or spinal fluids are often limited and can range from a few hundred picoliters (10^{-12} L) to tens of nanoliters (9). A nanoliter of renal fluid typically contains approximately 4.3 ng of chlorine (Cl), 3.2 ng of sodium (Na), 80 pg of potassium (K), 40 pg of calcium (Ca), 35 pg of phosphorous (P) and 24 pg of magnesium (Mg) (10); therefore, ultratrace sensitivity is mandatory for elemental analysis. Fluids from smaller invertebrates would also be volume limited and would require an ultratrace analytical technique for analysis.

Ultratrace Analytical Techniques

Presently, most trace analytical techniques require sample amounts in the order of 0.1 g to several grams and volumes in the range of milliliters to make such low concentrations detectable; however, there are several techniques which are capable of analysis of small volume samples. Microtechniques employed by the National Heart, Lung and Blood Institute for the analysis of nanoliter biological samples have been summarized by Bowman and Vurek (9) while a more general review of microsample analysis has been given by Little (11). The most widely used techniques for the trace analysis of small volume samples, particularly biological samples, include helium glow photometry (9-11), electron microprobe analysis of microdroplets (12, 13) and graphite furnace atomic absorption spectrometry (GF-AAS) (1-3).

In helium glow photometry, a radio frequency helium plasma is utilized to excite samples to produce their characteristic emission spectra. Aqueous samples are deposited directly onto an iridium wire which can be electrically heated. The plasma is initiated while the wire is heated to volatilize the sample into the discharge. Metastable helium atoms transfer their energy to the atoms of the sample and, thus, excite them. The emitted radiation is then recorded. Limits of detection for Na, K and Pb are 1.4 pg, 1.6 pg and 2 pg, respectively, where limit of detection is defined as the amount of an element needed to give a signal increment equal to twice the standard deviation of the blank (9).

Electron microprobe analysis involves bombarding samples with an electron beam. The resulting x-ray intensity of the element in the unknown solution is correlated to the x-ray signal emitted from the same volume of a standard solution of known composition and similar matrix (12, 13). This technique requires that the liquid samples first be dried on a beryllium support, which has a low x-ray background, prior to analysis, for the technique is limited to the analysis of solid samples such as crystals. Concentrations as low as 0.5 mmol/L in the original volume of material as small as 20 pL can be accurately measured for such elements as P, Mg, Cl and K (13).

The third technique, GF-AAS, is perhaps the most commonly used method for microsamples. Small volume samples are deposited into a graphite furnace which converts the sample into free atoms electrothermally. The atoms then absorb radiation of a characteristic wavelength, and this absorption is related to the concentration of the element in question. Hollow cathode lamps or electrodeless discharge lamps are

frequently employed as sources for this method (1-3). The technique can achieve extremely low absolute detection limits. For example, the limits of detection for Pb, Zn and manganese (Mn) are 5 pg, 0.2 pg and 0.8 pg, respectively (2).

Each of these techniques has drawbacks associated with it. The main disadvantage of the helium glow technique lies in the need to dilute the samples prior to analysis. A spectroscopic buffer of cesium nitrate and ammonium phosphate is added to the sample in order to swamp interelement interferences (9); however, the addition of the buffer can also result in contamination. Problems associated with electron microprobe analysis include the necessity of drying the samples in such a way that very small crystals are formed, homogeneously dispersed on a dry spot, and that these dried spots are of the same shape and dimensions for a given analysis. GF-AAS is also plagued with difficulties. Again, atomization is based on thermal volatilities, and often components found in the matrix can interfere with and alter the rate of atomization. The addition of matrix modifiers are frequently warranted. Blackbody emission, light scatter and molecular absorption can be sources of background which must be considered. The large power consumption of the graphite furnace is also a drawback of this method.

New Approaches to Ultratrace Analysis

Although most trace analytical methods require large sample volumes, atomic fluorescence spectrometry with a graphite furnace electrothermal atomizer (GF-AFS) is a promising technique for ultratrace analysis, especially when a laser is employed as the source. It has been well documented in the literature that laser excited atomic fluorescence spectrometry in a graphite furnace atomizer (GF-LEAFS) is capable of

achieving extremely low absolute detection limits, in the range of femtograms, for several elements (5, 14-16). Moreover, sub-femtogram sensitivity has been demonstrated for the measurement of Pb in aqueous solutions with a copper vapor laser pumped dye laser system (5). With this technique, atoms produced electrothermally are excited by photon absorption at a particular wavelength. As a result of the absorption, the atoms emit photons of a characteristic wavelength; this method is exceptionally selective. The resulting fluorescence emission is then correlated to the concentration of the element in question. The picometer resolution potential of the laser sources contributes to the high sensitivity and selectivity of this technique. However, as mentioned earlier, the graphite furnace atomizer has several disadvantages which prevent the widespread application of the technique.

Recently, there has been increased interest in the use of glow discharge atom reservoirs for ultratrace analysis of solutions. Glow discharges (GDs) are rather modest plasmas that are initiated upon electrical breakdown of an inert gas and simply consist of two electrodes immersed in a low pressure, rare gas environment (17). These self-sustaining discharges are easily maintainable at pressures between 1 to 10 torr, voltages up to 2 kV and currents ranging from 1 to 1000 mA.

Harrison and Prakash (18) first proposed employing GDs in the analysis of solutions. With this approach, solutions are deposited directly onto the cathode of the GD and are dried as a residue. Atomization of the residues is accomplished through sputtering, which will be discussed more fully in the following chapter. The atoms can then be analyzed by atomic fluorescence, emission or absorption spectrometry, or the atoms may be ionized and measured by mass spectrometry.

The feasibility of utilizing GDs for the analysis of small volume biological samples has been demonstrated by several groups. Caroli *et al.* (19) reported the determination of Al, As, Ca, Cu, gallium (Ga) and Zn in kidney, liver, brain and blood samples of mice with atomic emission detection. More recently, Williams *et al.* (20) have reported detection limits in nanoliter samples of 9 and 20 pg for P and Cl, respectively. Sub-picogram limits of detection were reported for lithium (Li), Na, K and Ca. The researchers also used atomic emission spectrometry (AES) as the method of detection and hoped to apply the technique to the analysis of renal fluids. Several others have had success with GD-AES for the analysis of microsamples (21, 22), and this technique appears promising.

Intent of Dissertation

The present work was performed to evaluate a laser excited atomic fluorescence spectrometric system which employed a miniature GD device as the atom reservoir. It was thought that by combining the most appealing elements of the two, newly established, ultratrace analytical methods, GF-LEAFS and solution analysis with a GD atom source, extremely low detection limits would be feasible. A copper vapor laser pumped dye laser system is employed for the measurement of nanoliter samples containing Pb, europium (Eu), yttrium (Y) and thulium (Tm). Two GD systems are evaluated with optimum operational conditions being determined. The figures of merit are documented, and the application of the technique to the measurement of real samples is investigated, noting any matrix interferences. Future research directions are suggested.

CHAPTER 2
LASER EXCITED ATOMIC FLUORESCENCE IN A GLOW DISCHARGE ATOM RESERVOIR

Principles of Laser Excited Atomic Fluorescence

In LEAFS, incident laser radiation is absorbed by an atom, causing the promotion of electrons from a lower state to a higher excited state for a given transition. The subsequent relaxation of the electrons produces fluorescence radiation which is collected and ultimately detected by a spectrometer. Atomic fluorescence spectrometry (AFS) was first demonstrated as an analytical technique in 1964 by Winefordner and Vickers (23). At that time, the relation of the fluorescence signal to the analyte concentration was recognized. The sensitivity and selectivity of AFS were further established when lasers were incorporated as excitation sources (24, 25). As mentioned earlier, the picometer resolution capabilities of these intense sources enhance the inherent selectivity of AF, and, not surprisingly, single atom detection can likely be achieved with LEAFS (26-30).

General Atomic Fluorescence Flux Expressions

The exact relationship of the analyte signal to the concentration of the analyte can be seen through the derivation of the fluorescence flux expression. In this mathematical treatment outlined by Ingle and Crouch (1), a simple two-level atom under resonance fluorescence conditions, such that the excitation wavelength and emission wavelength are identical, is utilized. A representation of this atom is shown in Figure 2-1 with the rate constants for the possible excitation and de-excitation processes indicated.

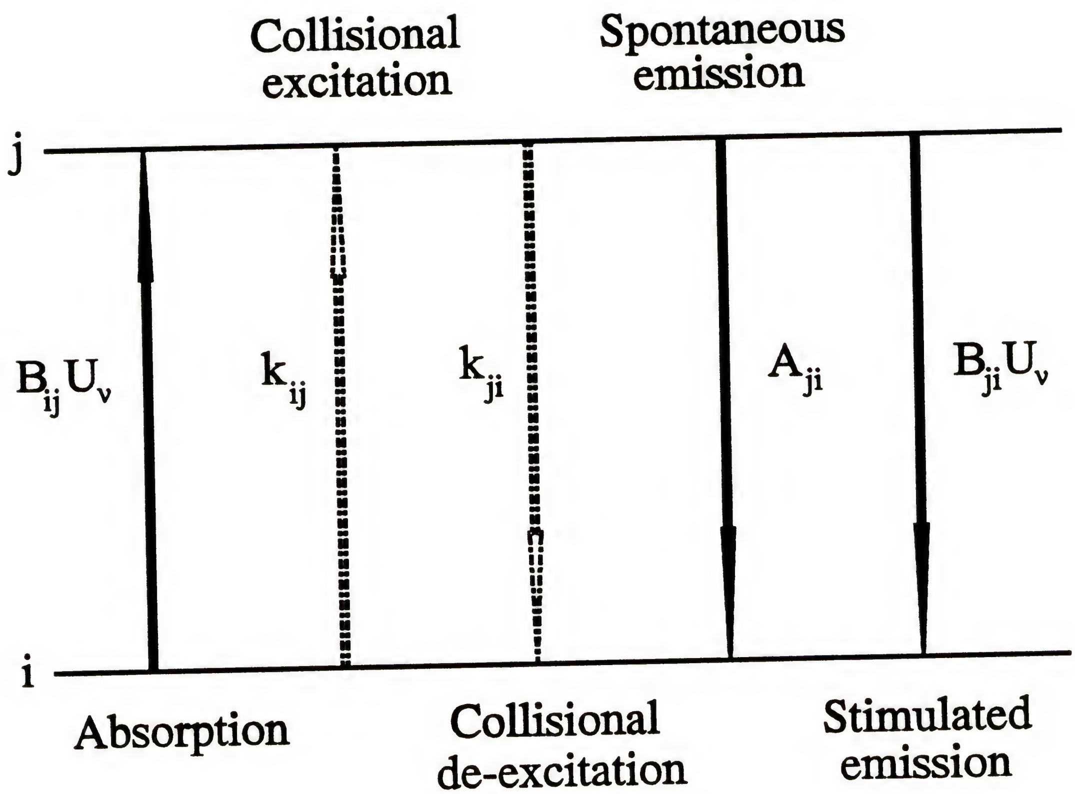

Figure 2-1. Excitation/de-excitation processes in a two-level atom (1).

For atomic fluorescence with a conventional line source, the absorption rate, $B_{ij}U_{\nu}n_i$ where B_{ij} is the Einstein coefficient of stimulated absorption ($m^3\ s^{-1}\ J^{-1}\ Hz$), U_{ν} is the spectral energy density ($J\ Hz^{-1}\ m^{-3}$), and n_i is the number density (m^{-3}), generally exceeds the collisional excitation rate, $k_{ij}n_i$. Stimulated emission is also considered negligible. With these assumptions, the efficiency of the fluorescence process can be related to its atomic parameters, but first, the terminology of AF must be defined.

The fluorescence quantum yield, ϕ, is the fraction of absorbed photons that are emitted as fluorescence photons of the appropriate wavelength while the fluorescence power yield, Y, is the fraction of absorbed radiant power emitted as fluorescence radiant power at the appropriate wavelength. Since radiant power is equal to the flux (photons s^{-1}) multiplied by the photon energy, for a resonance transition the fluorescence quantum yield and power yield are equivalent and can simply be given as

$$Y=\phi=\frac{A_{ji}}{A_{ji}+k_{ji}} \tag{2-1}$$

where A_{ji} is the rate constant for spontaneous emission (s^{-1}), and k_{ji} is the rate constant for collisional de-excitation (s^{-1}) (1).

The total fluorescence power produced, Φ_F, in the volume element V by absorption over pathlength l is given by

$$\Phi_F=\Phi_o\alpha_L Y \tag{2-2}$$

where Φ_o is the incident source radiant power ($J\ s^{-1}\ m^{-1}$), and α_L is the absorption factor

for a line source (m) (1). This absorption factor under optically thin conditions can be expressed as

$$\alpha_L = k_m l \tag{2-3}$$

where l is the pathlength (m), and k_m is the maximum absorption coefficient (m^{-1}) and can be expressed as

$$k_m = \frac{e^2 \lambda_m^2 n_i f_{ij}}{4 \varepsilon_o m_e c^2 \Delta\lambda_{eff}} \tag{2-4}$$

where e is the electron charge (C), λ_m is the wavelength of the transition (m), f_{ij} is the absorption oscillator strength (dimensionless), ε_o is the permittivity of free space (J^{-1} C^2 m^{-1}), m_e is the electron mass (kg), c is the speed of light (m s^{-1}), and $\Delta\lambda_{eff}$ is the effective width of the absorption line (m) (1). The effective width is defined as the width of an equivalent rectangular profile with the same peak value and area as the spectral profile.

After substituting equations (2-3) and (2-4) into (2-2) and evaluating constants, the total fluorescence power produced can be written as

$$\Phi_F = \frac{8.82 \times 10^{-15} \lambda_m^2 n_i f_{ij} l \Phi_o Y}{\Delta\lambda_{eff}} \tag{2-5}$$

where the constant has units of meters. Hence, the observed radiant power of fluorescence is directly proportional to the number density of the ground state which can be related to the analyte concentration and the radiant power. This relationship is the basis of AFS.

At high analyte concentrations when conditions are not optically thin, the absorption factor as expressed in equation (2-2) approaches unity and

$$\Phi_F=\Phi_o Y \qquad (2\text{-}6);$$

therefore, the fluorescence signal becomes independent of the atomic population in the ground state because all the radiation from the narrow line source is absorbed by the analyte. Self-absorption may also be present in this case. The observed fluorescence radiant power (J s^{-1} m^{-1}), Φ_F', is then given by

$$\Phi_F'=\Phi_F f_s \qquad (2\text{-}7)$$

where f_s is the fraction of fluorescent photons which are not reabsorbed (1). Atomic fluorescence is as a result only linearly related to the analyte concentration at low concentrations when a line source is utilized.

Although self-absorption is the major cause of non-linearity at high analyte concentrations, two other phenomena may also play a role. These effects, termed pre-filter and post-filter effects, are related to the right angle fluorescence detection geometry which is frequently utilized (31-33). In this configuration, the fluorescence is observed at 90° from the path of the radiation beam. The fluorescence intensity may be reduced near the front of the illuminated volume, where fluorescence is not detected, by the absorption of source light by the atoms. The cell is completely illuminated by the source; however, the fluorescence is incompletely measured. This is the pre-filter effect which leads to bending of the calibration graphs at lower concentrations. The post-filter

effect involves incomplete illumination of the volume; the fluorescence intensity is reduced due to the re-absorption of fluorescence by atoms that are outside the illuminated volume in the direction of the detector. This effect may lead to a decrease in the linear dynamic range by orders of magnitude.

Saturated Atomic Fluorescence Flux Expressions

When a laser is used as the excitation source instead of a conventional line source, saturation conditions can be achieved. Under saturation conditions, the rate of excitation is equal to the rate of de-excitation, and the maximum fluorescence signal is obtained. The fluorescence signal becomes independent of the quantum efficiency and the source intensity. The mechanism for level population now becomes dominated by the stimulated absorption and emission rates.

Under saturation conditions for the case of resonance fluorescence in the two-level atom illustrated in Figure 2-1, the fluorescence flux can be expressed as

$$\Phi_F = h\nu A_{ji} n_j V^* \tag{2-8}$$

where h is Planck's constant (J s), ν is the frequency (s^{-1}), A_{ji} is once more the Einstein coefficient of spontaneous emission (s^{-1}), n_j is the number density of the excited state (m^{-3}), and V^* is the volume of collected fluorescence (m^3) (1).

Because the rate of absorption and the rate of deactivation by collisions, spontaneous emission and stimulated emission are balanced, the following expression can be given:

$$B_{ij} U_\nu n_i = \left[k_{ji} + A_{ji} + B_{ji} U_\nu\right] n_j \tag{2-9}$$

with all of the variables being previously defined. The spectral energy density, U_ν, can also be defined as

$$U_v = \frac{(E_\lambda)_i}{c} \tag{2-10}$$

with $(E_\lambda)_i$ being the spectral irradiance at level i ($Hz^{-1}\ J\ s^{-1}\ m^{-2}$) (1). Substituting equation (2-10) into (2-9),

$$\frac{B_{ij}(E_\lambda)_i n_i}{c} = \left[k_{ji} + A_{ji} + \frac{B_{ji}(E_\lambda)_i}{c}\right] n_j \tag{2-11}$$

with all variables again being previously explained. Furthermore, the Einstein coefficients of stimulated absorption and emission, B_{ij} and B_{ji}, can be related through the statistical weights of the two levels i and j, g_i and g_j, such that

$$B_{ij} = \frac{g_j}{g_i} B_{ji} \tag{2-12}$$

and substituting equations (2-12) and (2-1) into (2-11) and rearranging so that

$$\frac{g_i n_j}{g_j n_i} = \left[1 + \frac{A_{ji} c g_j}{Y B_{ij} (E_\lambda)_i g_i}\right]^{-1} \tag{2-13},$$

the ratio of the number densities of the states i and j can be solved.

Under saturation conditions, the spectral irradiance, $(E^s_\lambda)_i$, must also be considered. As shown in equation (2-14),

$$(E^s_\lambda)_i = \left(\frac{A_{ji}c}{YB_{ij}}\right)\left(\frac{g_j}{g_i + g_j}\right) \qquad (2\text{-}14),$$

and the saturation spectral irradiance can be defined as the value of $(E_\lambda)_i$ for which the measured fluorescence signal is 50% of its maximum value (1).

When optical saturation is achieved, n_j is equal to n_i, and the total number density, n_T, which is the sum of n_i and n_j, can be related to n_j by the expression

$$n_j = n_T\left(1 + \frac{n_i}{n_j}\right)^{-1} \qquad (2\text{-}15).$$

Using this expression and combining with equations (2-8), (2-13) and (2-14), the equation

$$\Phi_F = h\nu A_{ji} V^* n_T \frac{g_j}{g_i + g_j}\left[1 + \frac{(E^s_\lambda)_i}{(E_\lambda)_i}\right]^{-1} \qquad (2\text{-}16)$$

can be derived and defines the fluorescence flux under saturation conditions; however, when a high intensity laser excitation source is employed, the spectral irradiance is much greater than the saturation spectral irradiance, and the bracketed term in equation (2-16) approaches unity. The fluorescence flux can then be simplified so that

$$\Phi_F = h\nu A_{ji} V^* n_T \frac{g_j}{g_i + g_j} \qquad (2\text{-}17).$$

The relationship between the resulting fluorescence and the number density or analyte concentration is evident and again shows a linear relationship at low analyte concentrations.

Atom Reservoirs for Atomic Fluorescence Spectrometry

Although LEAFS appears to be the ultimate trace analytical technique, there are several drawbacks to the method. No commercial instruments are available mainly due to the associated unreliability, complexity and high cost of the required lasers (26, 31, 32), and LEAFS is inherently a single element technique. The performance characteristics of LEAFS are exceptional, however. It offers a large linear dynamic range, good precision and accuracy and extremely low limits of detection. The detection limits and precision are often only limited by the atomizer through its efficiency and associated noise (1). The selection of an atomizer is, therefore, critical.

When considering an atom source for AFS, there are several desirable characteristics (1). The ideal reservoir would have an atomization efficiency of unity with all of the analyte being converted to an atomic vapor. The atomizer should cause minimal thermal excitation of emission from the analyte and other species present in the sample. Furthermore, the environment should be such that the fluorescence power yield is maximized. In other words, it should be free from species that could cause the fluorescence to be quenched. A chemically inert atmosphere is also ideal in order to minimize compound formation. Several atom sources have been routinely utilized in LEAFS with these points in mind, including most often flames, inductively coupled plasmas (ICPs), graphite furnace electrothermal atomizers and, more infrequently, low

pressure discharges or GDs (1, 32, 33). Each atom reservoir has certain advantages and disadvantages.

Flames are very simple to use; however, the associated high background emission can be a substantial source of noise. Inert gases can be utilized in order to reduce quenching, but this may result in a reduction in atomization efficiency. Also, the laser can be scattered by particles in the flame, adding further to the noise level.

ICPs, which are plasmas maintained by a magnetic field usually in an argon atmosphere, have high atomization efficiencies mainly due to the high temperatures associated with the plasmas. The high temperature, which is typically around 9000 to 10,000 K, also helps to reduce chemical interferences while the inert atmosphere reduces quenching. The ICP has a rather high excitation efficiency as well and a large continuum background so that the power, temperature and observation region must be carefully optimized (1).

As mentioned previously, GF-LEAFS is a promising ultratrace analytical technique, for electrothermal atomizers have several advantages. First, discrete analysis of small sample amounts in the microliter range is possible, resulting in low absolute detection limits. Both the ICP and flame sources require milliliters of sample in contrast. The atomization time is extremely short so that a high instantaneous number density is obtained. An inert atmosphere is again employed which reduces quenching. There are problems, however, with analyte interferences, blackbody emission and background absorption by molecular species which were previously mentioned in regards to GF-AAS.

The GD has been described as the ideal atom reservoir mainly because atoms are produced non-thermally through sputtering (18). As a result, these plasmas are less

prone to effects arising from matrix variations. The low pressure, inert gas environment is a reduced quenching environment, and as stated earlier, the discharges are capable of discrete, solution analysis. Disadvantages associated with these sources include poor precision and atomization efficiency. Nevertheless, the sources appear to be an excellent choice as an atomizer for LEAFS, and single atom detection with GD-LEAFS seems probable (29, 34).

Principles of Glow Discharge Operation

A GD is initiated by the application of a sufficiently high voltage between two electrodes immersed in a gas, most often argon (Ar). The applied potential causes the atoms and molecules of the gas to electrically break down, and the gas undergoes the transition from being a poor electrical conductor, with a resistivity of 10^{14} Ω m, to a good conductor, with a resistivity of approximately 10^{3} Ω m depending on the particular conditions (35). The potential difference between the electrodes at which this transition occurs is called the breakdown potential and depends on the identity and pressure of the gas, the electrode material and interelectrode separation (35, 36).

Breakdown of the gas results in the formation of positively and negatively charged ions and electrons. Electric fields develop between the electrodes so that the positively charged species travel toward the cathode (-) and negatively charged species are accelerated toward the anode (+). Collisional processes within the discharge produce more charged species, and the discharge becomes self-sustaining with the continued application of a potential which is most often lower than the breakdown voltage (35, 36).

The discharges are dark at currents up to about 10^{-6} A; however, at a current of approximately 10^{-4} A, a visible glow is produced between the electrodes. The luminous glow usually occurs at potentials of 200 to 300 V, and this potential remains practically constant for large variations of current, from about 10^{-4} A to 0.1 A (37). At the onset of the glow discharge regime, the cathode surface is only partially covered by the discharge, and increases in current do not effect the current density. As the current is further increased, the discharge eventually covers the entire surface of the cathode (35-38). At this point, any increase in current causes an increase in current density, requiring an increase in the discharge voltage. Discharges of this type are most frequently used in atomic spectroscopy and typically operate in an inert gas, reduced pressure atmosphere between 0.1 and 10 torr at powers of less than 10 W.

Glow Discharge Features

The electrical processes occurring in the GD are indeed numerous and quite complex. Penning (39) summarized these processes as early as 1957 as shown in Figure 2-2. The most significant of these in relation to the present work are the excitation and ionization processes which arise in the two analytical "zones" comprising the GD.

Visually, the GD consists of a number of alternating dark and luminous regions or zones. The number of these zones is dependent upon the experimental conditions, but as many as 4.3×10^7 have been distinguished (40). From the analytical standpoint, only two of these regions are of interest (35, 40-42). As depicted in the simple, planar electrode GD representation (Figure 2-3), the zones are termed the cathode dark space and the negative glow.

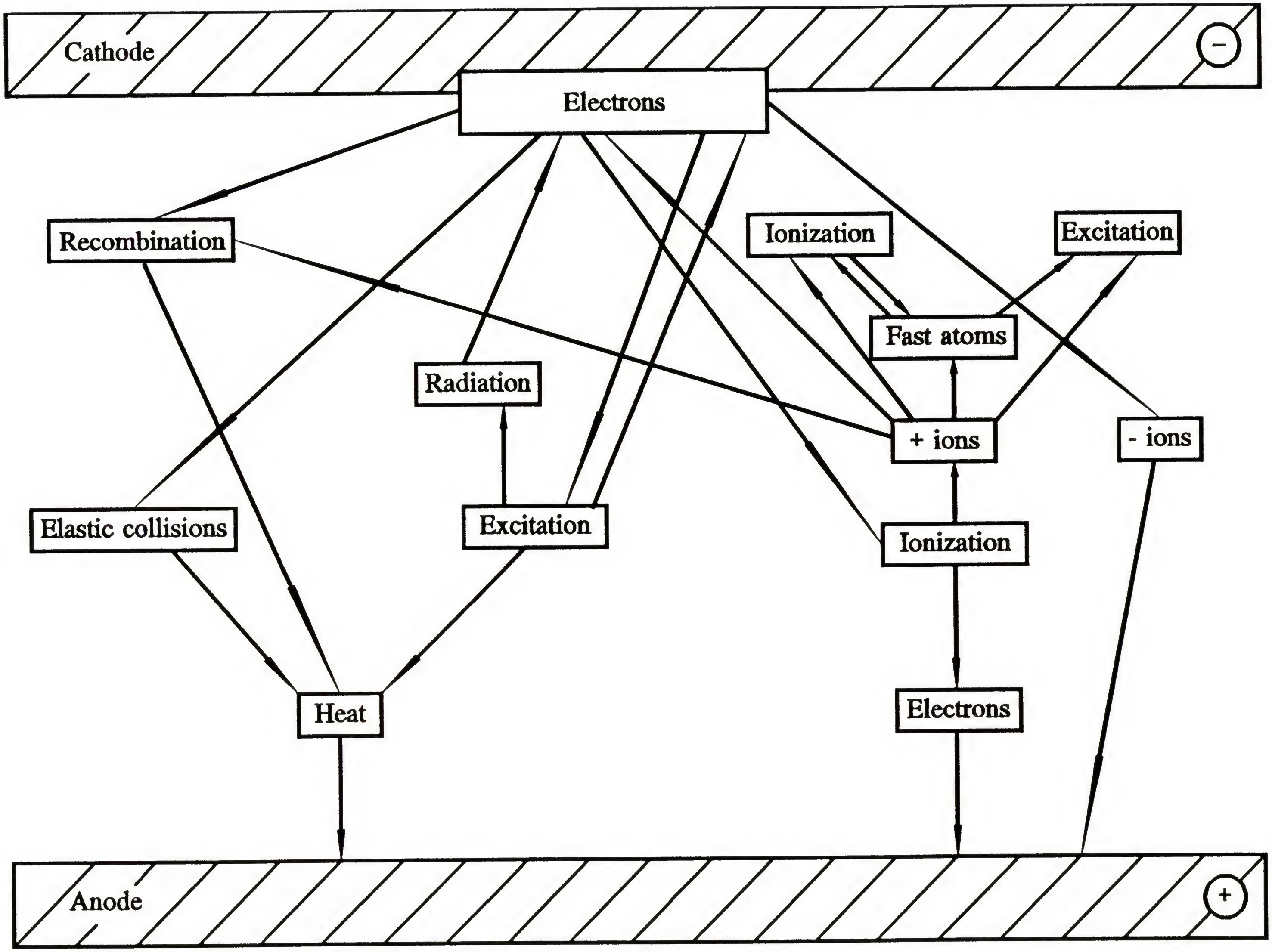

Figure 2-2. Elementary processes occurring in a low pressure glow discharge from (39).

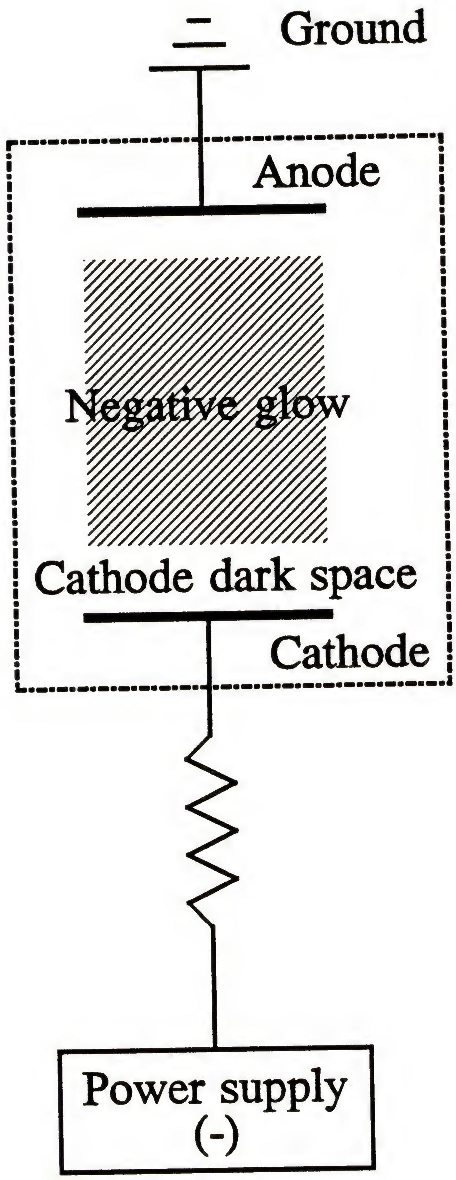

Figure 2-3. Representation of a simple, planar electrode glow discharge.

The cathode dark space is a very thin region with a thickness approximately three times the Debye length, λ_D, so that

$$\lambda_D = \left(\frac{kT_e\varepsilon_o}{n_e e^2}\right)^{\frac{1}{2}} \tag{2-18}$$

where k is Boltzmann's constant (N m K^{-1}), T_e is the electron temperature (K), ε_o is the permittivity of free space (C^2 N^{-1} m^{-2}), n_e is the electron number density (m^{-3}), and e is the electron charge (C) (35, 37, 18). Near the cathode in the cathode dark space, electrons are repelled, resulting in the development of a positive space charge. Almost the total potential difference between the cathode and anode is dropped fairly linearly across this region (35, 37, 39). It is the only region of the plasma where positively charged rare gas ions can gain energy on their way to the cathode surface (40). Fast, secondary electrons, which are emitted by the cathode as a result of the positive ion bombardment, inelastically collide with particles located in the cathode dark space and, consequently, lose a large fraction of their energy in this region.

The negative glow is the most important region in terms of analytical applications. The negative glow is characterized by a highly luminous glow which is a result of collisions of slow electrons entering the zone. These slow electrons are either fast, secondary electrons that have been collisionally cooled or are those created as a result of an ionization reaction (35, 36, 41, 42). Fast, secondary electrons which have not undergone collisional energy losses are also found in the negative glow (35, 36, 41, 42). This region is essentially a field-free or neutral region with the number of positive ions

nearly matching the electron density (36), and it has a thickness of the order of the mean free pathlength of the particles (37).

The excitation occurring in the negative glow is produced by the numerous electrons which result from the ionization processes arising in the cathode dark space as well as by the few, fast, cathode electrons which are again caused by positive ion bombardment. These positive ions, produced in the negative glow, impact the cathode and cause atoms, molecules and electrons composing the cathode to be ejected. This process is described as "sputtering," and this atomization process is perhaps the greatest advantage of the GD.

The Sputtering Process

In a GD, the positive ions in the negative glow may be accelerated across the cathode dark space and impinge on the cathode. Ion bombardment energies typically range from 100 to 500 eV (43). An ion striking the cathode surface either is backscattered from a surface atom or penetrates the solid and transfers its energy to surface atoms (18, 35, 43). The transfer of momentum between the incident ion and a matrix particle, neutral atom, ion, cluster or electron occurs through a collisional cascade caused by numerous inelastic and elastic collisions (18). If a sufficient amount of energy is transferred to atoms near the surface so that their energies are greater than the surface binding energy, the atoms can escape the cathode and enter the gas phase. The ejected atoms have energies around 5 to 15 eV and originate from the first few ångstroms of the sample (43). This process has been summarized by McHugh (44) as shown in Figure 2-4. Over 90% of the sputtered particles are ground state, neutral atoms with a few

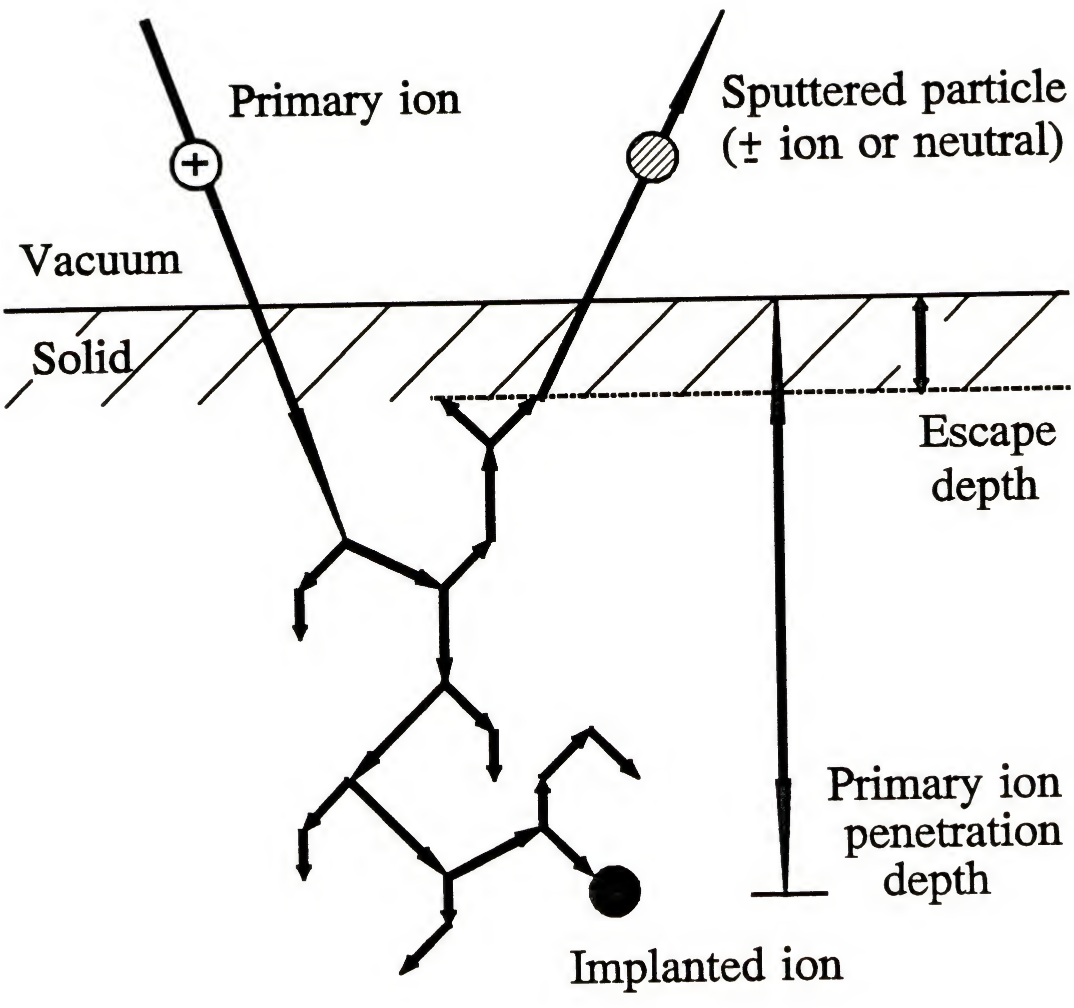

Figure 2-4. Representation of sputtering process from (44).

percent of ions, electrons, molecules and photons being ejected (45, 46). It should be noted that any atoms present on the surface, such as a solution residue, will also be sputtered. This is the basis of the present work involving GD-LEAFS.

The efficiency of this sputtering process or the sputtering yield, S, is defined as the number of sputtered atoms per incident ion and can be expressed as

$$S=\left(\frac{3}{4}\right)\pi^2\alpha\left[\frac{4M_1M_2}{(M_1+M_2)^2}\right]\frac{E}{U_o} \tag{2-19}$$

where M_1 and M_2 are the masses of the ion and the sputtered atom, respectively, in grams, E is the incident ion energy (eV), U_o is the surface binding energy (eV), and α is a function of the relative masses and the angle of incidence of the impinging ion (47,48). Experimentally, the sputtering yield can be considered as

$$S=\frac{10^{-6}\ WNe}{Mi^{+}t} \tag{2-20}$$

where W is the weight loss of the sample (μg), N is Avogadro's number (mol^{-1}), e is the electronic charge (A s), M is the atomic mass (g mol^{-1}) of the sputtered atom, i^+ is the ion current (A), and t is the sputtering time (s) (38). The ion current is related to the total discharge current, i, by

$$i^{+}=\frac{i}{1+\gamma_1} \tag{2-21}$$

where γ_1 is the number of secondary electrons released by one atom (38), typically around 0.1 for Ar discharges (35).

Sputtering yields vary little from element to element. As shown in Figure 2-5 which is based on the work of Laegreid and Wehner (49), the yields typically differ by a factor of 3 to 5. In comparison, elemental thermal volatilities can vary by 4 or 5 orders of magnitude (50). On this basis, GD atom reservoirs should be less prone to effects arising from matrix variations than atomization methods that rely on thermal volatilities.

Collisional Processes in the Glow Discharge

Once in the gas phase, sputtered atoms are subjected to a variety of gas phase collisions. Figure 2-6 from Harrison and Bentz (43) illustrates these processes. The sputtered neutral atoms rapidly lose their initial energy as a result of collisions with atoms of the discharge gas. In a discharge at 1 torr, these collisions may cause as much as 94% of the sputtered atoms to be redeposited on the cathode surface (51). Those that escape back-diffusion and redeposition enter the negative glow and may become excited or ionized as they diffuse through the region.

There are two primary ionization mechanisms: electron impact and Penning ionization (42, 52, 53). Electron impact ionization occurs when a sputtered neutral atom, M^o, collides with an electron such that

$$M^o + e^- \rightarrow M^+ + 2e^- \tag{2-22}$$

to form a positive ion, M^+. Between 0.1 and 1% of the sputtered population is ionized

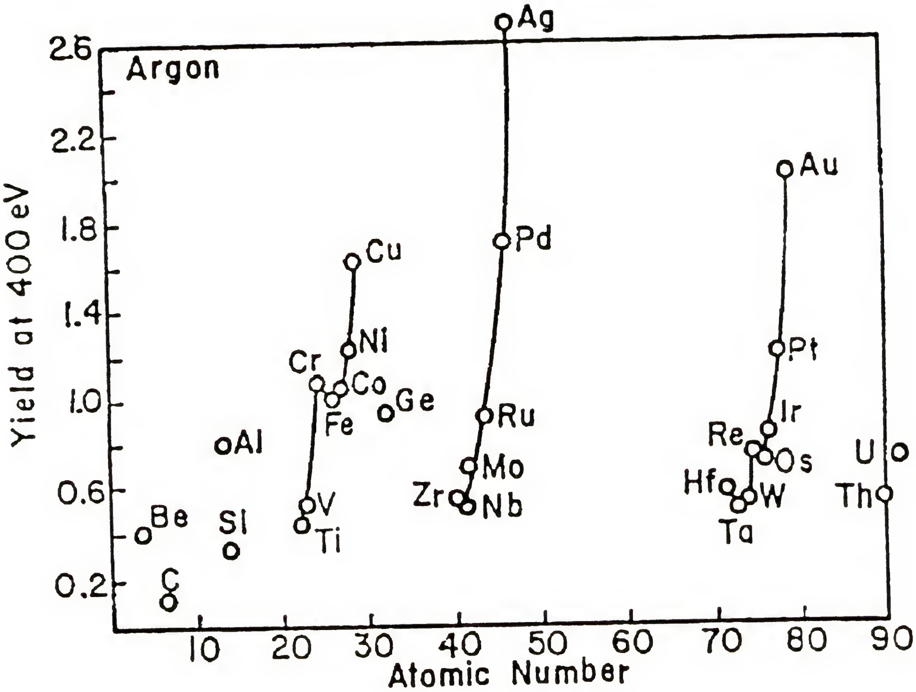

Figure 2-5. Sputtering yields for various elements in argon (49).

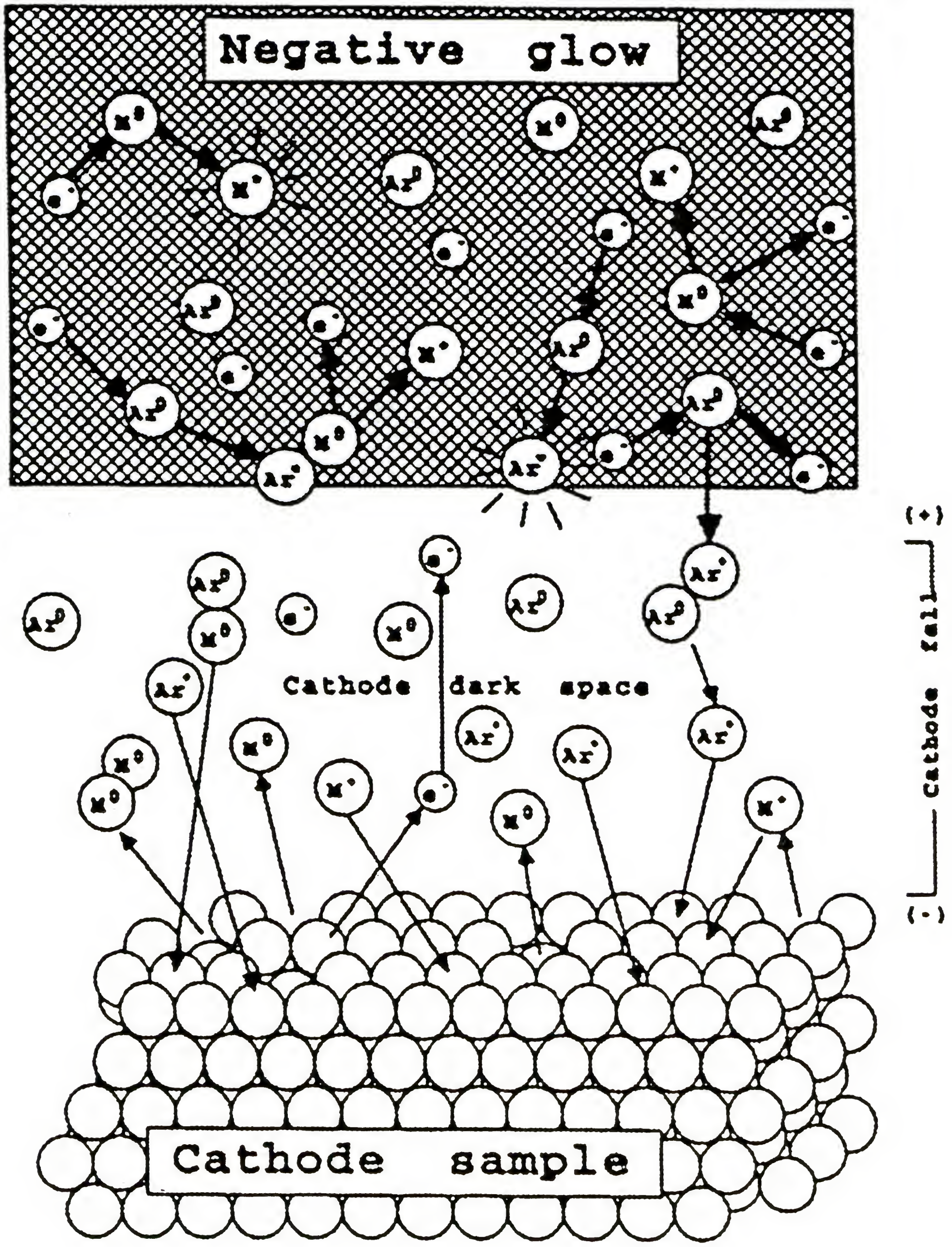

Figure 2-6. Fundamental collision processes in a glow discharge (43).

in this manner (54, 55). Electron densities are high, of the order of 10^{11} to 10^{13} cm^{-3}; therefore, this is likely to be the primary mechanism for ionization (44). Discharge gas atoms also undergo electron impact collisions, resulting in the production of metastable gas atoms (35, 42, 51, 52). These metastables often have energies greater than the first ionization potentials of neutral species. Argon has, for example, metastable energy states at 11.55 eV and 11.72 eV. Metastables are efficiently produced in a glow discharge and have reported densities around 10^{10} to 10^{11} cm^{-3} in 20 millitorr of Ar with the total density of Ar atoms being near 10^{16} cm^{-3} (52, 53). These metastable species can collide with a neutral atom causing ionization. This is termed Penning ionization as illustrated in equation (2-23)

$$M^{o} + Ar^{*} \rightarrow M^{+} + Ar^{o} + e^{-} \tag{2-23}$$

where Ar^{*} represents a metastable argon species. As much as 95% of the overall ionization may be due to Penning ionization (56); however, the contribution is widely debated and is dependent upon the experimental conditions.

Again, most of the sputtered atoms, around 99%, remain as neutrals. This is extremely important in the GD-LEAFS application to be presented herein. Furthermore, due to the low gas operational pressures of the discharges, analyte densities usually range from 10^{11} to 10^{14} atoms cm^{-3} so that the plasmas can be considered optically thin (41). Optically thin conditions are advantageous in this study as discussed in the section on LEAFS principles.

CHAPTER 3
REVIEW OF LITERATURE ON GD-LEAFS

Although the GD theoretically appears to be the ideal atom reservoir for AFS, relatively little research has been devoted to the subject of GD-AFS. In 1973, Gough *et al.* (57) first proposed that cathodic sputtering be used as a source of atomic vapor for the chemical analysis of metals by AFS. Their GD chamber was fashioned from pyrex and was maintained at a reduced pressure of 5 torr with a continuous flow of Ar. Currents near 35 mA were applied to the water-cooled cathodes. A commercial hollow cathode discharge lamp was utilized as the excitation source and was modulated so that the fluorescence signal could be separated from the dc emission in the GD by synchronous demodulation. The flat, metallic, disk-shaped cathodes, which served as the analytical samples, were placed 1 cm from the anode. The fluorescence, from a region 2 cm below the cathode surface, was detected at a right angle from the excitation beam. Since fluorescence is isotropic, this detection geometry minimized any noise attributed to scattered radiation from the source. Detection limits of 20 ppm for Ni, Cr and Cu, 70 ppm for Mn and 400 ppm for silicon (Si) were obtained in Fe based alloy samples with a 1% reproducibility. The researchers concluded, however, that there was a need for more intense excitation sources in order to improve the sensitivity of the technique.

Two years later, Butler *et al.* (58) utilized the GD designed by Gough *et al.* (57) as a resonance detector (RD). Resonance detectors simply indirectly measure atomic

emission. In their approach, an emission line from an atom source was employed as the excitation source to induce atomic fluorescence in the GD. This fluorescence was directly proportional to the atomic emission. In this way, a single, relatively weak emission line could be isolated from many. Although the GD was identical to that presented by Gough *et al.* (57), one important innovation was made. The GD was operated in a pulsed mode, whereas the source had previously been modulated. The fluorescence signal was measured several ms after (between 30 to 40 ms) the sputtering cell current had been switched off. Emission from the GD subsided to near zero after 20 ms while there were still sufficient numbers of free, neutral atoms to cause absorption and subsequent fluorescence. The measuring system did not "see" the high emission intensity from the GD; the shot noise caused by this high signal level was eliminated from the analytical signal. Work in this area was continued by Human, Ferreira, Kruger and Butler (59) who designed a brass GD chamber as a RD in 1978 and Bubert (60) who designed a multielement RD system in 1984.

Lasers were first incorporated as excitation sources for GD-AFS in 1982 by van Dijk *et al.* (61). An Ar ion continuous wave laser pumped dye laser was utilized to excite fluorescence in a pyrex GD chamber. Quartz windows were added to the cell so that the laser beam could pass. The system was a flowing system, and, once more, the GD was pulsed. Spatial and temporal diagnostics were performed with the distribution of sputtered atoms, the level populations of the fill gas and the axial profiles of the emission from the fill gas being measured.

Hannaford and Lowe (62), shortly afterwards, began measuring the radiation lifetimes of excited atomic levels by recording the time decay of the atomic fluorescence

emitted by the cathodes in a GD. These researchers employed a pulsed nitrogen laser pumped dye laser as the excitation source with the hope of determining the absolute atomic transition probabilities for the elements composing the cathodes. The GD was pulsed at 8 Hz with a pulse width of 3 ms. The triggered pulse to the laser was delayed between 1 to 15 ms so that it coincided with the dark time of the GD. This represented yet another important development, for both the source and the GD were now being pulsed. This work represents an on-going research study, and, as of late, fluorescence decay curves for neutral and singly ionized atoms of most elements, including the refractory elements, have been recorded (63-65).

Using a system similar to Hannaford and Lowe's (62), Smith *et al.* (66) first studied aqueous solutions by GD-LEAFS. A pulsed nitrogen laser pumped dye laser was again employed as the radiation source. Argon was continually introduced, and the pyrex GD chamber was pulsed at 20 Hz. The laser was triggered 300 μs after the discharge was extinguished with no decrease in fluorescence being noted when compared to continuous operation. This indicated that there was no significant loss of atom population during the time that the discharge was off; however, the background emission noise was 10 to 100 times greater if the discharge was not shunted off prior to the fluorescence measurements. Lead was chosen as the model element with non-resonance fluorescence, excitation at 283.3 nm and detection at 405.8 nm, being measured. Two types of samples, both aqueous and solid, were measured. Copper cathodes which contained trace levels of Pb were studied as were Pb solution residues deposited onto graphite electrodes. In the case of the Pb residues, 5 μL of the solutions were dried on

the cathode prior to analysis. Detection limits of 0.1 μg/g for Pb in Cu and 20 pg for Pb solution residues were obtained with 1-2% reproducibility. Ultimately, the measurements were found to be limited by radio frequency pick-up from the firing of the nitrogen laser.

In 1982, two years following the initial study involving the analysis of solution residues, Patel and Winefordner (67) reported detection limits of 8 ng and 11 ng for indium (In) solutions deposited on graphite and Cu electrodes, respectively. A dc GD was employed with a nitrogen laser pumped dye laser serving as the excitation source. In the course of their study, the researchers found that several diatomic species, Cu_2, copper oxide (CuO) and Pb_2, were present in the sputtered vapors of a Pb containing Cu cathode (68). It was concluded that the spectral interferences from these molecular species were contributing to the background noise level. Moreover, the formation of the diatomics resulted in a reduced number density of atoms, leading to reduced analytical sensitivity. The researchers did verify, however, that a simple, dc glow discharge was an efficient atom reservoir and that pulsing was not essential.

The possibility of detecting a single atom within the laser probe volume with GD-LEAFS was investigated in 1989 when Smith *et al.* (34) studied the fluorescence of Pb in a commercial hollow cathode lamp. According to the researchers, in order to detect a single atom, several conditions had to be met. First, an atom reservoir with low background emission noise was needed. Secondly, non-resonance, saturated fluorescence had to be measured, and, finally, the experimental system needed to have a good probing efficiency with good fluorescence collection efficiency and detector efficiency. It was

deduced that these conditions could be satisfied with a high repetition rate laser excitation system, such as a copper vapor laser (CVL) pumped dye laser system, which utilized a commercial glow discharge device as the atom reservoir. In order to investigate their theory, the output from a pulsed, 6 kHz CVL pumped dye laser at 283.3 nm was used to excite the Pb atoms in a hollow cathode lamp. The density of the Pb atoms was controlled by controlling the current to the discharge over the range of 0.001-10 mA by varying a ballast resistor in series with the lamp. The experimental system as shown in Figure 3-1 used front surface illumination and detection with fluorescence in the lamp at 405.8 nm being monitored. The limit of detection obtained was 6000 atoms or 1.8 ag (1.8 x 10^{-18} g) of Pb in the laser probe volume. The system was limited by a rather poor detection efficiency. Nevertheless, the results were promising, and pulsing of the hollow cathode lamp was proposed in order to decrease the background emission noise and, consequently, the limit of detection.

Glick *et al.* (69), encouraged by this work with the commercial hollow cathode lamp, continued studying the non-resonance fluorescence of Pb atoms with GD-LEAFS. Solutions containing both Pb and iridium (Ir) were deposited onto graphite electrodes, and the sputtered atoms were excited by a tuneable dye laser pumped by a xenon chloride (XeCl) excimer laser, a high power, pulsed laser. The GD was pulsed so that the laser pulses coincided with the dark period. The emission from the GD completely disappeared within 20 μs, and the laser pulse was timed to arrive 100 μs after the GD voltage had been switched off. The chamber was constructed from a six-way vacuum cross with Ar being continually introduced. Front surface illumination and detection

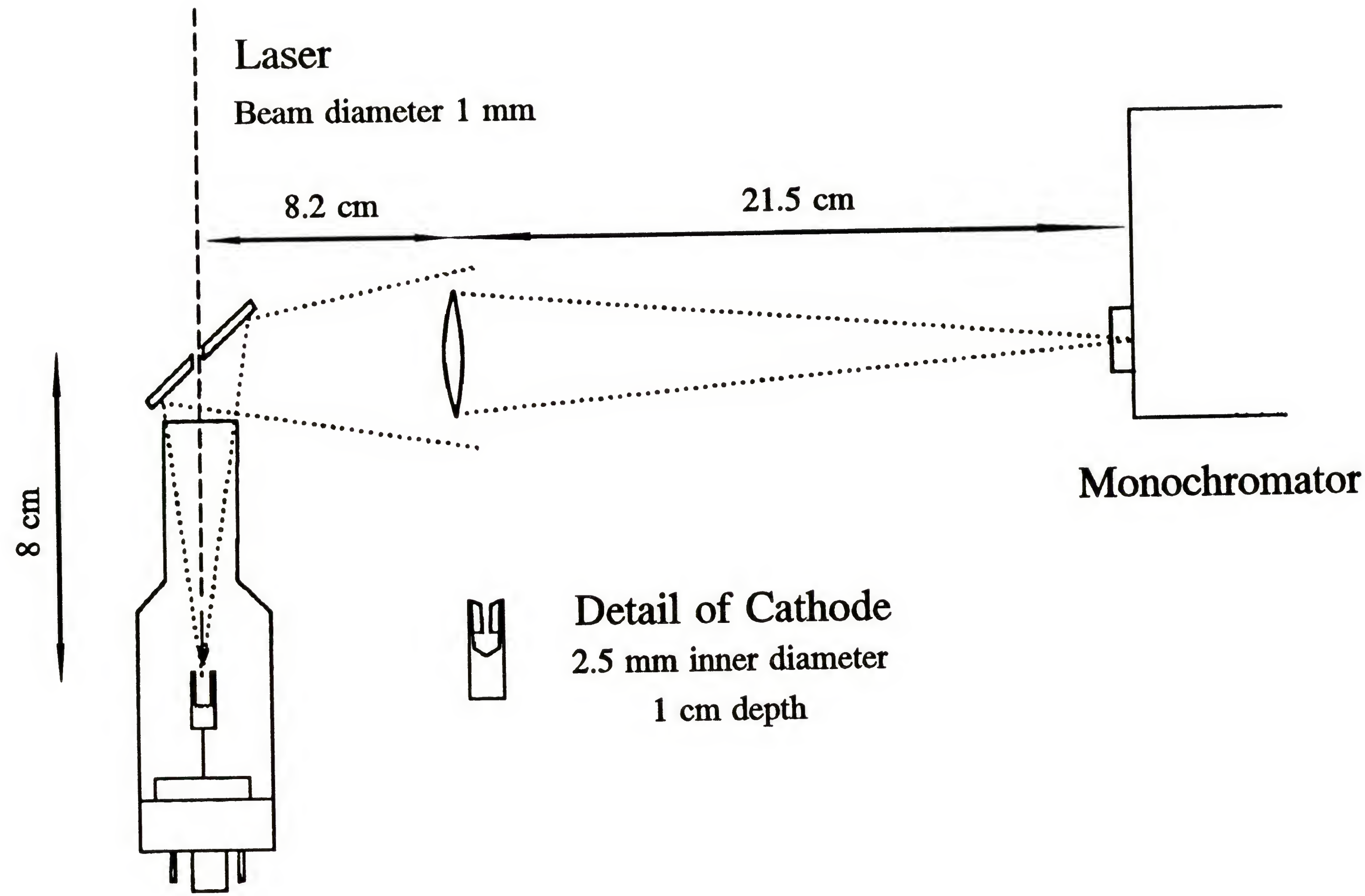

Figure 3-1. Optical layout utilized by Smith and co-workers for collection of fluorescence in a hollow cathode lamp (34).

were again employed. Limits of detection of 500 fg and 20 pg of Pb and Ir, respectively, were obtained. Suggested improvements included increasing the atomization rate, temporal probing efficiency and spatial probing efficiency in order to obtain analyte detection limits that approached the theoretical, intrinsic detection limit of 25 atoms for Pb. The same system, substituting a pulsed CVL operating at 6 kHz for the excimer laser, was studied the following year by Womack *et al.* (70), and a detection limit of 15 pg of Pb deposited onto a graphite electrode was acquired.

Dashin *et al.* (71) used a pulsed GD-LEAFS system similar to that described by Glick *et al.* (69) in order to investigate the resonance fluorescence of Pb contained in solid Cu standards. A XeCl excimer laser pumped dye laser served as the excitation source. The cathode, which was composed of the sample material, was fashioned into a cup or hollow cathode in contrast to the planar cathodes employed by Glick *et al.* (69). A detection limit of 40 ng/g for Pb in Cu resulted. These researchers continued this work, and their results involving the direct analysis of planar, solid metallic samples by GD-LEAFS were published in 1993 (72). The newly developed system used a planar magnetron sputtering device, similar to those found in the thin films industry, in hopes of improving the sputtering efficiency. High purity In and Ga were analyzed for Si content, and limits of detection of 0.4 ng/g for Si in In and 1 ng/g for Si in Ga were acquired.

The depth profiling capabilities of GD-LEAFS were investigated by Grazhulene *et al.* (73) in 1991. A nitrogen laser pumped dye laser was used to excite the fluorescence of Na contained in high purity molybdenum (Mo) in a pulsed, stainless steel

GD chamber. The time of discharge ignition and quenching did not exceed 10 μs with the laser pulse occurring 0.1 ms after the GD had been switched off. The chamber was operated at pressures from 0.1 to 1 kPa at currents between 30 to 50 mA. Fluorescence was collected at 90° from the excitation beam and passed through a 10 nm band pass interference filter before being detected by a photomultiplier tube. This non-dispersive system had the advantages of increased solid angle collection and throughput, resulting in increased sensitivity. The researchers were able to detect 24 μg/g of Na when etching an amount of Mo corresponding to a mean layer thickness of 1 nm. The possibility of achieving depth resolution in depth profiling down to tens of ångströms was clearly shown.

Like Dashin *et al.* (71), Lunev *et al.* (74) were interested in a hollow cathode GD device as an atom reservoir for LEAFS. A pyrex chamber with quartz windows was utilized at neon fill pressures of approximately 2 kPa. Aqueous solutions containing varying amounts of Co were dried onto graphite electrodes prior to analysis. The electrodes with deposited residues were then annealed in the chamber at currents near 250 mA for 1 min before atomization when currents were increased to 600 mA. The cathodes could also be heated so that the thermal contribution to the atomization rate could be determined. Maximum Co fluorescence, excited by a neodymium: YAG (Nd:YAG) laser pumped dye laser, was measured 20 s after the GD was initiated. Pulsing of the GD was investigated; the researchers found that the atom population remained constant some 300 μs following extinction of the GD while the emission fell to near zero. A limit of detection of 0.6 pg was obtained with pulsing. Lunyov and

Oshemkov (75) have recently acquired a detection limit of 200 pg for aqueous Ni residues deposited onto graphite electrodes with this system.

In 1993, the pulsed CVL pumped dye laser GD-LEAFS system initially studied by Womack and co-workers (70) was re-evaluated by Deavor *et al.* (76). The experimental set up is illustrated in Figure 3-2. The system was identical to the one described by Womack with the exception of the planar mirror that was added in order to reflect the laser radiation back into the GD which resulted in a two-fold increase in the fluorescence signal. The GD chamber (Figure 3-3) was constructed from a stainless steel, six-way vacuum cross with a total volume of 240 mL. The discharge, which could also be pulsed, operated under optimal conditions with an Ar pressure of 5.5 torr and a current of 25 mA. Argon could be continuously introduced, or the chamber could function under stop-flow conditions. A planar Cu rod was utilized as the electrode with aqueous Pb solution residues being measured. Graphite electrodes were also studied; however, the associated high porosity led to sample loss, increased atomization time and substantial memory effects. Non-resonance fluorescence was monitored at 90° from the beam path, and maximum signals were obtained 100 ms after the GD was ignited.

Several parameters of the system were studied such as the benefits of pulsing the GD and the significance of the position of the laser beam relative to the cathode surface. The fluorescence signal measured between the cathode and anode in region AB of Figure 3-3 was compared to that recorded below the anode in region BC. It was found that the atomic vapor uniformly filled the entire chamber; however, the background emission decreased significantly when measurements were obtained in the area below the anode,

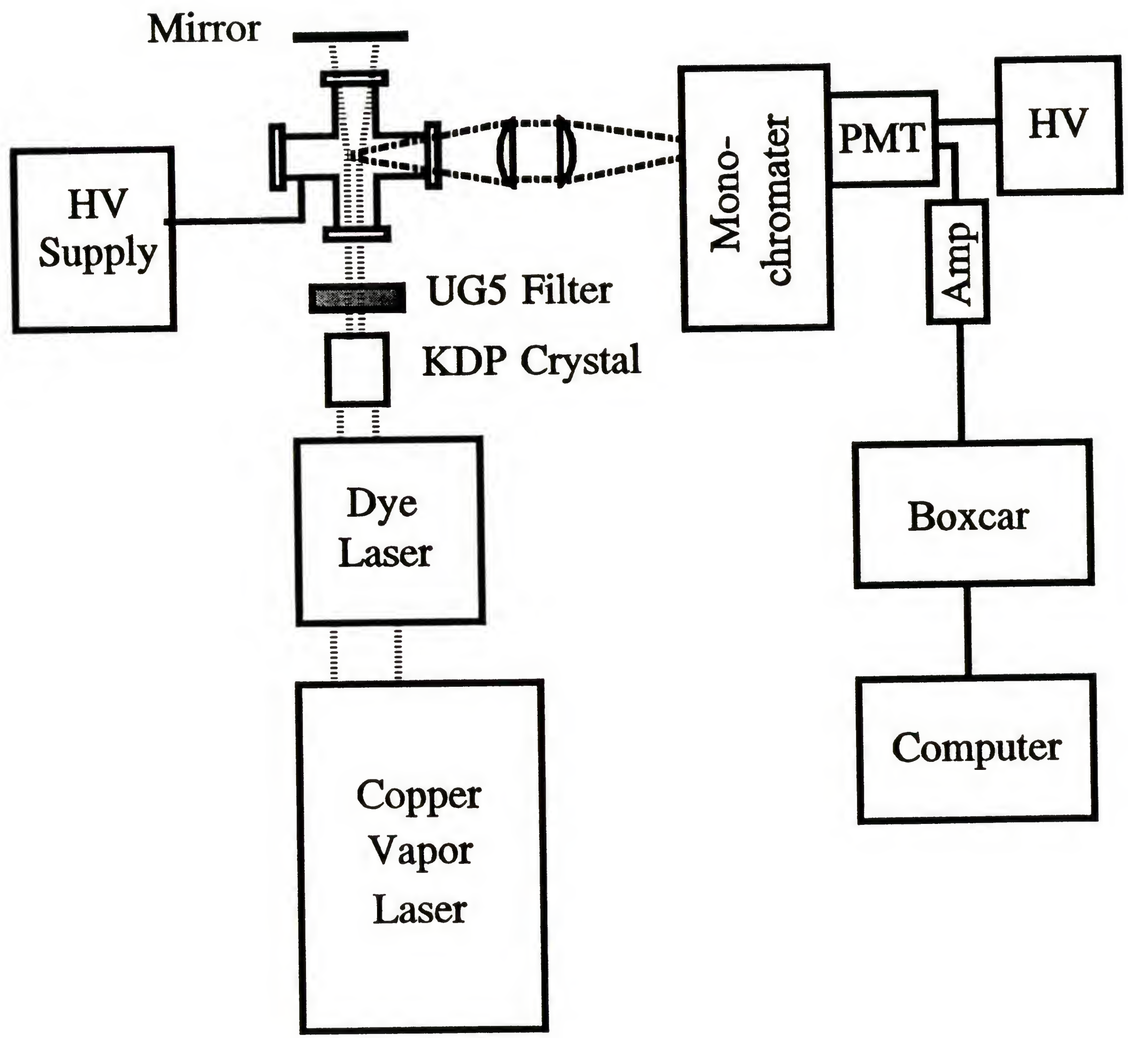

Figure 3-2. Schematic of the GD-LEAFS experimental system of Deavor and co-workers (76).

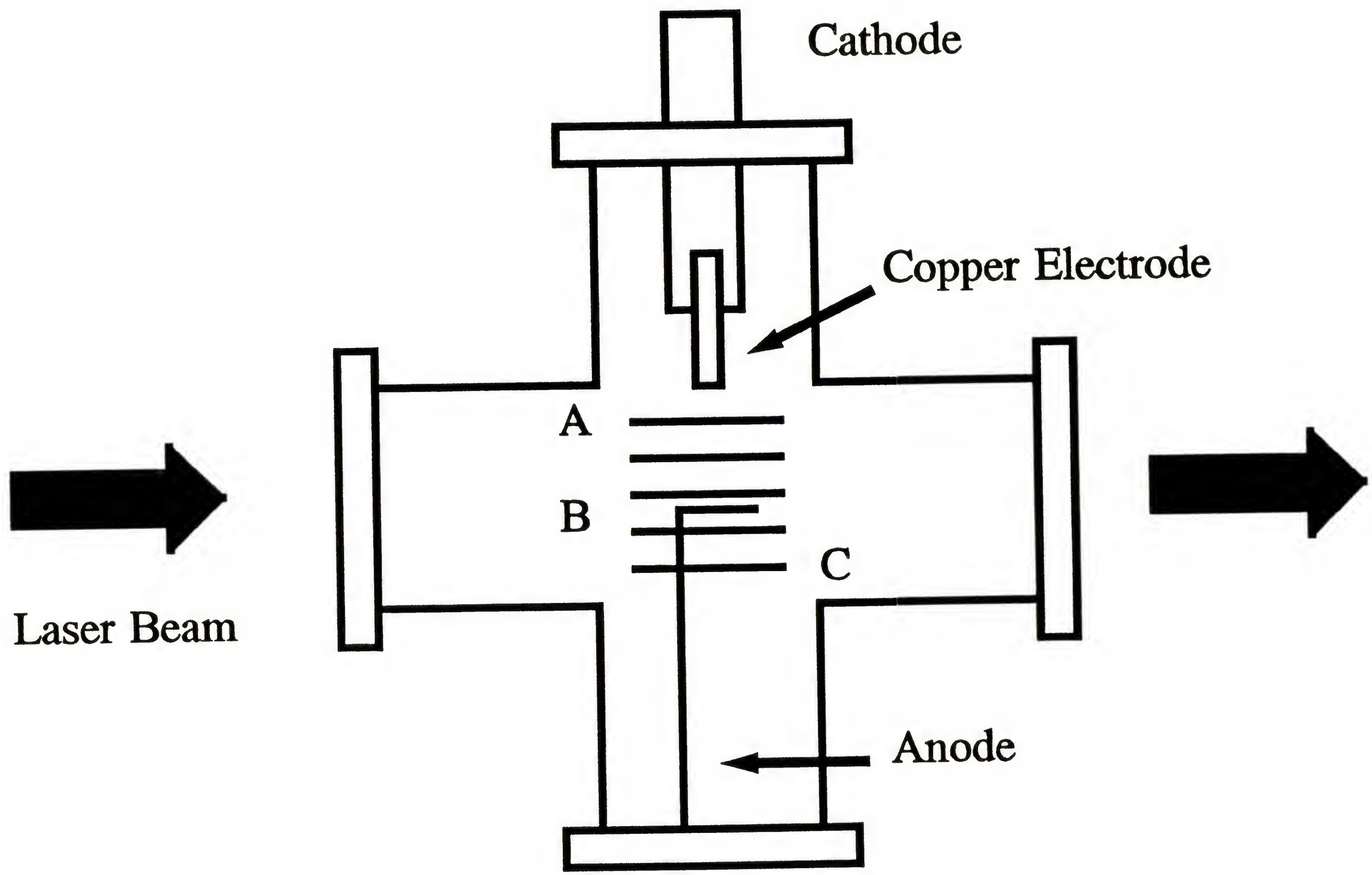

Figure 3-3. Representation of the GD chamber designed by Deavor and co-workers (76).

at distances greater than 1 cm from the cathode. Pulsing the GD at 6 kHz did not result in a similar increase in the signal to noise ratio (S/N). The researchers found that the background emission did not decrease substantially during the 163 μs dark time of the GD. Therefore, pulsed operation held no advantage over dc operation. Stopped-flow operation was also found to offer no benefits. It was thought that the atomic vapor could be confined in the chamber if the gas inlet and vacuum port were closed prior to ignition of the GD. As a result, the atoms would be probed many times by the laser; however, this did not appear to be the case. The fluorescence signal decreased when the stop-flow mode was utilized. The limit of detection, utilizing peak height as the means of comparison, of 2 pg for Pb was limited by background fluorescence due to Pb impurity in the Cu cathodes. It is interesting to note that a slightly poorer detection limit of 60 pg was obtained when peak areas were compared. In conclusion, the researchers suggested that a smaller volume chamber be constructed which would minimize dilution of the atomic vapor and that stop-flow operation be studied more thoroughly. A search for cathodic materials which are free of Pb was strongly recommended.

The research presented herein is a continuation of the work by Deavor and co-workers (76). Their suggestions have been carefully considered and investigated with the results being documented in the following pages.

CHAPTER 4
DESIGN OF THE QUARTZ GLOW DISCHARGE ATOM RESERVOIR AND THE SPECTROMETRIC SYSTEM FOR THE MEASUREMENT OF LASER EXCITED ATOMIC FLUORESCENCE

Chamber Design

The goals of the design strategy were developed in light of the previous research performed in this laboratory. The first goal was to reduce the physical size of the chamber. As stated earlier, Deavor and co-workers (76) found that the atom cloud immediately diffused away from the planar cathode to the walls of the chamber, decreasing the concentration of the analyte species in the probe volume of the laser. The atoms uniformly filled the entire chamber. It was thought that by reducing the volume of the atom reservoir, one could cause a subsequent increase in the atom density and minimize dilution of the analyte. The new, miniature chamber was to be approximately one-forth the volume of the chamber employed by Deavor *et al.* (76) so that a direct comparison of the analytical figures of merit could be made.

Efficient sample exchange was also a desired characteristic of the miniature chamber, and this formed the basis of the second goal of the chamber design. It was determined that a chamber could be constructed from a modified 19/22 quartz outer taper joint and that the cathodes could be made from the corresponding inner taper joints. Cathodes could, therefore, be easily removed and quickly exchanged. The exact design of the cathodes will be discussed in the following section. The vacuum requirements

could also be met with this configuration. Three optical quality windows were added to the original outer taper joint to allow for 90° collection of the fluorescence.

The final objectives involved the design of the anode which was critical. In order to investigate the effect of the laser sampling area on the S/N, the anode needed to allow for placement of the laser both above and below it without physically obstructing the viewing window. Furthermore, the distance between the anode and the cathode was to be variable in order to monitor its effect on the S/N as well. A hook-shaped, stainless steel wire was ultimately found to meet these criteria. Several anodes of varying lengths were fabricated so that the role of the anode-to-cathode distance could be studied. A 7/15 quartz outer taper joint was added directly opposite to the 19/22 taper to facilitate anode exchange. A 1/16 in diameter stainless steel rod was epoxied with vacuum epoxy into the mating 7/15 inner taper joint flush with the end. This rod was held at electrical ground. A small hole, with a diameter slightly larger than the anode wire and a depth of approximately 1/8 in, was drilled into the rod. The anode wires were placed into this depression and were, as a result, also at ground potential.

A schematic of the GD chamber is shown in Figure 4-1 with the dimensions of the reservoir indicated. The volume of the chamber was 60 mL. The system was a flowing system with the fill gas, Ar, being continually introduced. A dual stage rotary pump (Trivac A, Leybold-Heraus Vacuum Products, Inc., Export, PA) was used to maintain the desired pressure within the chamber. This pressure was monitored by a capacitance manometer (Baratron Type 221AHS-A-10, MKS Instruments, Inc., Burlington, MA). A length of 1/8 in inner diameter Tygon tubing, which was connected

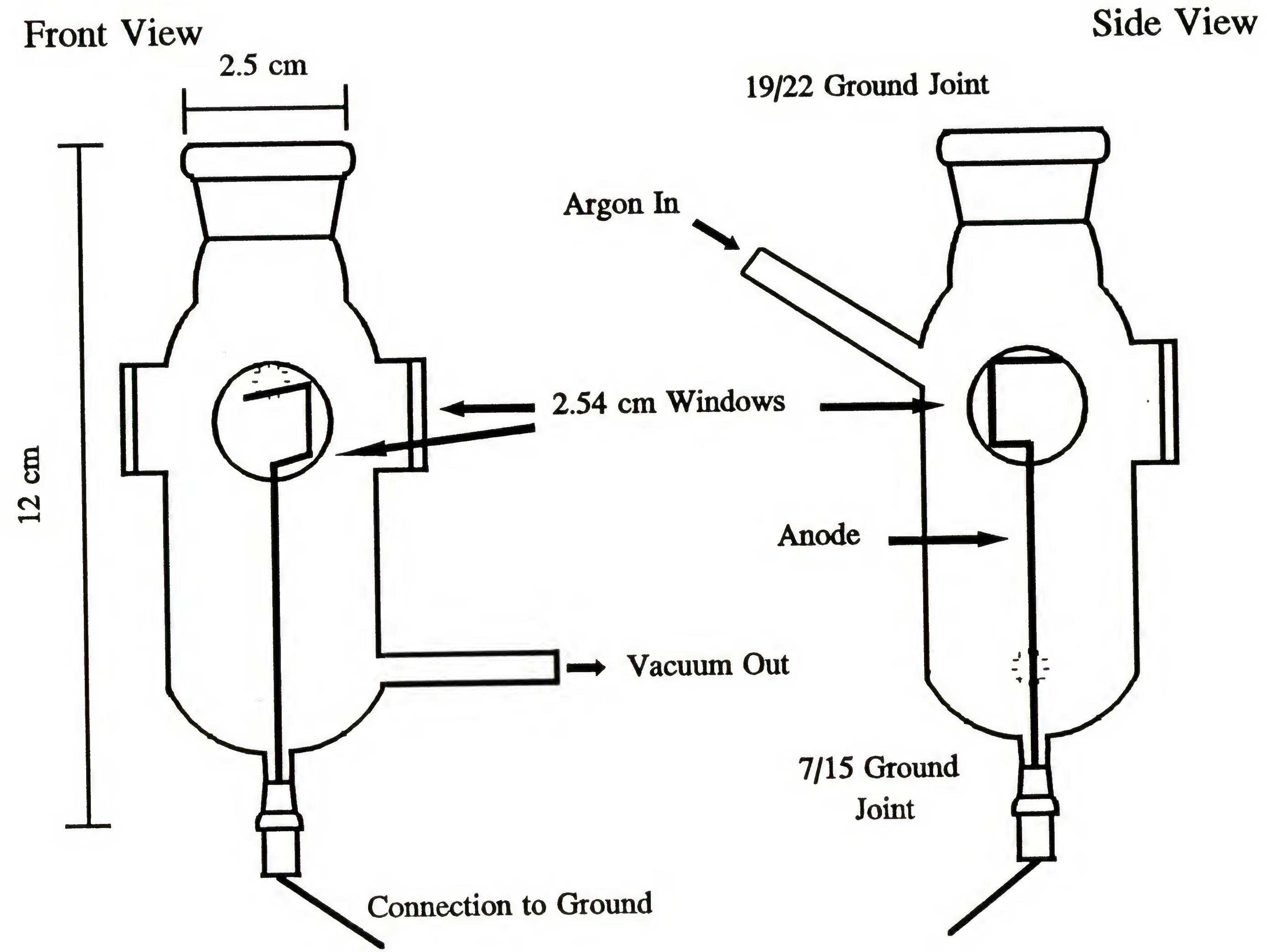

Figure 4-1. Schematic design of the quartz glow discharge chamber.

connected to a flowing chilled water supply, was wound around the outside of the 19/22 outer taper joint neck in order to provide some external cooling to the cathode. The chamber was mounted on an x-y-z translational stage to allow for alignment.

Cathode Design

The cathodes were demountable to expedite the sample analysis procedure. The basic design of the cathodes is illustrated by Figure 4-2. The cathode itself consisted of a 1/4 in diameter by 1 in long metallic rod with a slight circular depression on the planar surface. This depression was found to increase the reproducibilty of sample deposition. The metallic rod was epoxied with vacuum epoxy into a machineable Macor ceramic sleeve. This sleeve insured that the discharge was confined to the front, planar surface of the cathode. The metallic rod with the ceramic sleeve was then epoxied into the 19/22 quartz inner taper joint. An electrical connection to the negative pole of a current controlled, high voltage power supply (105-05R, Bertan Associates, Hicksville, NY) was also added. A 20.5 kΩ ballast resistor in series with the power supply limited the power provided to the cathode. The cathodes proved to have a rather long lifetime. All of the work which employed the quartz chamber was performed with a single cathode which is still functioning.

Instrumental Layout and Spectrometric System

With the fabrication of the atom reservoir completed, the instrumentation for the excitation and detection of atomic fluorescence could be assembled. An illustration of the experimental set up is shown in Figure 4-3. The system basically consisted of four major components: the atom reservoir, which has been described, the laser excitation

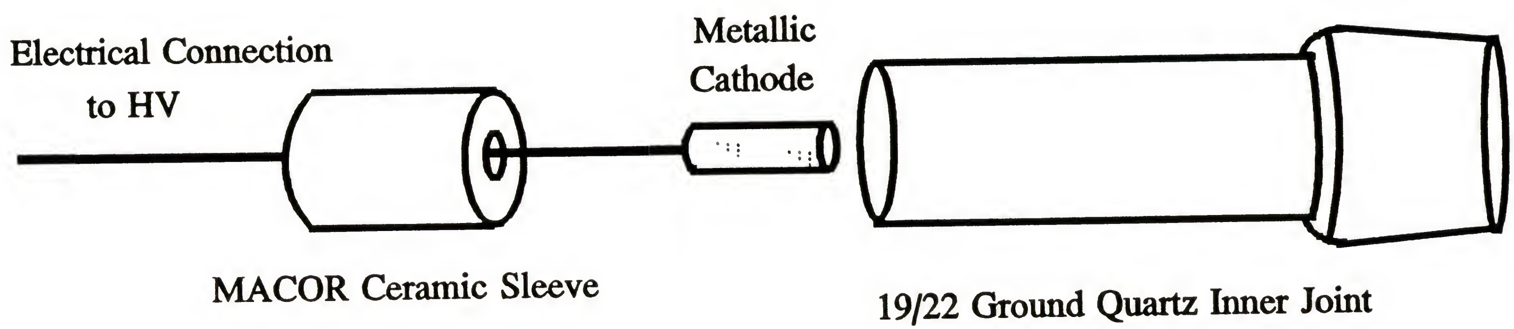

Figure 4-2. Exploded view of the demountable cathode.

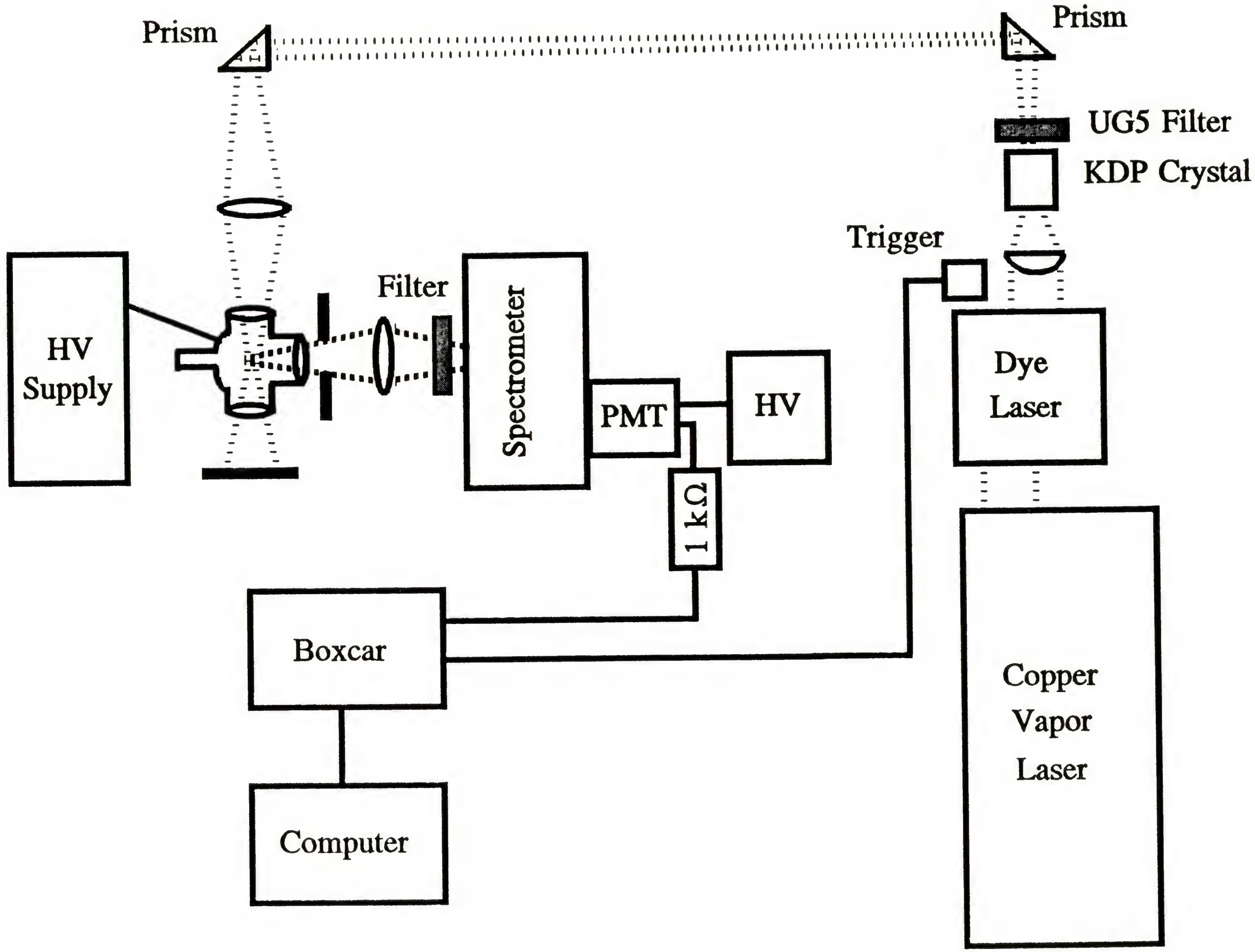

Figure 4-3. Instrumentation for GD-LEAFS.

source, the fluorescence collection system and the signal processing instrumentation. Each of the latter three will be examined.

Copper Vapor Laser Pumped Dye Laser Excitation Source

The CVL (CU-15A, Oxford Lasers, Ltd., Acton, MA) was a pulsed, compact, air-cooled laser which was equipped with an unstable resonator. The unstable resonator improved the output beam divergence which was 0.4 mrad. The laser operated simultaneously at two wavelengths, 510.6 nm and 578.2 nm, producing pulses 5-20 ns in duration with energies of several millijoules per pulse, at pulse repetition frequencies in the range of 9-13 kHz. The average power obtained was 20 W, and the overall, wall plug efficiency of the laser was approximately 1%.

The CVL was employed to pump a dye laser (DLII, Molectron Corp., Sunnyvale, CA). The energy from the CVL was sufficient to cause the flowing organic dye in the dye laser to fluoresce. The output wavelength of the dye laser could be varied from 530 nm to 850 nm through dye selection. This output was extended into the ultraviolet region by frequency doubling the fundamental output. This was achieved by focussing the dye laser beam with a 3 in focal length planoconvex lens into a nonlinear crystal (KDP-B, Model 562-126, Interactive Radiation Corp., Northvale, NJ). The resulting beam then passed through a colored filter (UG5, Corion Corp., Holliston, MA) which transmitted ultraviolet radiation. A 5 ns laser pulse with energy between 100 nJ and 4 μJ, depending on the dye utilized and the operating wavelength, was produced. Importantly, this energy was found to vary by as much as an order of magnitude from pulse to pulse. The frequency doubled beam was then directed toward the atom reservoir

by a series of prisms and was gently focussed by an 8 in focal length quartz biconvex lens.

There were certain unique advantages of the CVL pumped dye laser source. The high peak power of the CVL meant that the threshold for dye oscillation was easily achieved. This can be contrasted with continuous wave lasers which always operate close to threshold. Consequently, the CVL pumped dye laser was much easier to align and to optimize than comparable continuous wave laser systems; however, the most important benefit of this laser system was the high pulse repetition frequency. This was crucial in the transient signal applications presented in this dissertation. The high pulse rate translated into increased probings of the atom population per unit of time, which enabled sampling the analyte atom population as much as possible during the short time allowed. The transient nature of the fluorescence signals will be discussed in the following chapter.

Fluorescence Collection System

Fluorescence was collected at 90° from the beam path by a 3 in focal length quartz biconvex lens. This geometry was utilized in order to minimize laser scatter from reaching the monochromator. An iris diaphragm aperture was also employed for the same reason. The fluorescence was gently focussed onto the slit of the 0.25 m focal length monochromator (Minimate, Spex Industries, Inc., Edison, NJ) which had an f/# of 4 and a reciprocal linear dispersion of 40 Å/mm. A glass sharp cut filter (WG360, Corion Corp.) placed directly in front of the slit further reduced laser scatter.

Signal Detection and Processing System

An end-on type photomultiplier tube (Type R1547, Hamamatsu Systems, Waltham, MA) detected the fluorescence. The photomultiplier tube operated with an anode-to-cathode voltage of -1100 V supplied by a high voltage power supply (EU-42A, Heath, Acton, MA). The anode pulse was terminated into a 1000 Ω resistor. The resulting voltage pulse temporal profile had approximately a 200 ns full width at half maximum (FWHM).

The voltage pulse was sent to a boxcar integrator and gated detector (SR 250, Stanford Research Systems, Palo Alto, CA) which was set to average one thousand laser shots with a gate width of 209 ns and no delay. An analog processor (SR 225, Stanford Research Systems) provided an additional gain of a factor of ten.

The data from the boxcar was sent to a microcomputer (Northgate Computer Systems, Inc., Plymouth, MN) for processing and storage using the Stanford software supplied with the boxcar. The datum was transferred by an analog-to-digital computer interface (SR 245, Stanford Research Systems). This interface was triggered by the busy out signal from the boxcar, which is at the laser repetition rate; however, the interface was unable to transfer data faster than 1.2 kHz. A simple divider circuit was utilized to divide the trigger signal to the interface by a factor of one hundred.

With the system completely designed, the measurement of the model element, Pb, in aqueous solution residues was next to be performed. The results of this study were then to be compared with the results obtained for the determination of Pb by Deavor and co-workers (76).

CHAPTER 5
MEASUREMENT OF THE MODEL ELEMENT WITH THE QUARTZ GLOW DISCHARGE RESERVOIR AND LASER EXCITED ATOMIC FLUORESCENCE DETECTION

Introduction

The excitation and detection scheme for Pb is illustrated in Figure 5-1. This wavelength scheme is the one most frequently utilized for the atomic fluorescence detection of Pb partially due to the strength of the emission line at 405.8 nm. The considerable wavelength separation between the excitation and fluorescence wavelengths is also beneficial, allowing a cut off filter to be effectively used prior to the monochromator to minimize scattered radiation at 283.3 nm impinging upon the photomultiplier tube. Optical saturation was also achieved with this scheme due to the high energy of the dye laser at 283.3 nm, which was greater than 1 μJ per laser pulse. Glick *et al.* (69) had previously determined that optical saturation was achieved at a laser power of 1 μJ. As described in Chapter 2, this is a highly desirable situation because the fluorescence signal is then independent of the laser source power, giving the maximum fluorescence signal.

Experimental

Instrumentation

The instrumentation was fully described in Chapter 4. Rhodamine 6G laser dye (Exciton Corp., Dayton, OH) at the concentration of 0.46 g/L in methanol (Optima Grade, Fisher Scientific, Pittsburg, PA) was utilized in the dye laser.

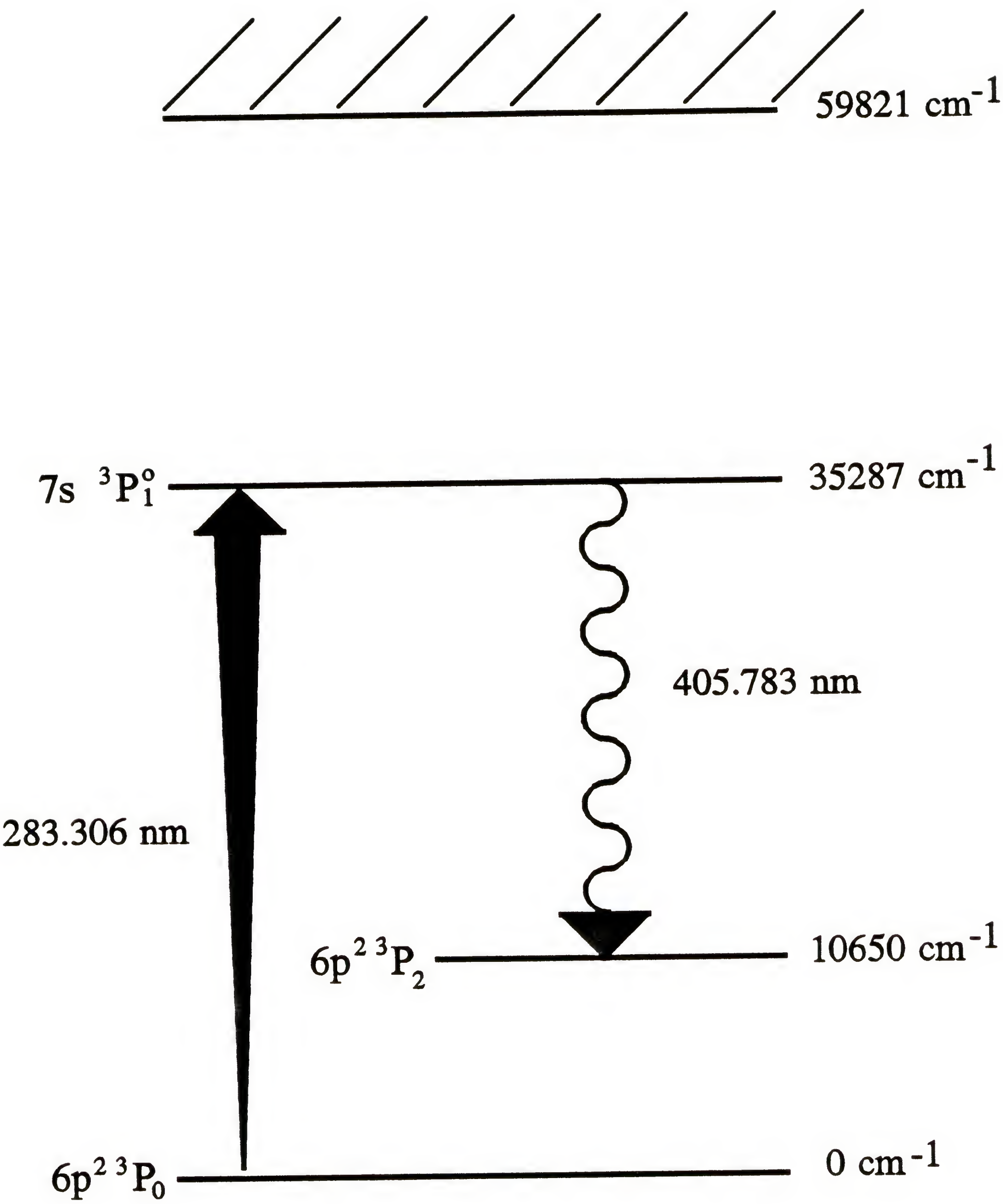

Figure 5-1. Partial Grotrian diagram for lead.

Sample Preparation

Solutions of various concentrations of Pb were prepared by serial dilution of a 1000 ppm research grade standard solution of lead nitrate in 1% nitric acid (HNO_3) (Fisher Scientific) with doubly deionized water. Volumetric flasks used in these preparations were thoroughly cleaned and soaked in a 50% solution of HNO_3 (Trace Metal Grade, Fisher Scientific).

Samples were deposited onto the cathode with a calibrated micropipet (Model P-2, Rainin Instrument Co., Inc.,Woburn, MA). Disposable, metal-free pipet tips were used throughout. The micropipet was calibrated to deliver volumes from 1 nL to 2 μL with precisions ranging from 14% for volumes below 50 nL to 0.3% for volumes above 500 nL. Volumes of either 400 or 500 nL were employed in this study.

Procedure

Samples were dried at atmospheric pressure under a moderate flow of dry nitrogen gas. The cathodes were inserted into the GD chamber, and the chamber was evacuated to a pressure of less than 50 millitorr. The chamber was next filled to atmospheric pressure with Ar and was once again evacuated. The pressure was set to the desired operating pressure with a needle valve. The GD was ignited through the use of a remote switch in series with the negative pole of the power supply and the cathode. The fluorescence signal was recorded and stored for future analysis with the Stanford software.

Both fluorescence peak height and peak area were measured for each sample. Peak heights were found to be more reproducible, with a relative standard deviation

(RSD) of approximately 10% for a series of twenty replicates. Peaks areas differed by 30% for this same data set; therefore, peaks heights were used for comparative purposes.

Optimization of the Operating Conditions

There were several operating parameters that needed to be optimized. These included the cathodic material, the monochromator slit width, the CVL pulse repetition rate, the cathode-to-anode distance, the laser sampling area, the pressure inside the discharge chamber and, finally, the current supplied to the cathode. Optimizations were performed by monitoring both the fluorescence signal peak and the noise corresponding to the standard deviation of a measurement of a blank, aqueous sample.

Cathodic material

Several cathodic materials were tested, namely graphite, Cu, Al, Mo, stainless steel and Ni. Initially, graphite was used because the cathodes were essentially disposable, eliminating any problems associated with memory effects; however, the graphite was extremely porous, resulting in a problem with sample recovery. Metallic cathodes were then studied, and of these Ni was found to be the most appropriate. High purity Ni (99.995%, Johnson Matthey, Ward Hill, MA) could be purchased that was free of Pb; purity had been a problem with Cu. Nickel also did not form the surface oxide layer as Al, Mo and stainless steel did which required frequent, time consuming cleaning. Importantly, Ni had few emission lines in the wavelength region of interest, and the memory effects associated with the Ni were less problematic. Figure 5-2 illustrates the difficulty encountered with memory effects. Run 0 represents the signal obtained from a 10 ng Pb residue deposited onto the Ni cathode. Immediately following

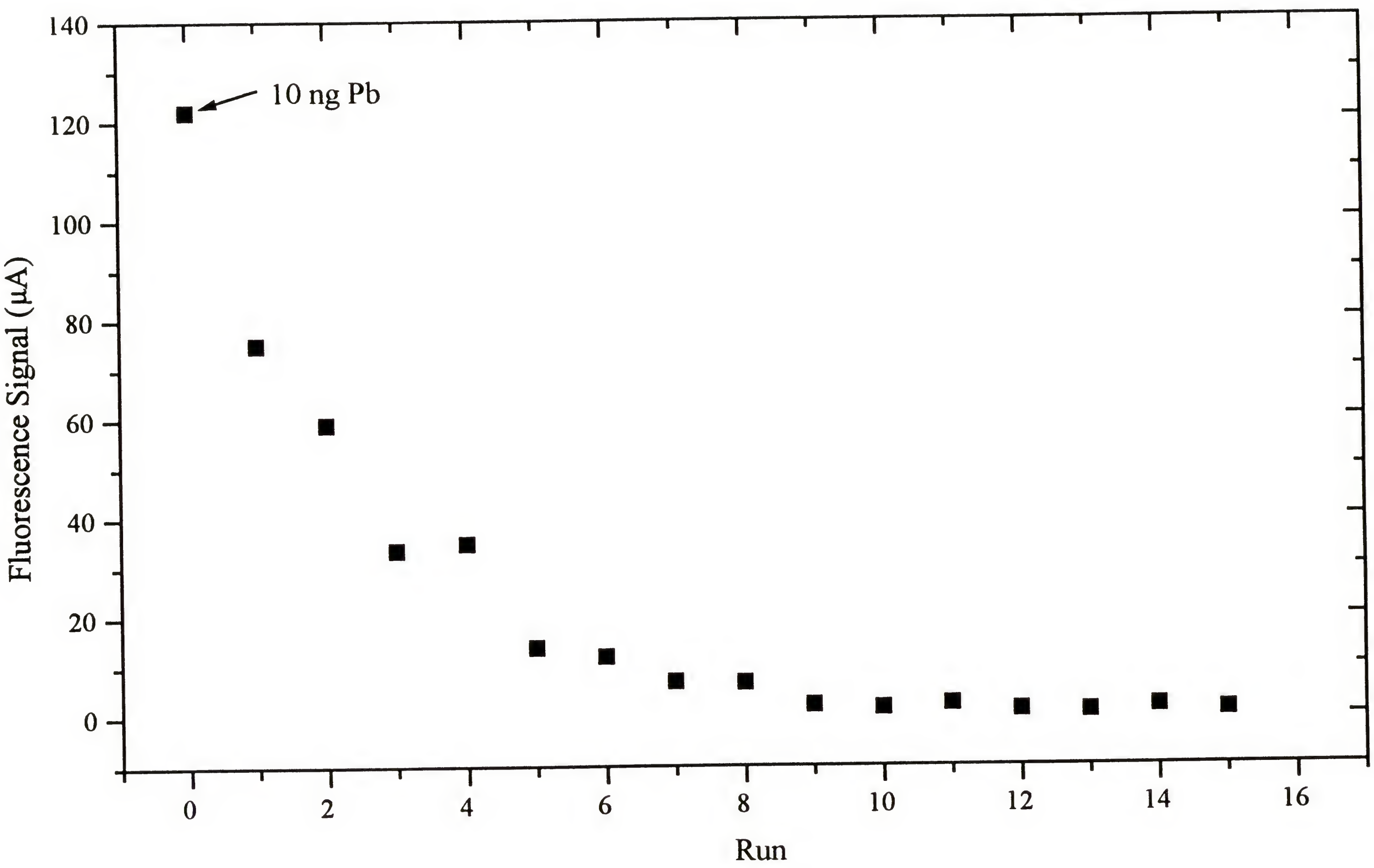

Figure 5-2. Memory effect associated with the nickel cathode.

that measurement, an equal volume of the blank was deposited onto the cathode and dried. A signal approximately 75% of the initial value was recorded (Run 2). This process of depositing and measuring blank samples was repeated fifteen times; at the end of which, the signal still remained above the baseline value. This memory effect, however, could be eliminated if the Ni cathodes were cleaned with concentrated HNO_3 (Optima Grade, Fisher Scientific) followed by rinsing with water after each run. The other cathodes were not as responsive to this simple, quick cleaning method.

Spectrometer slit width

Triplicate measurements of the fluorescence signals obtained for 500 nL samples of 500 ppm Pb were made at a pressure of 7 torr and a current of 20 mA, and the S/N was monitored. Slits widths of 0.25 mm, 1.25 mm, 2.5 mm and 5.0 mm were studied. The results are illustrated in Figure 5-3. Error bars represent one standard deviation. A slit width of 1.25 mm was determined to be ideal.

Laser pulse repetition rate

The effect of the CVL pulse repetition rate was also investigated. Samples of 500 nL of 590 ppb Pb were measured in triplicate at a pressure of 5 torr and at a current of 20 mA with the results being shown in Figure 5-4. Error bars again represent one standard deviation. It appeared that this parameter was not extremely critical within the limited range of variability, between 9 kHz and 13 kHz. A repetition rate of 10 kHz was chosen for all subsequent measurements.

Cathode-to-anode distance and the laser sampling area

Cathode-to-anode distances of 10 mm, 7 mm and 3 mm were investigated. Vertical profiles of fluorescence signal and noise were recorded with each spacing by

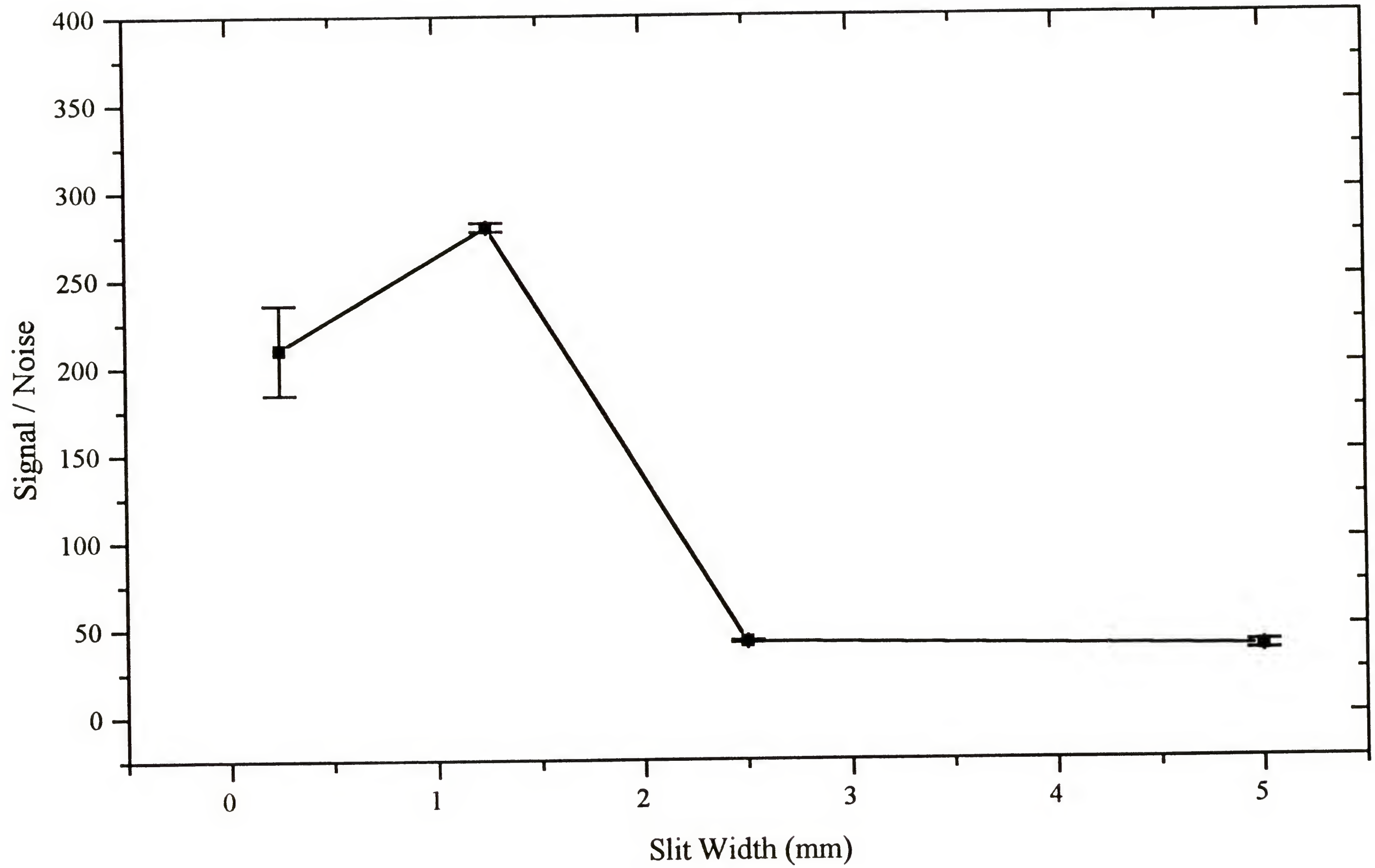

Figure 5-3. Optimization of the monochromator slit width.

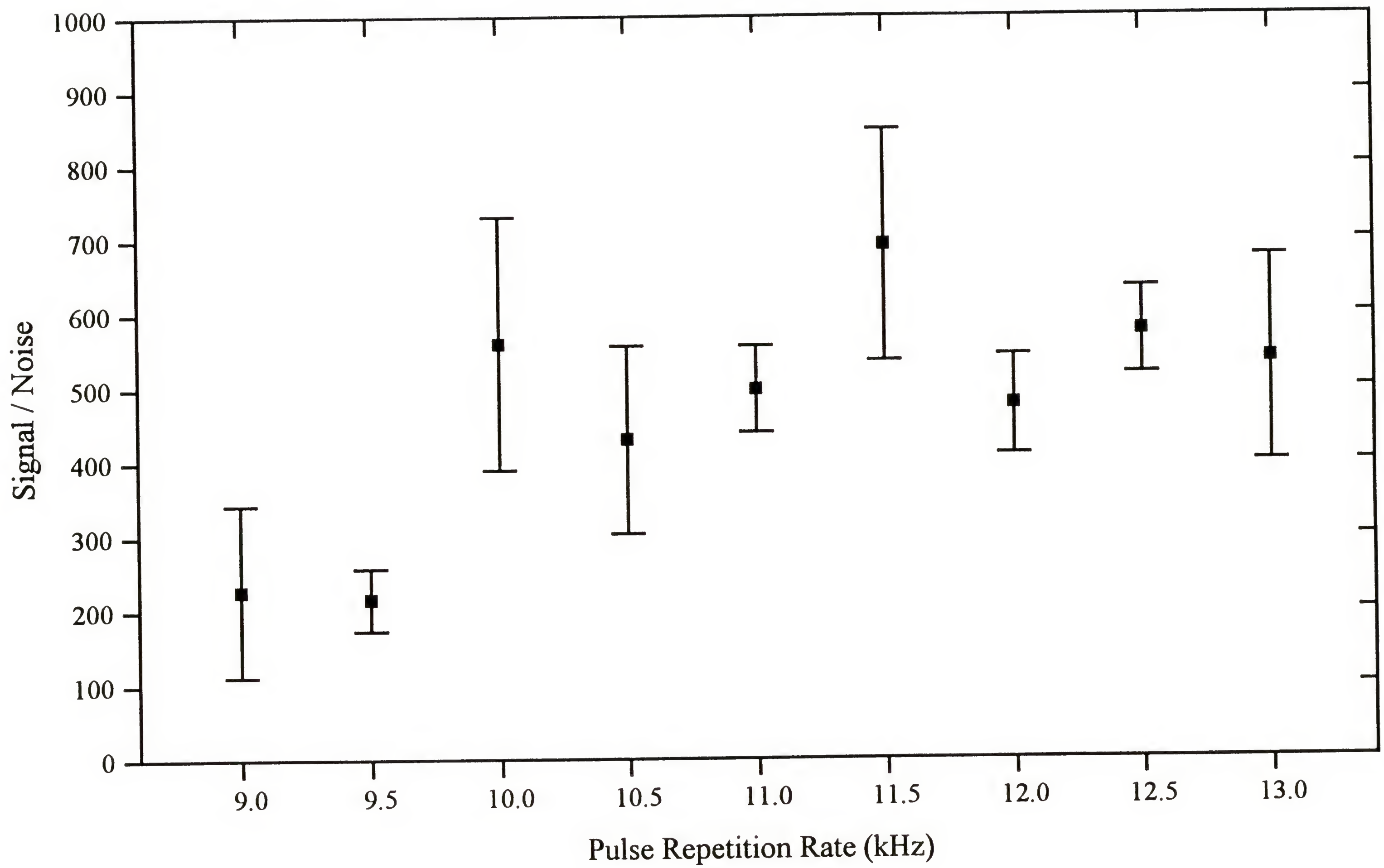

Figure 5-4. Effect of the CVL pulse repetition rate on the S/N.

varying the position of the laser beam relative to the surface of the cathode. Samples consisting of 5 ng of Pb were measured at 3 torr and 30 mA. The standard deviation of the background was utilized as a representation of the noise. These profiles are shown in Figures 5-5, 5-6 and 5-7. At 0 mm, the laser is essentially at the surface of the cathode. Both the Pb fluorescence signals and the associated noise are shown in each plot.

It can be seen in each plot that the highest fluorescence signals were obtained close to the cathode and that these signals slowly decayed. The noises reached a maximum near the cathode surface and often near the anode in the region of the bright anode glow. The best S/N ratios were obtained with the 3 mm cathode-to-anode distance at a laser beam position 10 mm from the cathode surface, corresponding to a position 7 mm below the anode wire. At this location, the signal was still significant while the noise had decreased to a much greater extent.

Pressure and current

Finally, the chamber pressure and the current supplied to the cathode were to be optimized. First, the pressure and current ranges for stable operation were determined. Stable plasmas were formed between 1 and 10 torr with currents up to 80 mA depending on the pressure. The optimum pressure and current were determined by varying the current in increments of 10 mA at a given pressure in the pressure range while monitoring either the fluorescence signal produced by a 5 ng Pb sample or the standard deviation associated with a blank measurement. The response surface obtained is

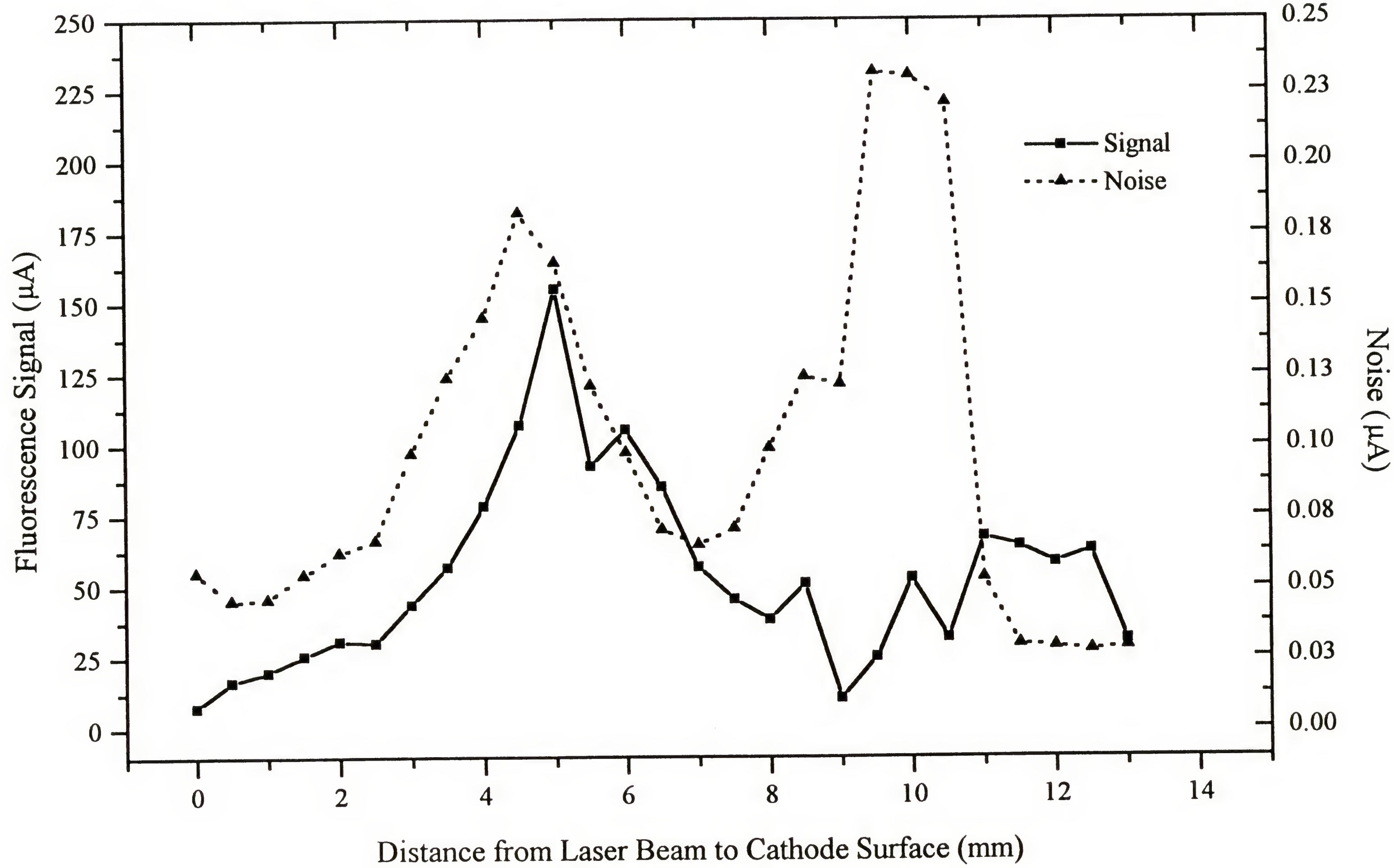

Figure 5-5. Vertical profile of the glow discharge obtained with a cathode-to-anode distance of 10 mm.

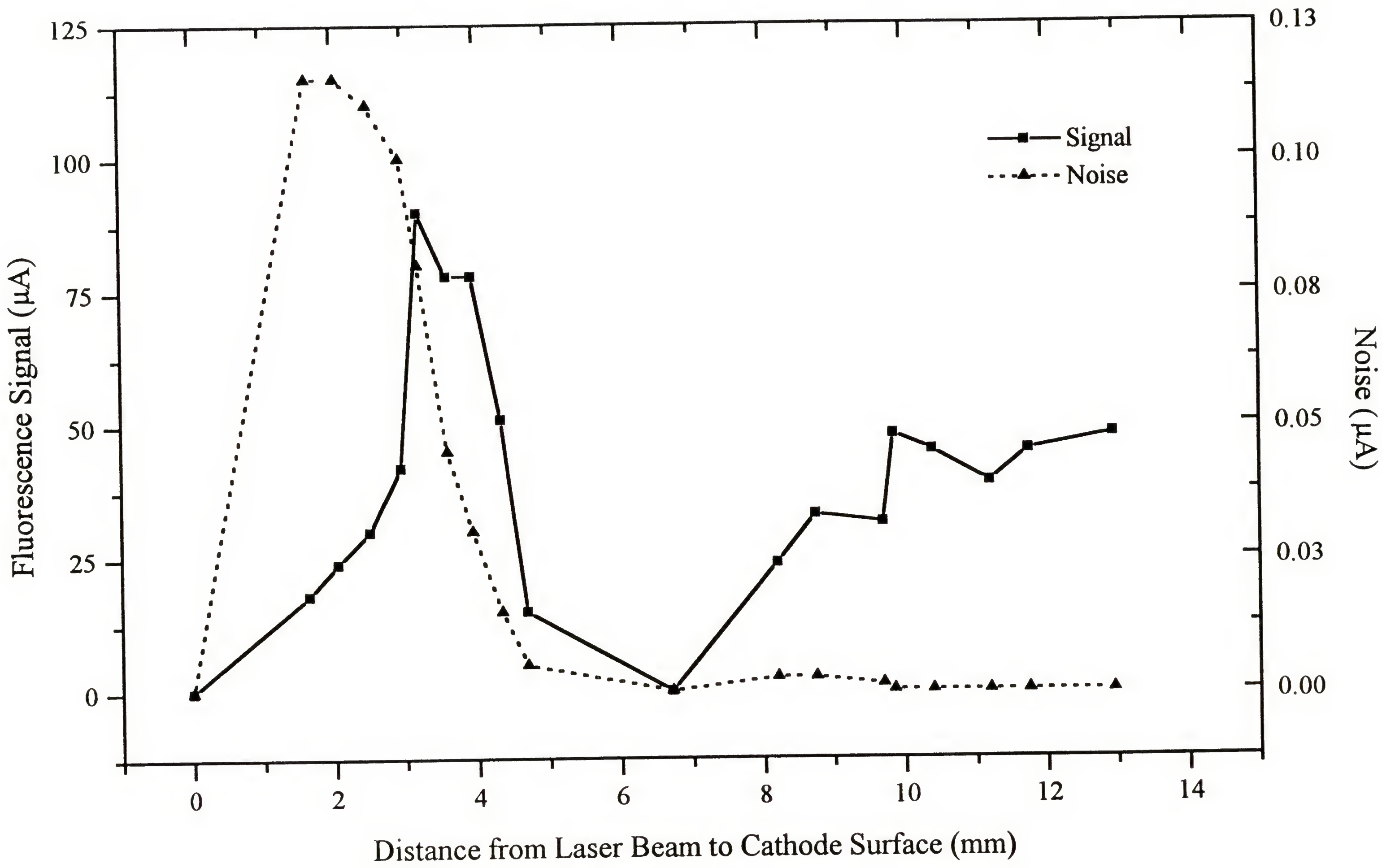

Figure 5-6. Vertical profile of the glow discharge obtained with a cathode-to-anode distance of 7 mm.

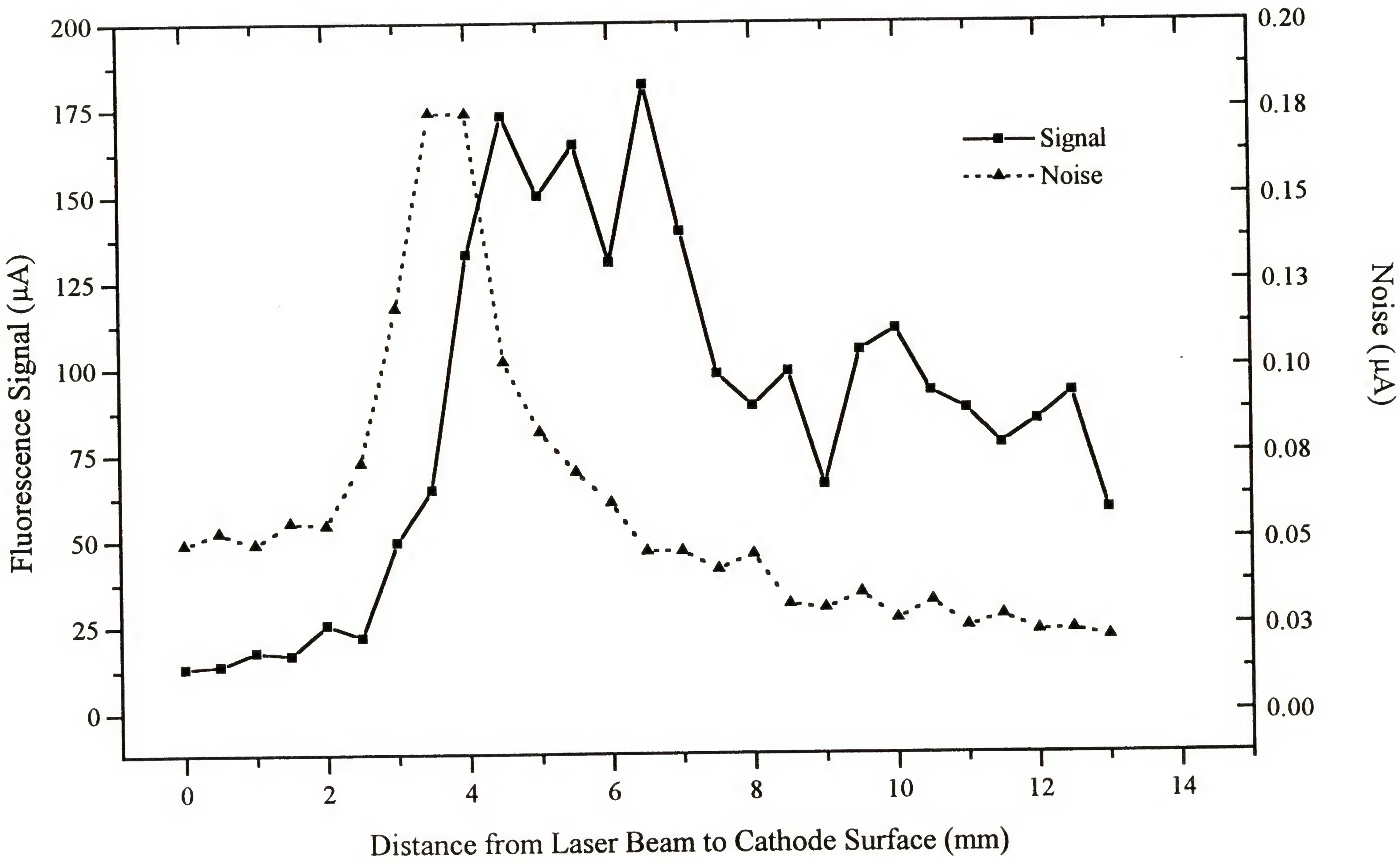

Figure 5-7. Vertical profile of the glow discharge obtained with a cathode-to-anode distance of 3 mm.

shown in Figure 5-8. All signal measurements were performed in triplicate; however, error bars were not added for clarity and simplicity in interpretation of the results. The highest S/N was found to occur at 4 torr and 20 mA.

A second response surface was then taken by varying the pressure near the ideal pressure in smaller increments. The S/N ratios at pressures of 3, 3.5, 4, 4.5 and 5 torr with currents up to 60 mA were monitored. This plot, as shown in Figure 5-9, does not indicate that there was a clear optima. The pressure did not seem to be a critical parameter as long as it was within $\pm$ 2 torr of the ideal value.

The current was optimized more carefully by varying it in 2.5 mA increments near the value of 20 mA. As illustrated in Figure 5-10, the S/N was not very sensitive to currents in the range of 15 to 25 mA. Error bars represent one standard deviation from a set of three measurements. Conditions of 4.5 torr and 20 mA were chosen for all other measurements.

Temporal Profiles

Accurate temporal profiles of the Pb fluorescence signal were obtained by recording the last out signal from the boxcar with no signal averaging. The profile of a 0.3 ng Pb solution residue is shown in Figure 5-11. This was recorded under the conditions found to be optimal. The signal was extremely fast with an exponential decay constant of 58 ms. It was desirable that the atomic population be sampled as often as possible during this short time period. The high pulse rate of the CVL was of particular importance in that respect. It was thought that the baseline did not return to the initial value due to redeposition of the analyte onto the cathode; however, the exact process

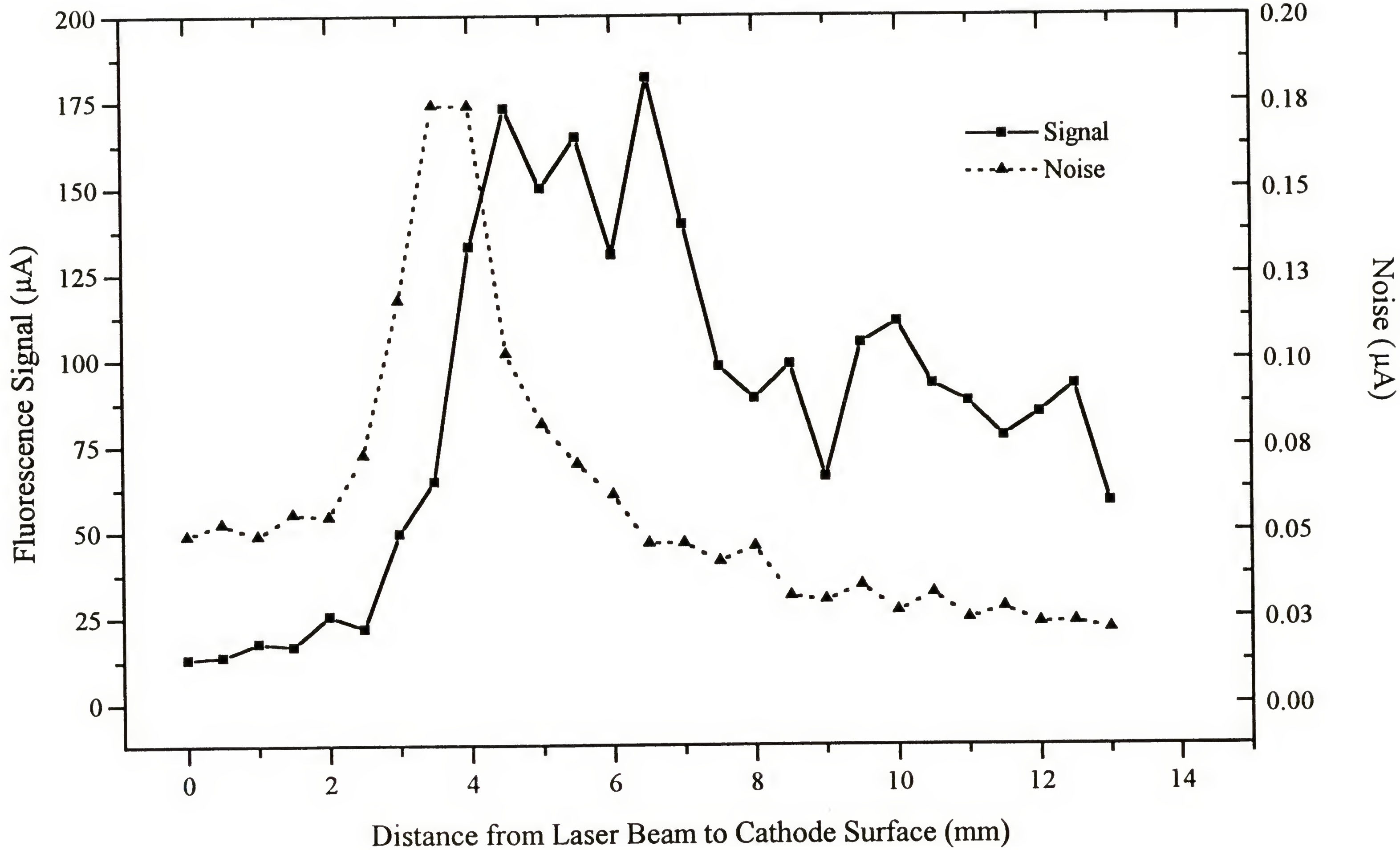

Figure 5-8. Entire response surface associated with the measurement of lead residues.

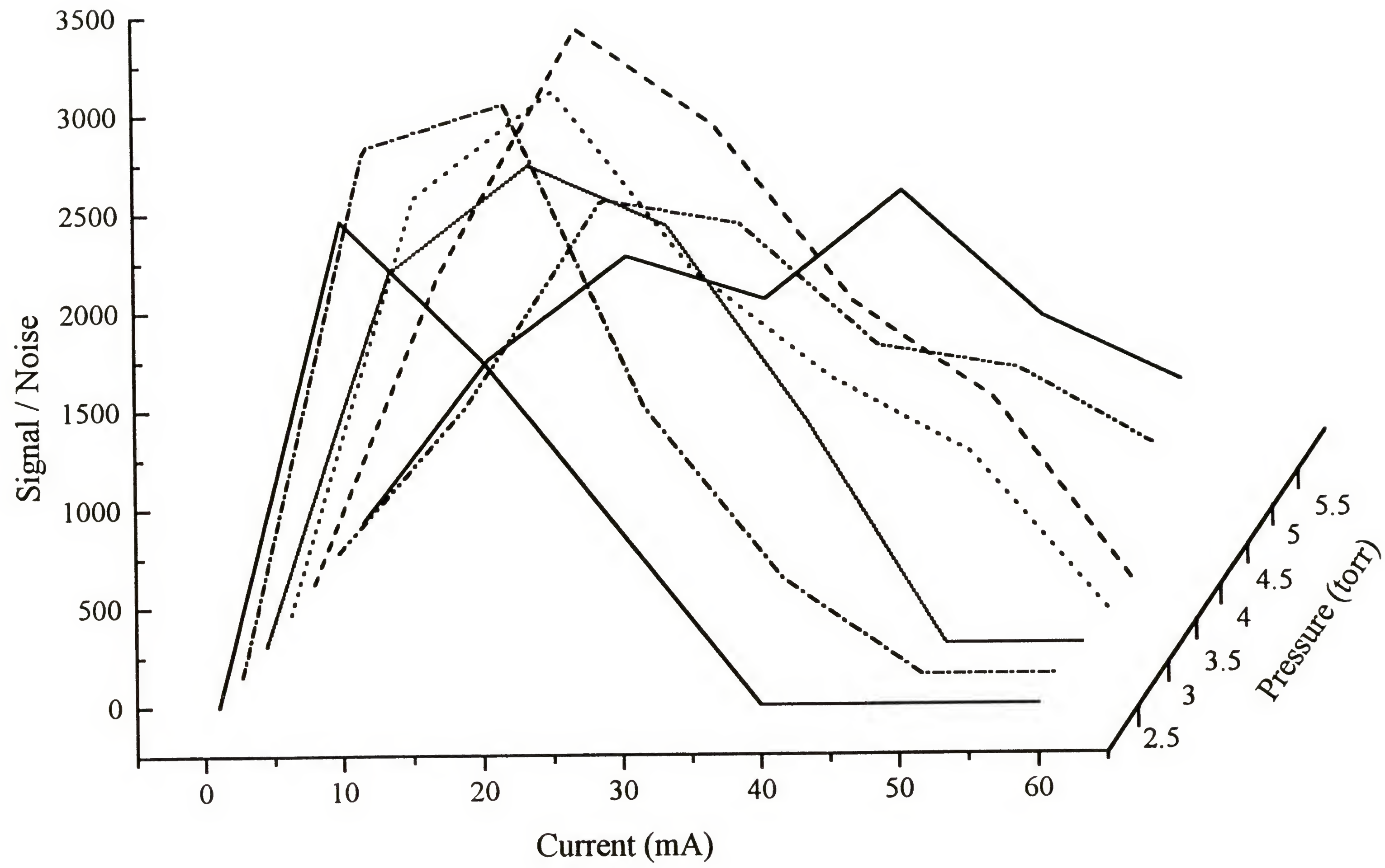

Figure 5-9. Lead response surface near the optimum pressure found in Figure 5-8.

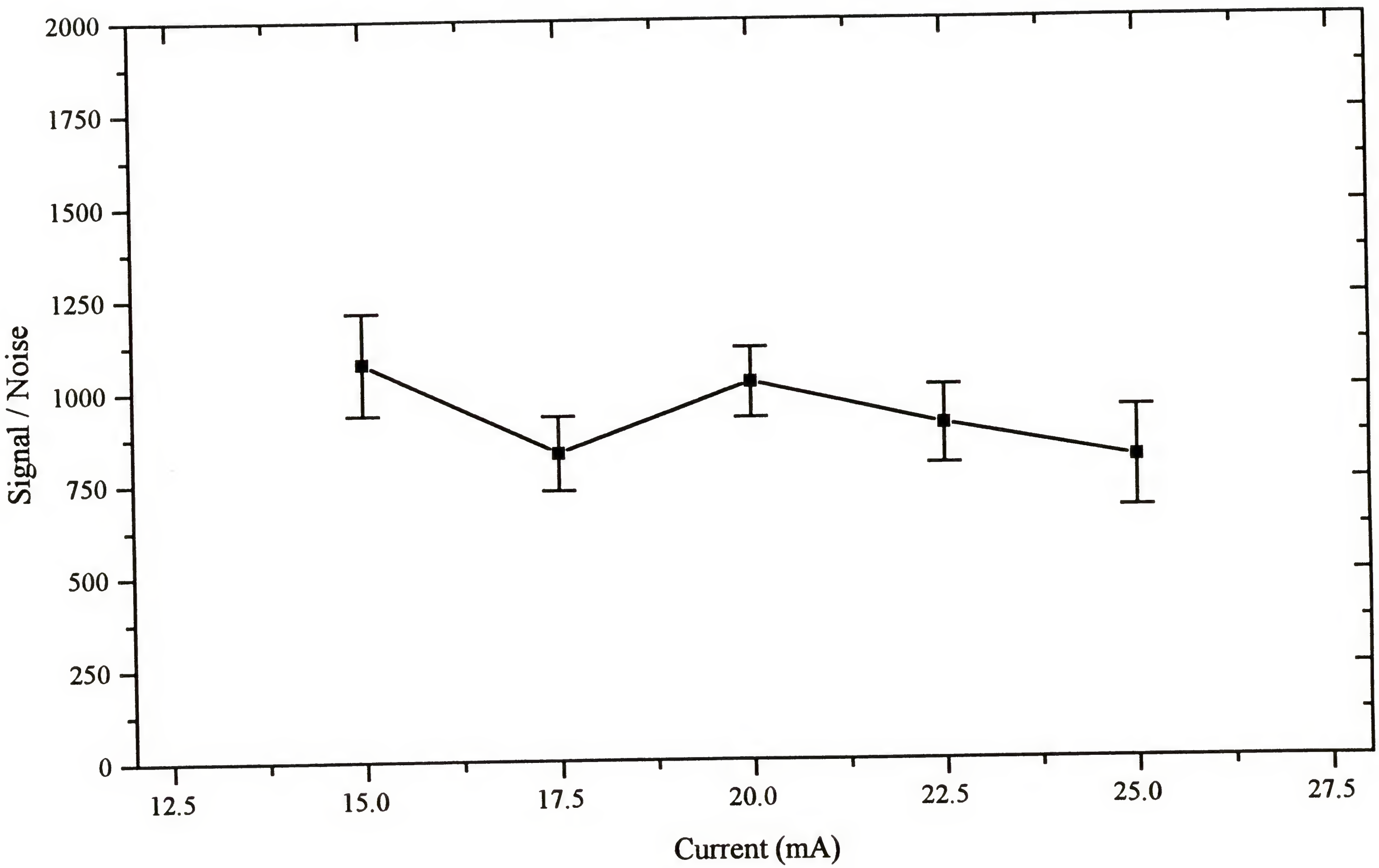

Figure 5-10. Current optimization for the measurement of lead at 4.5 torr.

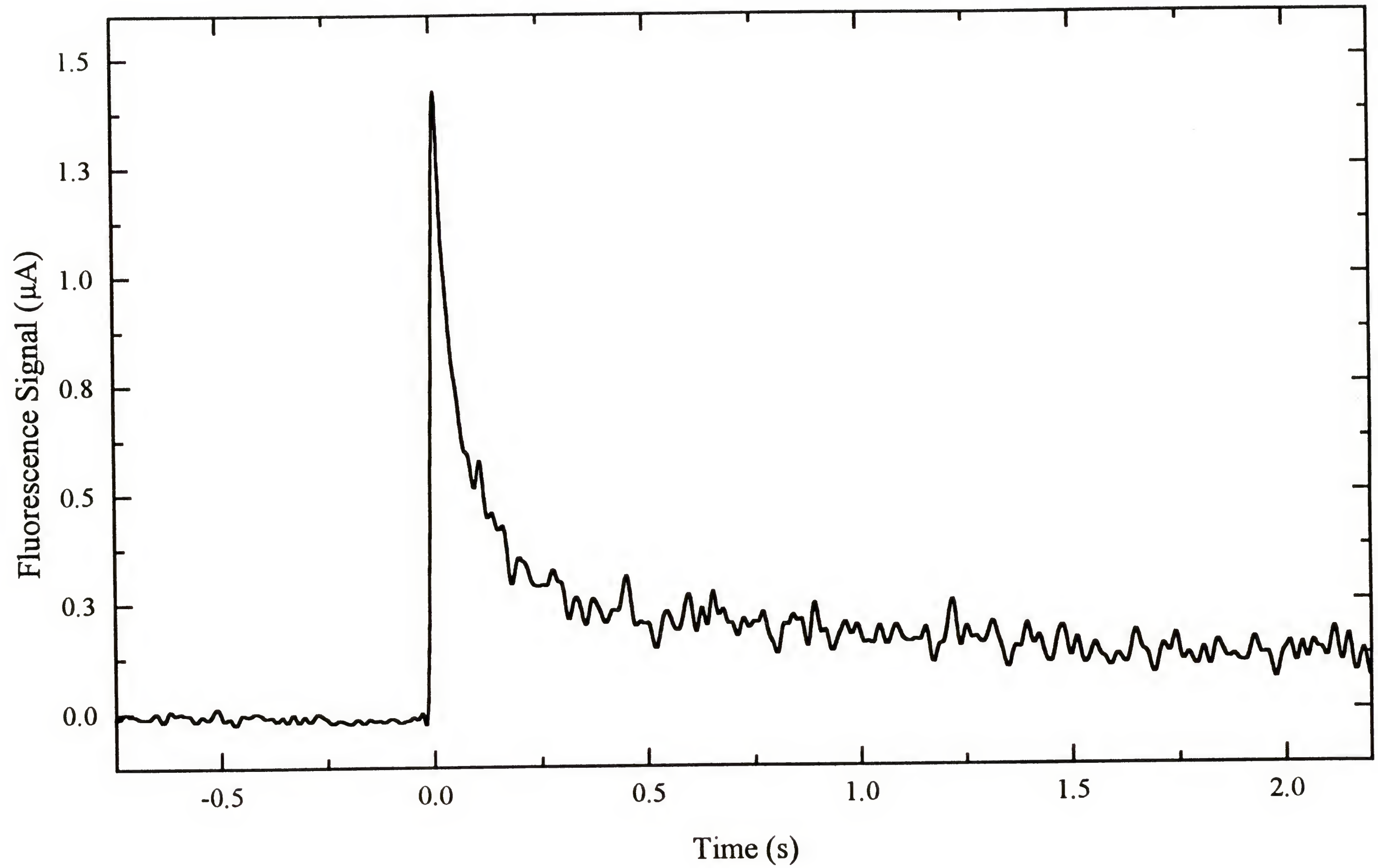

Figure 5-11. Temporal profile of a 0.3 ng lead solution residue.

which was occurring was not investigated further at that time. This redeposition theory will be discussed in a latter chapter.

Determination of the Figures of Merit

With all of the parameters optimized, a calibration curve was obtained for Pb solution residues (Figure 5-12). A Ni cathode was utilized with a 3 mm cathode-to-anode distance, the laser beam passed 10 mm below the surface of the cathode, and the pressure in the chamber was maintained at 4.5 torr. A current of 20 mA was supplied to the cathode, corresponding to a power of 7.5 W. The excitation beam had an energy of approximately 1 μJ which was sufficient to achieve optical saturation. Each measurement was performed in triplicate with error bars representing one standard deviation. Twenty blank measurements were also performed in order to obtain the standard deviation which served as a representation of the noise. Peak heights were employed as the means of comparison. The correlation coefficient obtained from the linear regression analysis was 0.99989; the data were linear over five orders of magnitude as testified by the slope of 1.090 obtained on the log-log plot depicted. The limit of detection based on 3σ was 0.6 pg, corresponding to a concentration detection limit of 1 ppb. The average RSD was 16%.

Peak heights were thought to be more reproducible than peak areas; however, at a much later date, the data shown in Figure 5-12 were analyzed with peak areas utilized as the form of comparison. Blank measurements were also necessarily interpreted based on areas. The analysis of the blank runs involved summing all of the data points, representing the voltage at a given time, taken during a 2 s time period.

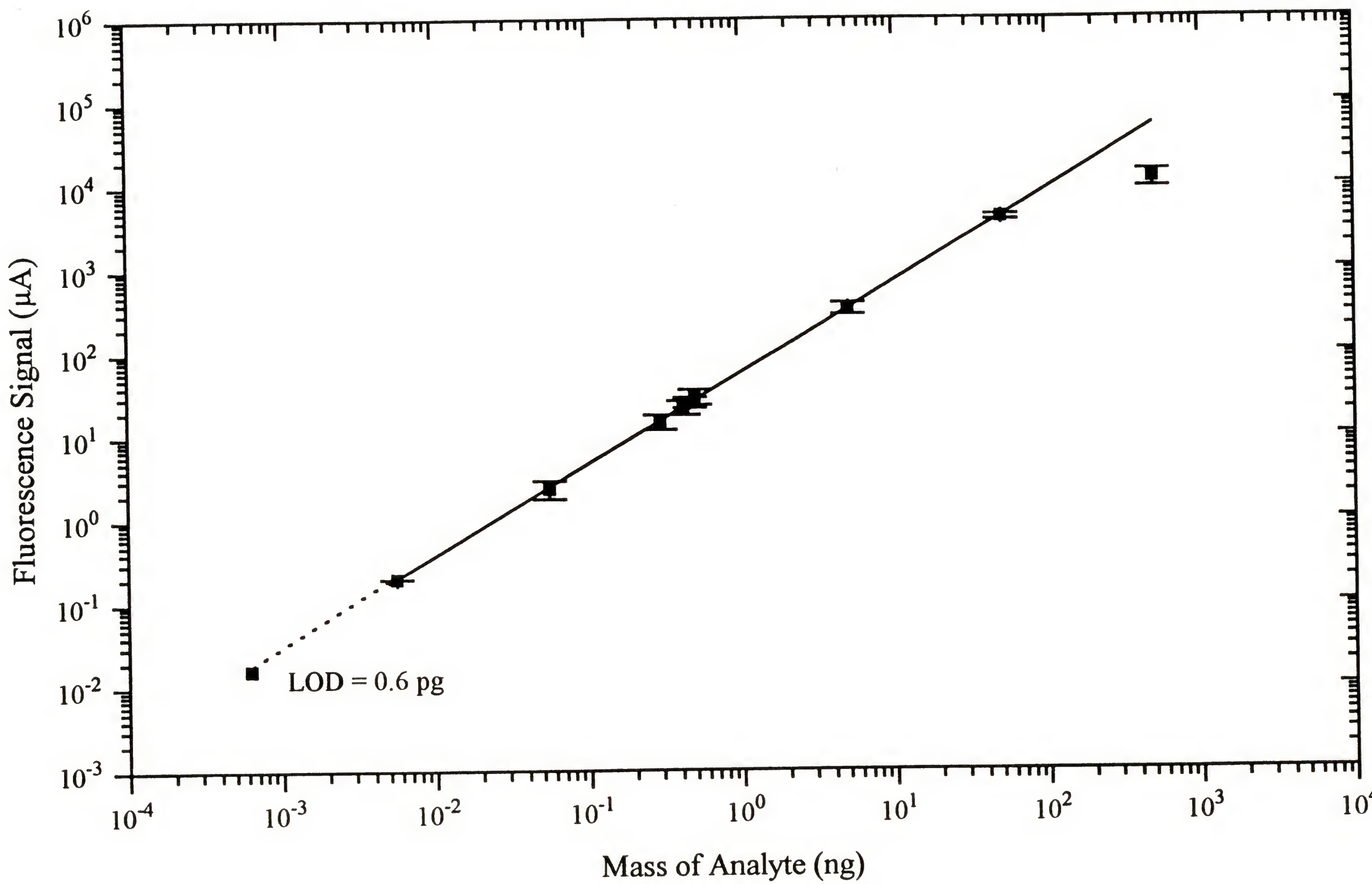

Figure 5-12. Calibration curve for lead solution residues.

It was thought that the majority of the signal would be contained in this time period. The sum of the voltages was then manipulated and set equal to zero. The area under the curves, which was equivalent to the sum of the voltages multiplied by the gate width of 209 ns, was recorded, and the standard deviation of the average area for the twenty blank samples was considered to be the representation of the noise. Analysis of peak area for the samples was much simpler. Data was gathered approximately 1 s prior to ignition of the GD. The sum of these points, accumulated during this time when the GD was off, was set to zero. The area under the curve for the 2 s duration following ignition of the plasma was recorded and served as the analytical signal. The calibration curve for the peak area measurements is shown in Figure 5-13. The correlation coefficient resulting from the linear regression was 0.99999, and the slope of the log-log plot was 1.058. The limit of detection based on 3σ was 2 fg. This detection limit required extrapolation over 3 orders of magnitude; unfortunately, at the time of data analysis, it was not feasible to repeat the experiment so that measurements closer to the theoretical detection limit could be taken. Peak area did seem to be a promising means of comparison although the average RSD, 28%, was somewhat higher than that recorded for peak height.

Results and Discussion

The detection limits compared favorably to that obtained by Deavor and co-workers (76) of 2 pg. It would seem that the reduced volume of the quartz GD was advantageous and did perhaps cause an increase in the atom density, minimizing dilution of the analyte.

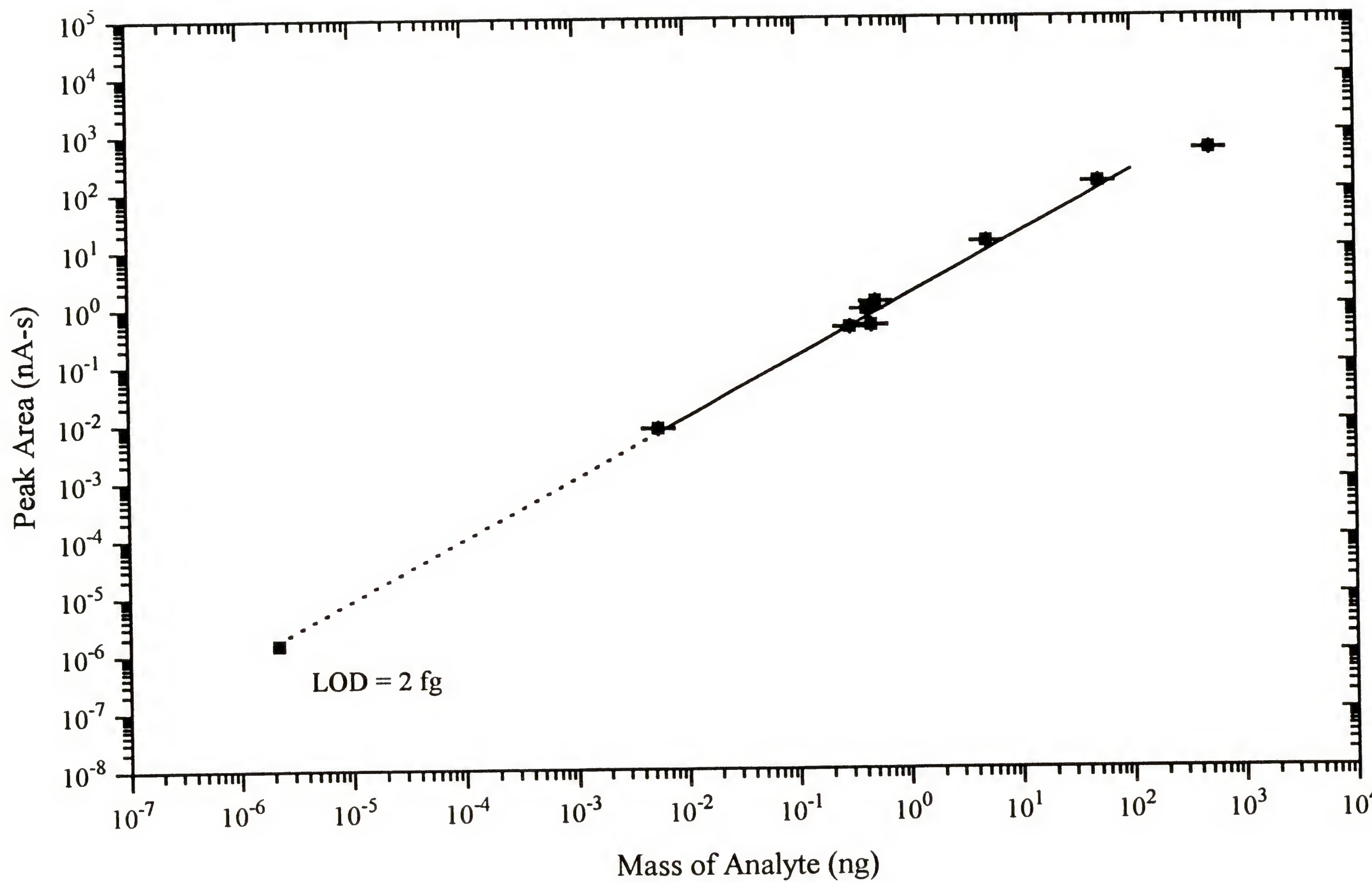

Figure 5-13. Calibration curve for lead solution residues based on peak area.

Gated Peak Integration Versus Peak Detection

Interestingly, the detection limit obtained using peak areas or gated peak integration with this system was several orders of magnitude better than that resulting from peak detection. There has been considerable debate in the literature as to which is the better method (77-83). Sasaki *et al.* (77) noted that replicate maximum peak amplitude measurements must result in maximum S/N for a Gaussian peak; however, Synovec and Yeung (78) and Williams (79) obtained maximum S/N utilizing peak integration techniques. Voigtman (84) has shown, through a series of theoretical calculations of S/N and through a simple computer simulation, that peak detection of a Gaussian peak in white noise works well only at high input S/N. There was a threshold input S/N below which the peak detector performance was seriously degraded, and as a result, the S/N was arbitrarily poor.

In the Voigtman computer simulation model, a unit amplitude Gaussian peak was generated by an impulse generator. It was then summed with Gaussian-distributed white noise to produce a typical signal waveform. This signal was processed by a series of integrating circuits which performed gated peak integration utilizing various gate widths and peak detection, which was treated as peak integration with an infinitely narrow gate width. The S/N results of this simulation and the theoretical values are compared in Table 5-1. Based on these results, peak area measurements should yield an improved S/N for a Gaussian peak.

The experimental results for Pb showed a more dramatic improvement in the S/N than was expected considering the work of Voigtman (84). The experimental conditions

Table 5-1. Comparison of theoretical and simulated S/N results from (84).

Method	Gate Width	Theoretical	Simulated
Gated Integration	$\pm\ 1.40\sigma$	0.9435	0.952
	$\pm\ 2.50\sigma$	0.8316	0.810
	$\pm\ 0.10\sigma$	0.3354	0.329
Peak Detection	$\pm\ 0.10\sigma$	--------	0.284

did obviously deviate from those considered in the simulation. The Pb signals were not Gaussian; the signals decayed slowly and exponentially over time. The noise was also not purely white noise, for flicker noise was a substantial component. The large improvement in the detection limit, however, was likely linked to the redeposition and resputtering of the analyte which was eluded to earlier. Statistically, the area under the curves representing the signals remained above the level recorded for the blank at concentrations where the peak height had long been lost in the fluctuations of the blank.

If only the area under the initial, fast peak of the profile was employed as the means of comparison, the improvement of the detection limit would have been more modest; however, when the "tail" of the profile was included, the lower limit of detection was obtained. By measuring just the peak height, much of the analytical signal was not considered, and a large amount of information was being neglected or overlooked, for the tail of the peak contained a significant amount of the total signal. The precise mechanism which produced this tailing was not yet identified, and this explanation was one of several theories proposed in an attempt to understand this phenomenon. A more detailed study of the tailing will be presented in Chapter 8.

Intrinsic Detection Limit

The experimental detection limits could also be compared with the calculated, intrinsic detection limit for Pb. Before an estimate of the intrinsic detection limit can be made, the efficiency of detection, ε_d^*, at the intrinsic noise limit must be determined. This efficiency can be defined as

$$\varepsilon_d^* = 1 - \exp\left[-gA_{ul}\Delta t_i \eta_{fl} \eta_d \eta_{el} p\right] \tag{5-1}$$

where ε_d^* is dimensionless, g is the saturation parameter relating the statistical weights of the upper and lower transitions (dimensionless), A_{ul} is the Einstein coefficient of spontaneous emission from level u to level l (s^{-1}), Δt_i is the interaction time or the laser pulse width (s), η_{fl} is the fluorescence collection efficiency (dimensionless), η_d is the detection efficiency of the photons reaching the photomultiplier tube (dimensionless), η_{el} is the efficiency of electronics or the counts per photoelectron (dimensionless), and p is the number of laser pulses during the atom residence time (29).

The saturation parameter, g, can be expressed as

$$g = \left(\frac{g_u}{g_l + g_u}\right) \tag{5-2}.$$

Since g_u is equal to 3 and g_l is equal to 1, g has a value of 0.75.

The collection efficiency of the fluorescence can be written as

$$\eta_{fl} = \frac{WH\Omega_F T_0}{4\pi A_{fl}} \tag{5-3}$$

where W and H are the width and height of the monochromator entrance slit (cm), Ω_F is the solid angle of collected fluorescence (sr), T_0 is the transmittance of the optical

system (dimensionless), and A_{fl} is the total surface area of the fluorescence (cm^2). For this system, the width of the slit was 0.125 cm and the height was 1.9 cm. The transmittance of the optics was estimated to be 0.8, and the solid angle of fluorescence was determined to be 0.05 sr with the area of fluorescence approximately equal to 0.03 cm^2. The fluorescence collection efficiency, η_{fl}, was as a result found to be 0.03.

The detection efficiency, η_d, or the quantum efficiency of the photomultiplier tube at 405.8 nm was determined by equation (5-4) so that

$$\eta_d = \frac{hcS}{\lambda e} \tag{5-4}$$

where h is Planck's constant (J s), c is the speed of light (m s^{-1}), λ is the detection wavelength (m), e is the charge of an electron (C), and S is the sensitivity of the photomultiplier tube (A W^{-1}) which was specified to be 0.065625 A W^{-1} for this system. Substituting all values into equation (5-4), the photomultiplier tube detection efficiency was determined to be 0.2.

If the values calculated for g, η_{fl} and η_d are substituted into equation (5-1) with A_{ul} equal to 9 x 10^7 s^{-1}, Δt_i as 5 x 10^{-9} s, η_{el} considered to be 1, and p equal to the FWHM of the temporal profile of Pb, which was 0.06 s, multiplied by the laser pulse repetition rate of 10,000 s^{-1}, the detection efficiency, ε_d°, can be determined to be 0.6.

There were several assumptions made in order to arrive at this estimate of the detection efficiency (29). The laser was assumed to be broad band so that its spectral profile was larger than the absorption profile of the atoms in the GD, and it was assumed to have a rectangular temporal profile. Also, the laser transition was considered to be optically saturated during the entire interaction time.

With the detection efficiency at the intrinsic noise limit, $\varepsilon_d°$, determined, the intrinsic limit of detection, N_L, as defined by Alkemade (27, 28) could be calculated with

$$N_L = \frac{k^2}{\varepsilon_d^{\circ}} \tag{5-5}$$

where N_L is the number of atoms, and k is the statistical confidence level of 3. The intrinsic detection limit was found to be 15 atoms.

Limiting Noises

The experimental detection limits of 1.8 x 10^9 atoms for peak heights and 6.4 x 10^6 atoms for peak areas are far from the calculated limit. The limiting source of noise in the case of the analysis involving peak heights was found to be background emission from the blank Ni cathode. The noise sources associated with the measurement of Pb are illustrated in Figure 5-14. These measurements were obtained by first blocking the slit of the monochromator, then opening the slit while allowing the laser beam at 283.3 nm to pass through the chamber, and finally, igniting the GD with a blank Ni cathode in place. The emission noise was reduced considerably due to sampling below the anode, at some distance from the surface of the cathode. It may be possible to reduce the noise further through pulsing of the discharge. Pulsed discharges, as mentioned in Chapter 3, have been employed by several researchers.

In the case of the peak area analysis, it was thought that the detection limit would be blank limited. It would be extremely difficult to find blanks that contained less than 1 fg of Pb. The detection limit obtained is again only hypothetical due to the large range of extrapolation.

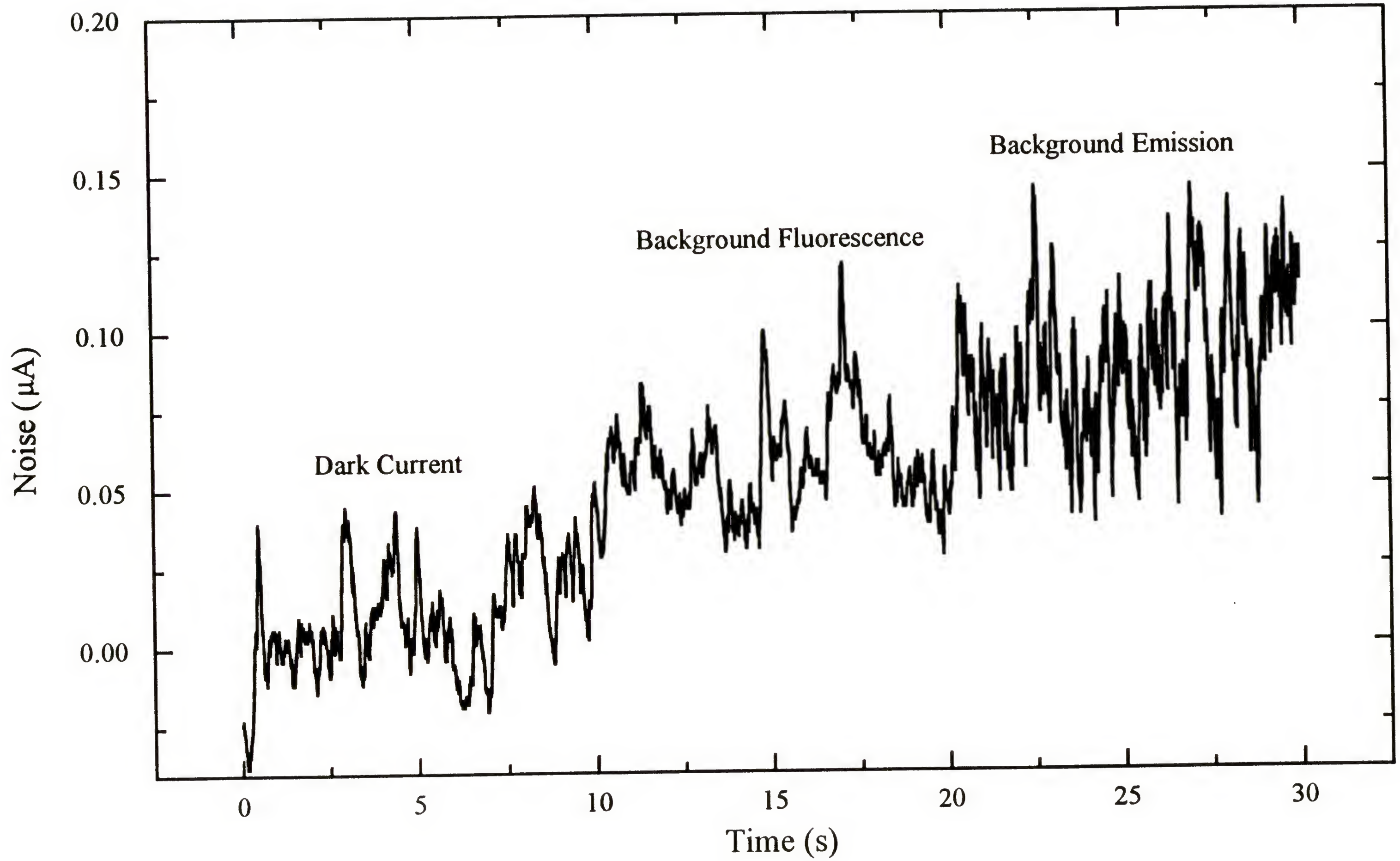

Figure 5-14. Noises associated with the measurement of lead.

Future Work

In order to improve upon the experimental detection limits, the dilution of the analyte could be reduced further. A GD chamber with a smaller total volume than the quartz chamber was to be constructed. The design of a miniature GD with a total volume of 1.5 mL was next undertaken and is presented in the following chapter.

CHAPTER 6
DESIGN OF THE MINIATURE GLOW DISCHARGE ATOM RESERVOIR AND THE INSTRUMENTAL LAYOUT FOR THE MEASUREMENT OF LASER EXCITED ATOMIC FLUORESCENCE

Chamber Design

The goals of the design strategy were identical to those mentioned in Chapter 4 with the exception that the total volume of the chamber was to be reduced. Several designs were initially investigated. Immediately, quartz was found to be unsuitable as a fabrication material, for it produced broadband fluorescence near 400 nm when exposed to the laser radiation at 283.3 nm. This background fluorescence proved to be a considerable problem. In order to circumvent this, stainless steel was chosen as the construction material, and a 7/15 outer taper joint, much like the 19/22 taper joint employed by the quartz chamber, facilitated fast and simple cathode exchange. A schematic of the chamber is shown in Figure 6-1 with the dimensions of the reservoir indicated.

The chamber was constructed almost entirely of steel and had a total volume of 1.5 mL. Three quartz windows were added to allow for placement of the laser and collection of the resulting fluorescence at 90° from the beam path. The chamber itself was electrically grounded and served as the anode. It was not feasible to add a separate anode that would allow for sampling below the anode due to the small size of the chamber. The gas inlet and the vacuum port were located on the bottom of the chamber,

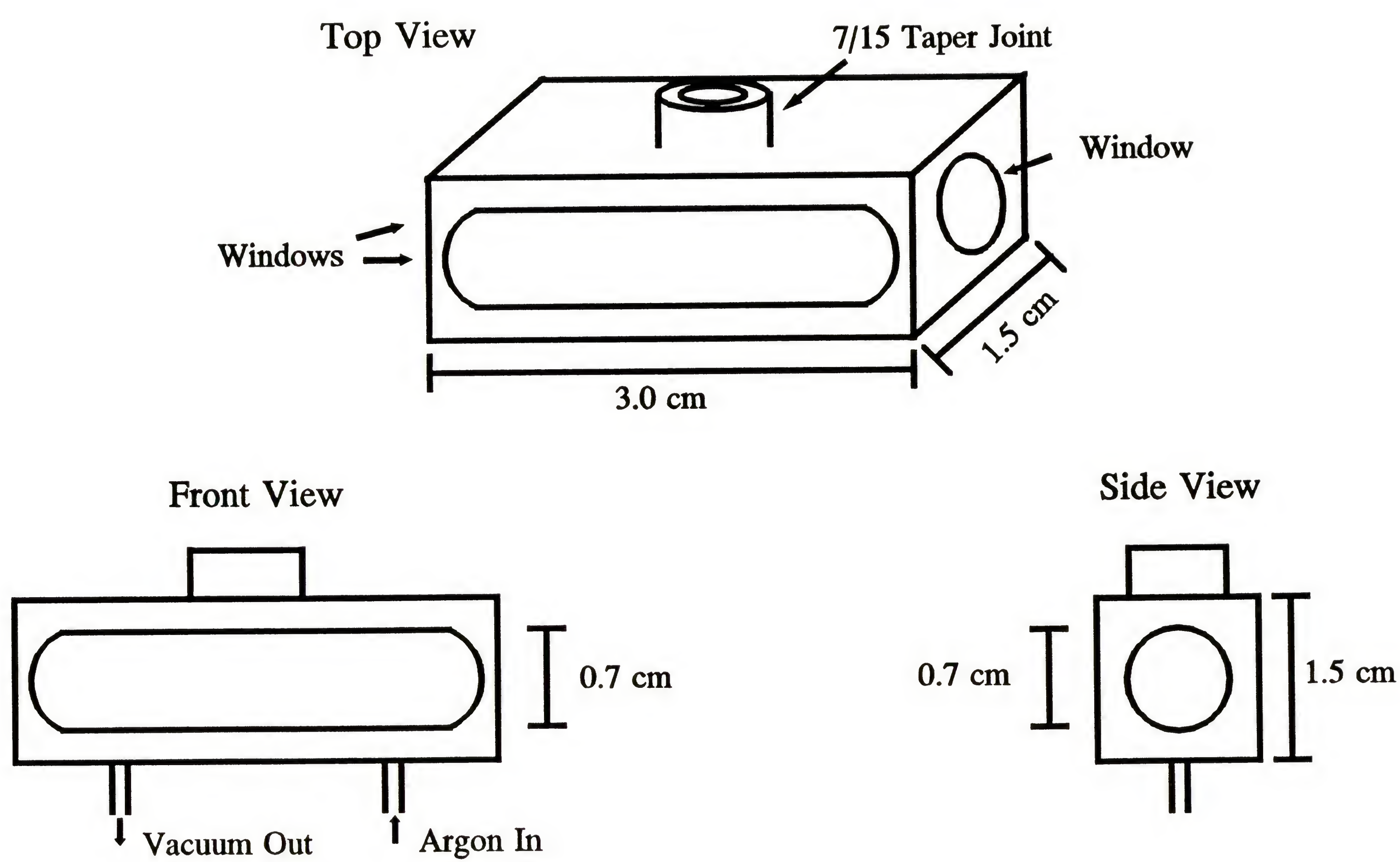

Figure 6-1. Schematic representation of the miniature glow discharge chamber.

and, unlike the gas introduction method utilized with the quartz chamber, the fill gas could be continuously introduced, or the system could operate under static conditions. Stop-flow operation was possible with the addition of two solenoid valves (ETO-3-12V, Clippard Instrument Laboratory, Inc., Cincinnati, OH) located as close as possible to the chamber at the gas inlet and vacuum port. These valves could be closed by the application of 12 V. The same remote switch, which ignited the discharge, was connected to a 12 V power supply and to the solenoid valves so that the valves were closed when the switch was closed. As a result, the chamber could be filled to the desired pressure with Ar, and at the time of ignition, the solenoid valves could be closed to theoretically prevent any loss of the analyte through the vacuum line during a measurement. Again, a dual stage rotary pump was used to achieve the desired pressure which was monitored by a capacitance manometer, and 1/8 in inner diameter Tygon tubing, which was connected to a flowing chilled water supply, was wound around the neck of the chamber to externally cool the cathodes. The chamber was also mounted on an x-y-z translational stage.

Cathode Design

The cathode design did not require much modification. Since a smaller outer taper joint was employed in the chamber construction, the cathode size was necessarily decreased. The design of the cathodes is illustrated in Figure 6-2. The cathodes consisted of a 3 mm diameter by 20 mm long Ni rod with a 2 mm diameter circular depression approximately 0.5 mm deep. The rods were epoxied into 7/15 quartz inner taper joints with vacuum epoxy. A Macor shield was not necessary since the rods tightly

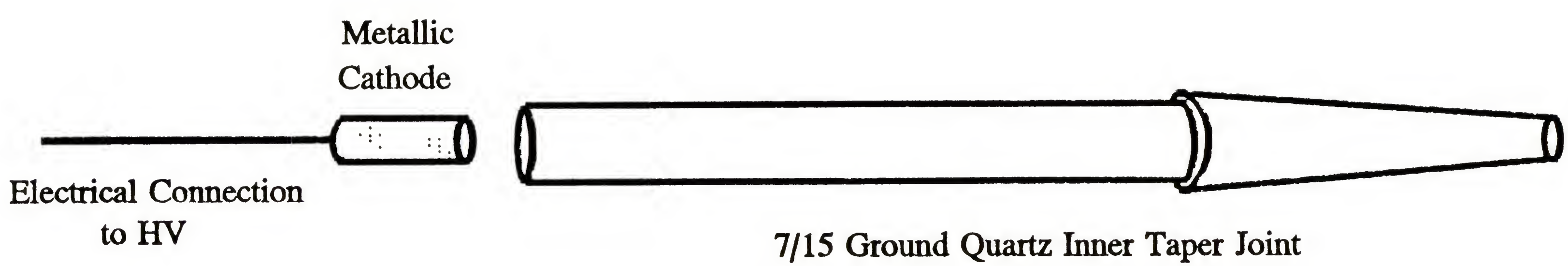

Figure 6-2. Exploded view of the cathode.

fitted into the taper joints. The Ni rods were connected to the negative pole of the high voltage power supply previously described in Chapter 4. A 20.5 kΩ ballast resistor in series with the cathode and power supply was again utilized.

Instrumental Layout and Spectrometric System

The experimental set up, as shown in Figure 6-3, is basically the same as that described in Chapter 4 with a few minor alterations. The CVL pumped dye laser served as the excitation source; however, a prism and focussable mirror were employed to direct the doubled beam toward the atom reservoir. An iris diaphragm was placed prior to the chamber in order to decrease the scattered radiation, and a mirror was added perpendicular to the beam path just after the chamber. This mirror reflected the laser beam back into the chamber, effectively doubling the probe volume when the reflected beam was positioned directly beside the original beam.

The signal detection and processing system was also modified slightly. The same end-on type photomultiplier tube was incorporated and operated at -1100 V; however, a laboratory constructed transimpedance amplifier, which was designed by D. Hueber, converted the current from the tube into a voltage with a gain of 1 x 10^4 V/A. The resulting voltage pulse was stretched to approximately 300 ns FWHM. A schematic of the circuit is shown in Figure 6-4. The voltage pulse was sent to the boxcar integrator and gated detector which was set to average a variable number of laser shots with a gate width of 272.5 ns and a delay of 17.5 ns. The analog processor provided an additional amplification of a factor of ten. The data was processed as described in Chapter 4 with the exception that the trigger signal to the interface was divided by a factor of ten so that data was collected at a rate of 1 kHz.

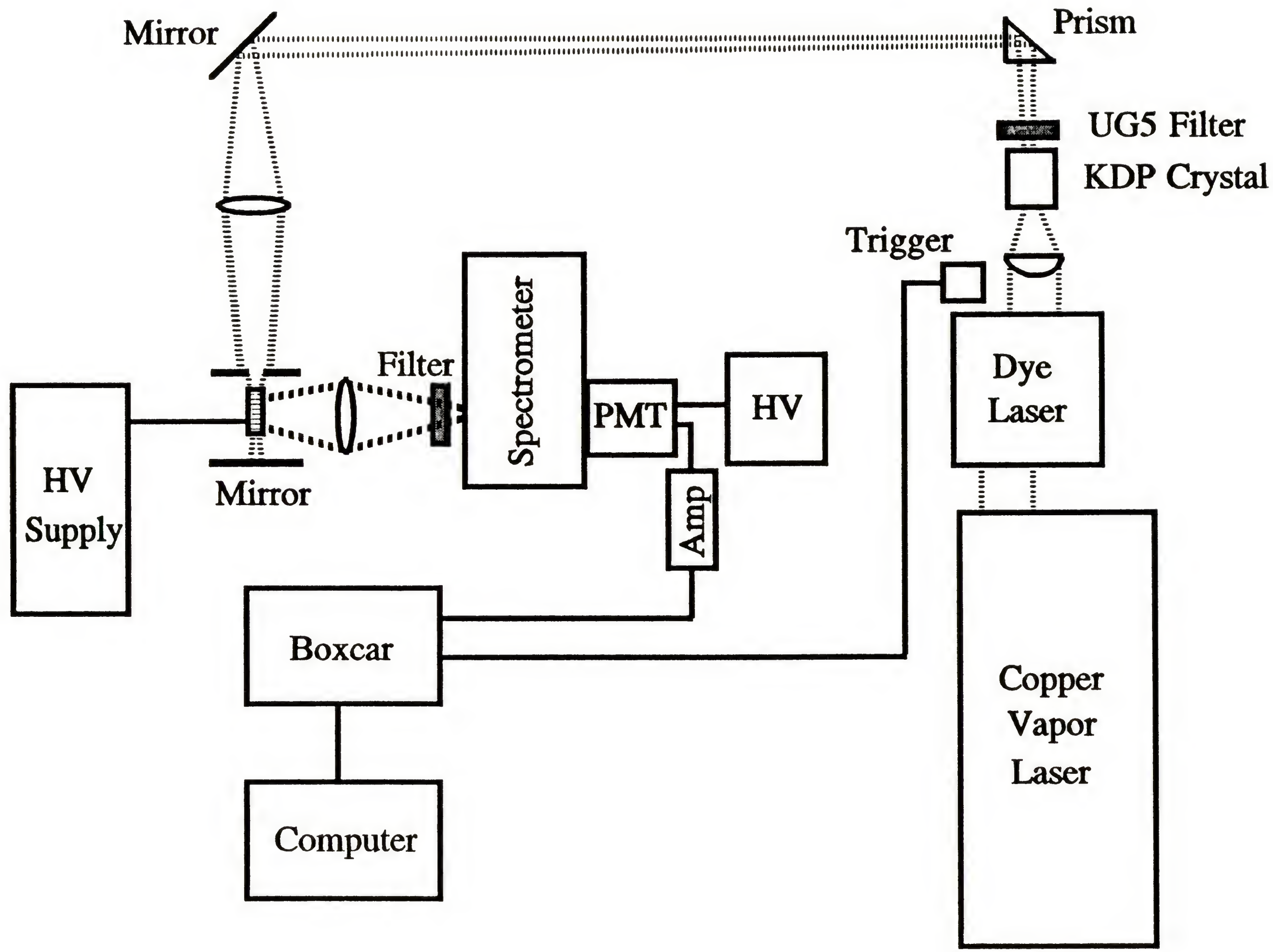

Figure 6-3. Instrumental set up for GD-LEAFS with the miniature reservoir.

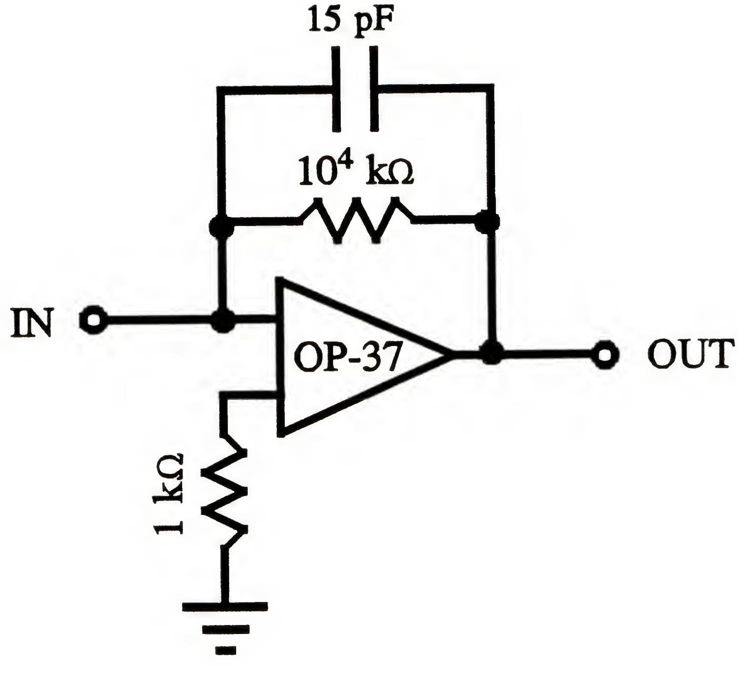

Figure 6-4. Schematic representation of the transimpedance amplifier.

Measurement of the model element, Pb, was next to be undertaken with this system. The results of this study were to be compared to those of Deavor and co-workers (76) as well as to the results obtained with the quartz chamber, for it was hoped that the atom density would be further increased in the miniature chamber, leading to a decrease in the limit of detection.

CHAPTER 7
MEASUREMENT OF THE MODEL ELEMENT WITH THE MINIATURE, STAINLESS STEEL GLOW DISCHARGE COUPLED WITH LASER EXCITED ATOMIC FLUORESCENCE DETECTION

Introduction

The same excitation and detection scheme presented in Chapter 5 for the measurement of Pb was used. Optical saturation of the 283.3 nm transition was achieved with a laser power of at least 1 μJ per pulse being recorded.

Experimental

Instrumentation

The instrumentation was described in Chapter 4 with any modifications being noted in Chapter 6. Rhodamine 6G laser dye at the concentration of 0.46 g/L in optima grade methanol was utilized by the dye laser.

Sample Preparation

The samples were prepared as described in Chapter 5.

Procedure

The procedure outlined in Chapter 5 was followed exactly for measurements under flowing conditions. The solenoid valves which facilitated stop-flow operation were connected to a 12 V power supply when in use; as stated earlier, these valves could be closed at the time of ignition. The chamber was, nevertheless, flushed with Ar and evacuated as described for the flowing system prior to measurement.

Optimization of the Operating Conditions

Because of the smaller, more restrictive size of the stainless steel chamber, there were fewer parameters to optimize. The laser sampling area and the cathode-to-anode distance were not truly variable, while the cathodic material had previously been optimized. The CVL pulse repetition rate had not been found to be critical in the earlier study; therefore, a pulse repetition rate of 10 kHz was once more used. The monochromator slit width as well as the chamber pressure and the current supplied to the cathode under both flowing and stop-flow operation could, however, be optimized. Peak detection was utilized for comparative purposes in order to minimize the time needed for signal processing and analysis.

Monochromator slit width

Triplicate measurements of the fluorescence signals obtained from 200 nL of 100 ppb Pb were made at a pressure of 6 torr and a current of 20 mA supplied to the Ni cathode. Slit widths of 0.25 mm, 0.5 mm, 1.25 mm, 2.5 mm and 5.0 mm were investigated with the S/N being monitored. The results are illustrated in Figure 7-1. Error bars represent one standard deviation. A slit width of 0.5 mm was found to be ideal; this slit width closely matched the diameter of the excitation beam passing through the GD.

Pressure and current

The chamber pressure and the cathodic current were optimized under both flowing and static conditions. The procedure outlined in Chapter 5 was followed. Measurement of signals arising from 200 nL of 100 ppb Pb were performed in triplicate. The entire

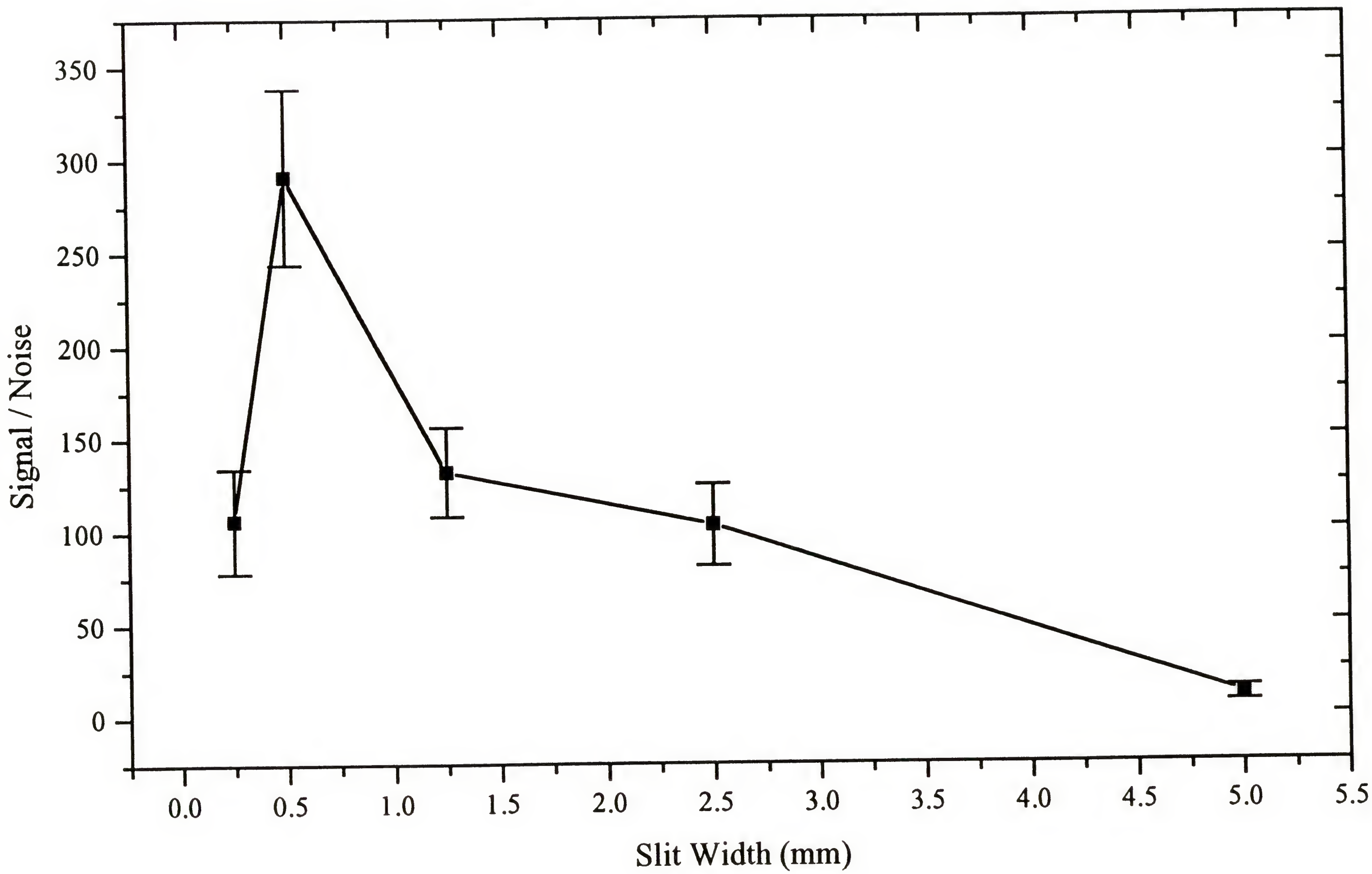

Figure 7-1. Optimization of the monochromator slit width.

response surface obtained with continuous Ar introduction is shown in Figure 7-2 with the results of the detailed look at the response surface and the more precise optimization of the current presented in Figures 7-3 and 7-4, respectively. A chamber pressure of 5.5 torr and a cathodic current of 20 mA appeared to be best. At this point, it was decided that both the detailed response surface and the detailed current optimization were not necessary. As stated in Chapter 5, the pressure did not appear to be critical as long as it was within a range of $\pm$ 2 torr of the ideal, and the current seemed to be even less sensitive.

Considering this, a single response surface was recorded for the system under static conditions, and this plot is shown in Figure 7-5. As can be deduced by the lower S/N measured with this configuration, no advantage was gained, and stop-flow operation was not investigated further. Although signals were enhanced with the static system, the noise level increased proportionally most likely due to fluctuations in the chamber pressure, which increased during stop-flow measurements. The taper joint was unable to maintain the chamber pressure when the chamber was disconnected from the vacuum system. The design of the chamber itself would need to be modified in order to eliminate this problem. Ideal conditions for the static system were found to be near 8 torr and 40 mA.

Temporal Profiles

Lead fluorescence temporal profiles were recorded under both static and flowing operation utilizing a gate width of 360 ns and a delay of 44.2 ns at the pressure and current found to be best. These profiles for a 0.03 ng Pb residue are depicted in

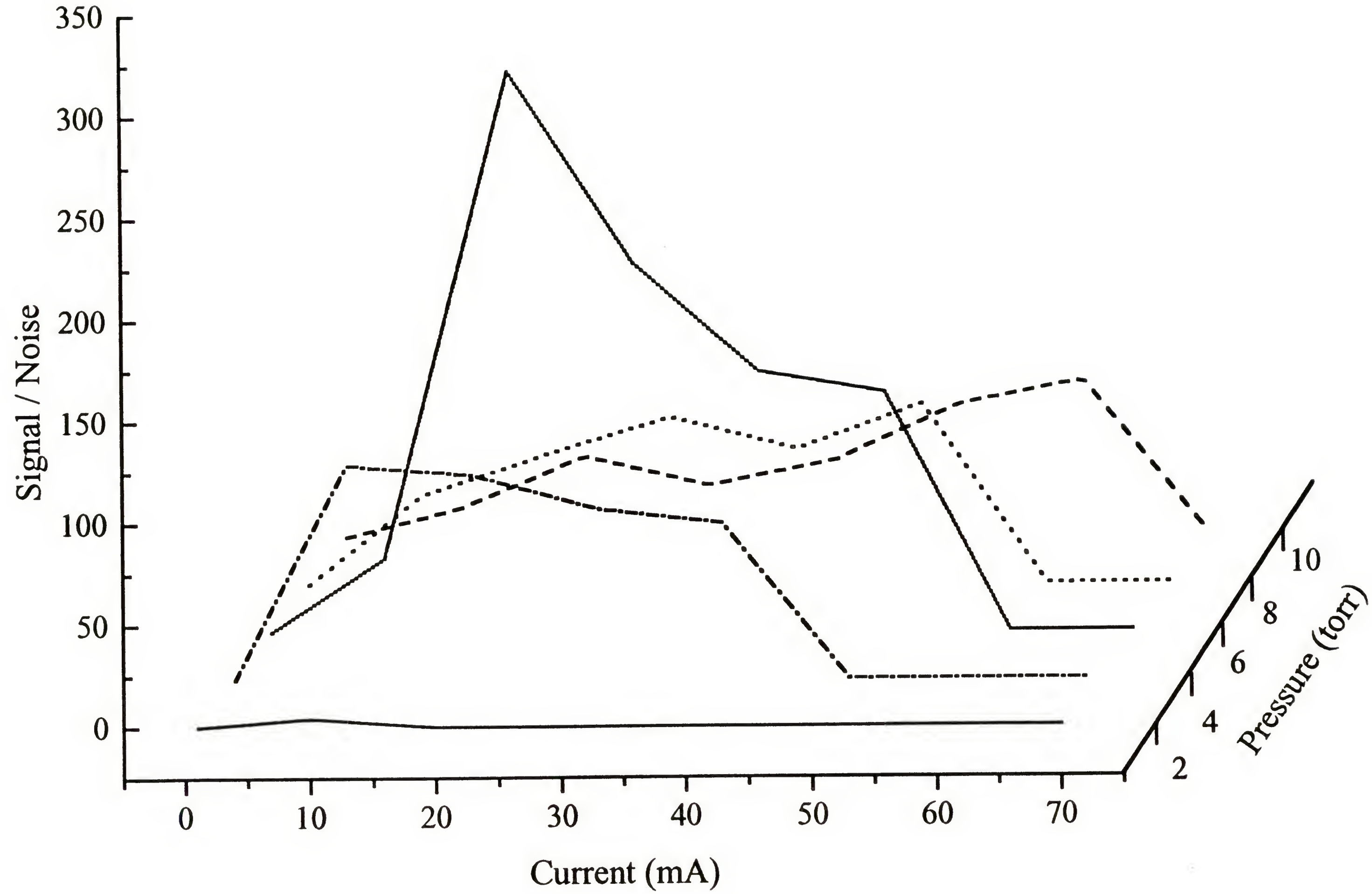

Figure 7-2. Entire response surface associated with the measurement of lead residues with continuous Ar introduction.

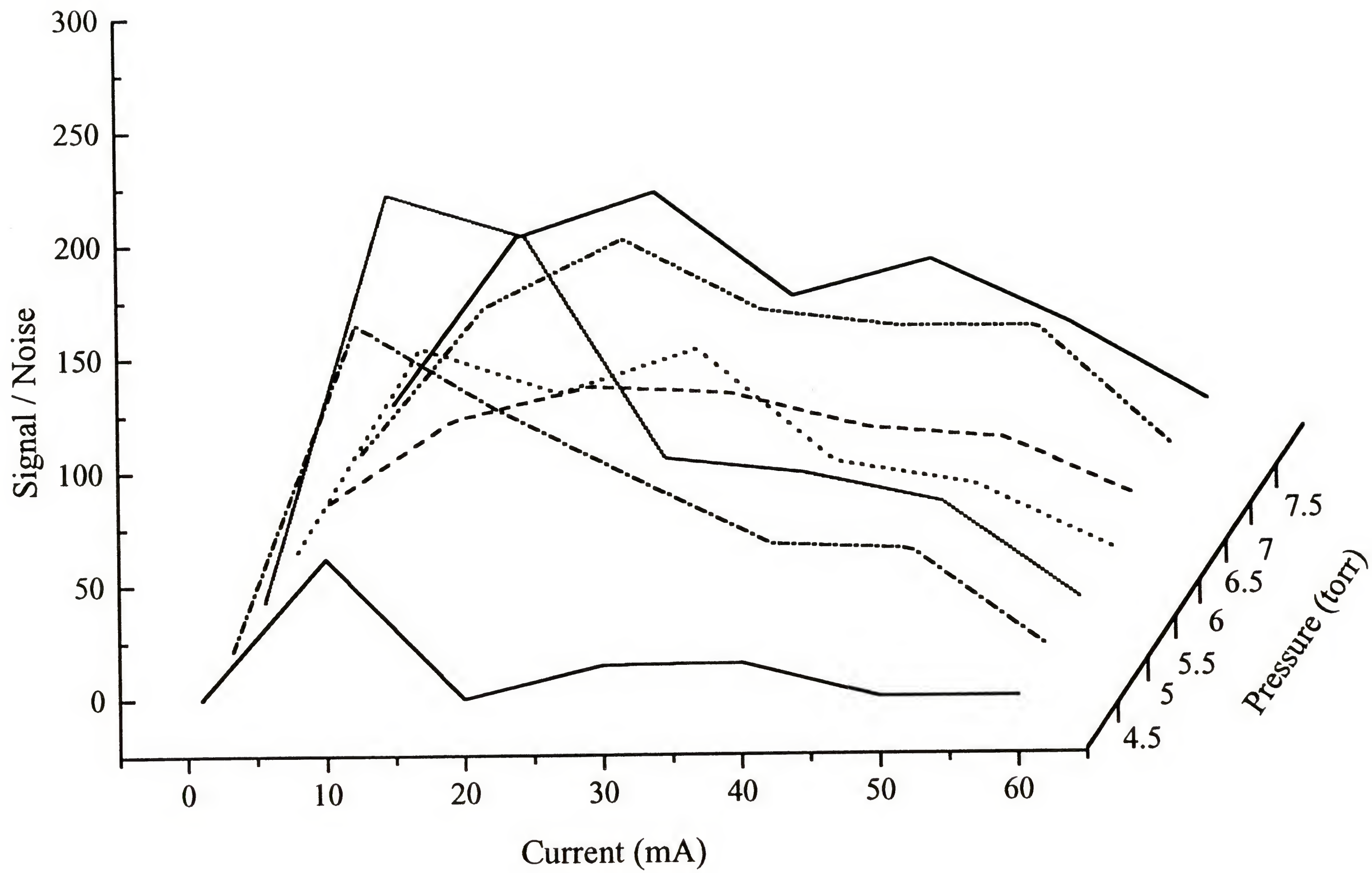

Figure 7-3. Lead response surface near the optimum pressure found in Figure 7-2.

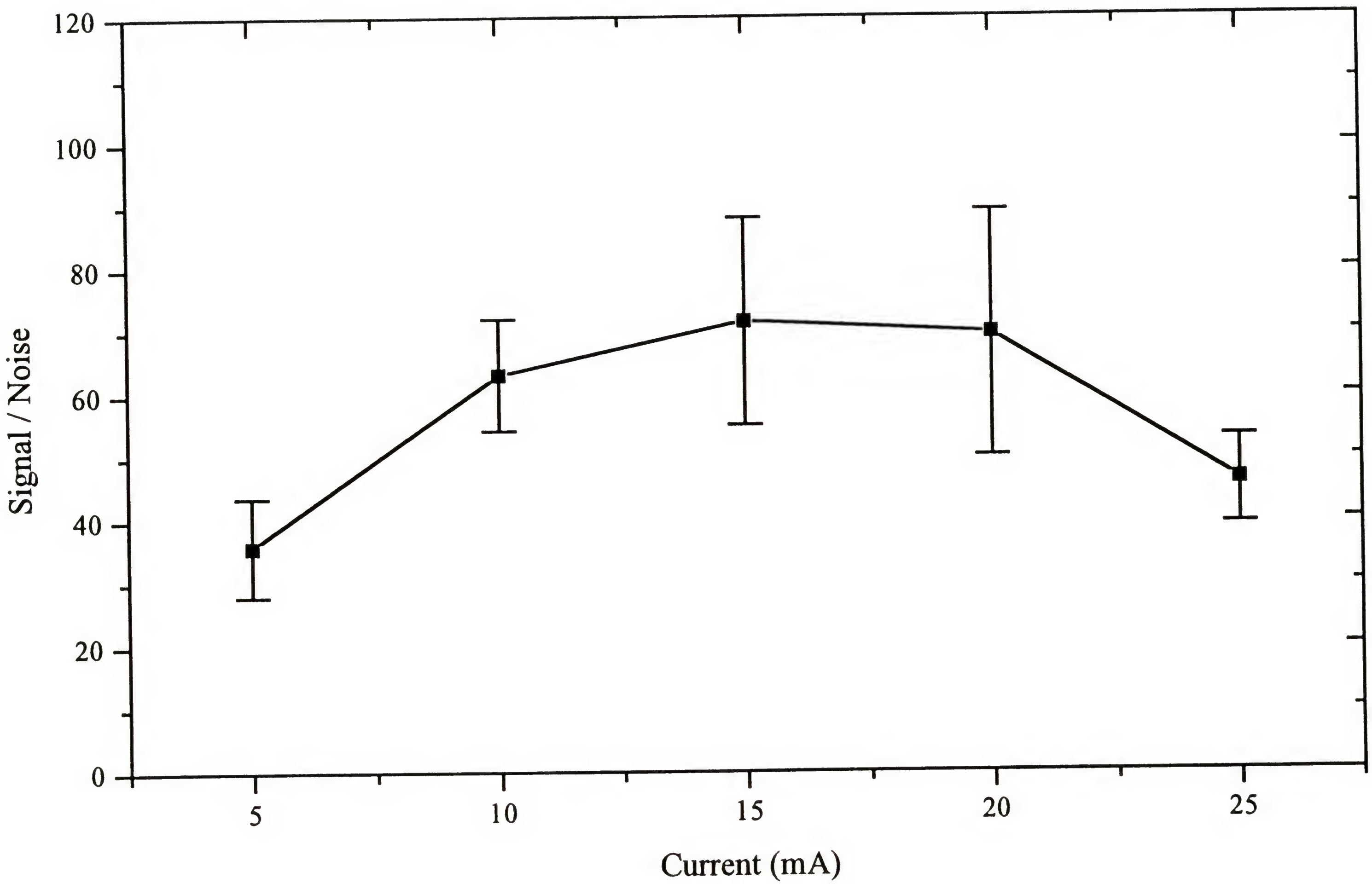

Figure 7-4. Current optimization for the measurement of lead at 5.5 torr.

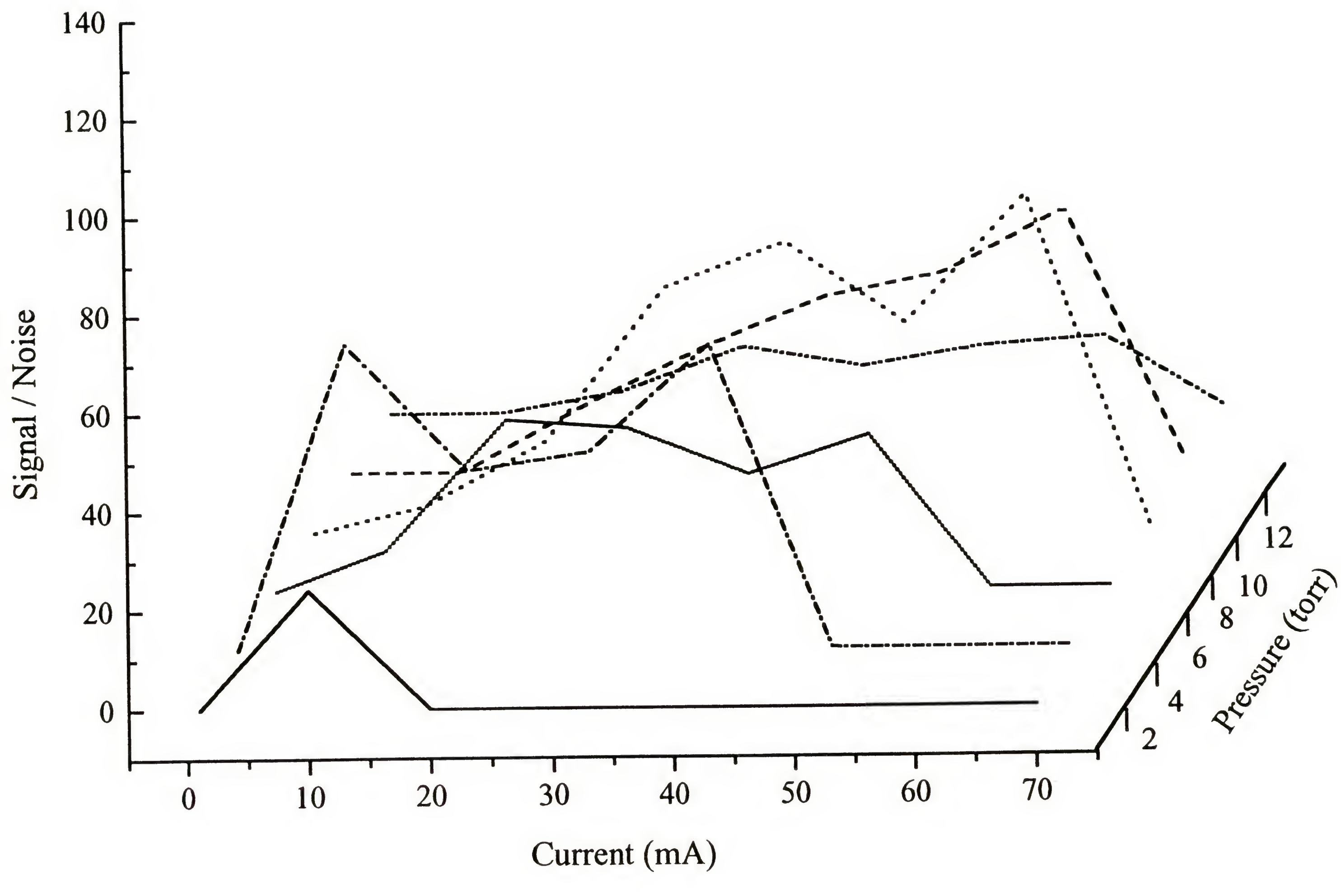

Figure 7-5. Entire response surface associated with the measurement of lead under static conditions.

Figures 7-6 and 7-7. The profile obtained with the flowing system seemed to indicate that the sputtering process was faster in the smaller system; the FWHM of the initial peak was 25.0 ms. The residence time of the atoms was apparently greater in the static system, for the FWHM of the peak was approximately 200 ms. Nevertheless, no improvement in the S/N when either peak heights or peak areas were used for comparison resulted with the static system due to the increased noise level.

Determination of the Figures of Merit

Calibration curves were obtained with both peak detection (Figure 7-8) and gated peak integration (Figure 7-9) under the conditions found to be ideal for the flowing system. The chamber was maintained at 5.5 torr with Ar as the fill gas, and a current of 20 mA, corresponding to a power of 5.5 W, was supplied to the cathode. The boxcar integrator and gated detector was set to average 100 laser shots. The excitation beam had a power of at least 1 μJ per pulse. Samples consisted of 400 nL volumes, and each concentration was measured in triplicate with error bars representing one standard deviation. Ten blank measurements were performed in order to obtain a representation of the noise. It should be noted that the data depicted in these plots were collected on two separate occasions; therefore, the peak areas obtained were not those recorded for the signals shown in Figure 7-8. Data analysis followed the general procedure presented in Chapter 5. The correlation coefficient obtained from the linear regression analysis of the signals shown in Figure 7-8 was 0.9848 with a slope of 1.013 on the log-log plot. The absolute detection limit based on 3σ was 0.6 pg, corresponding to a concentration detection limit of 1 ppb, with an overall average RSD of 14%. This limit of detection

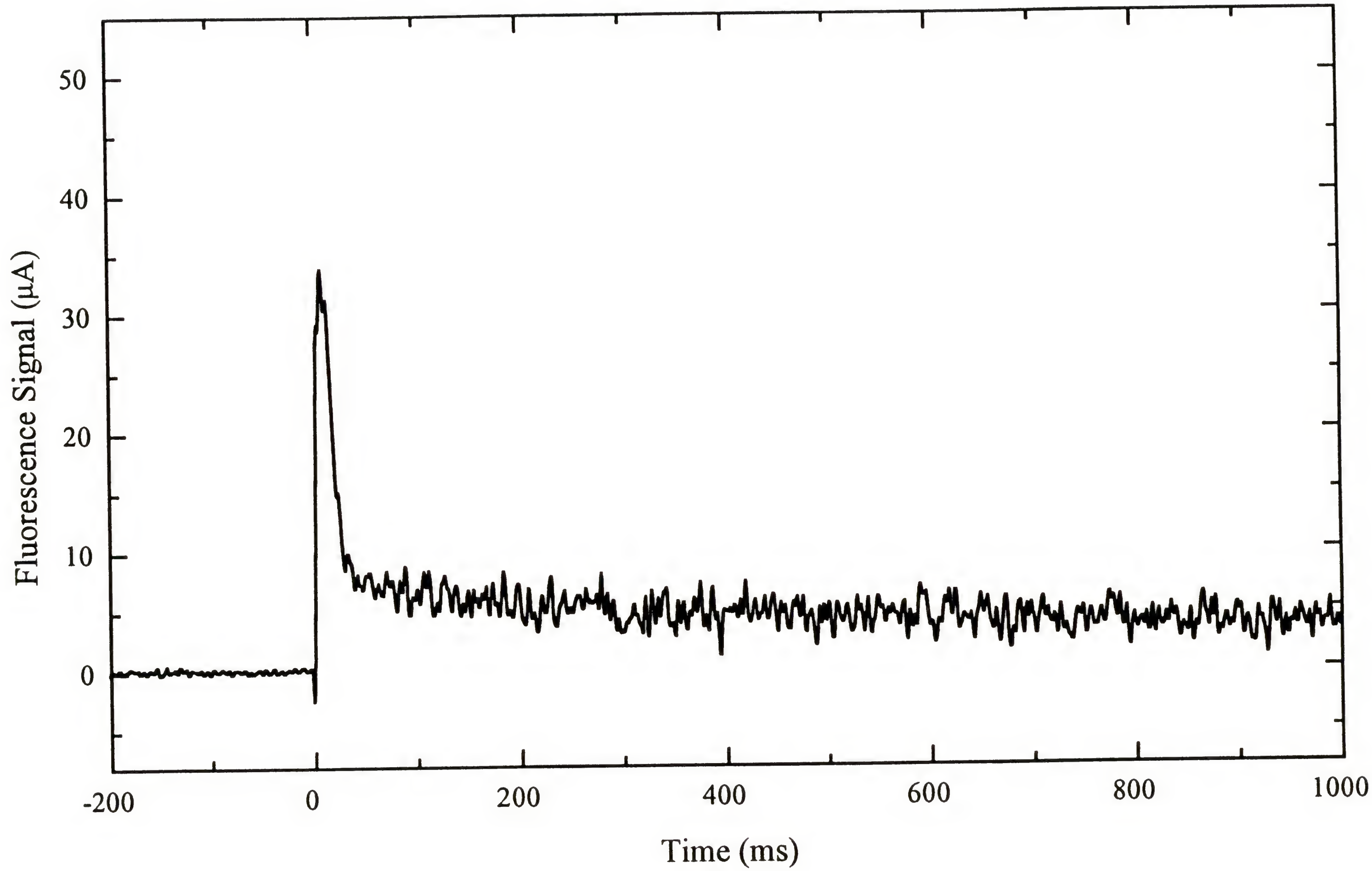

Figure 7-6. Temporal profile of a 0.03 ng lead solution residue with continuous gas introduction.

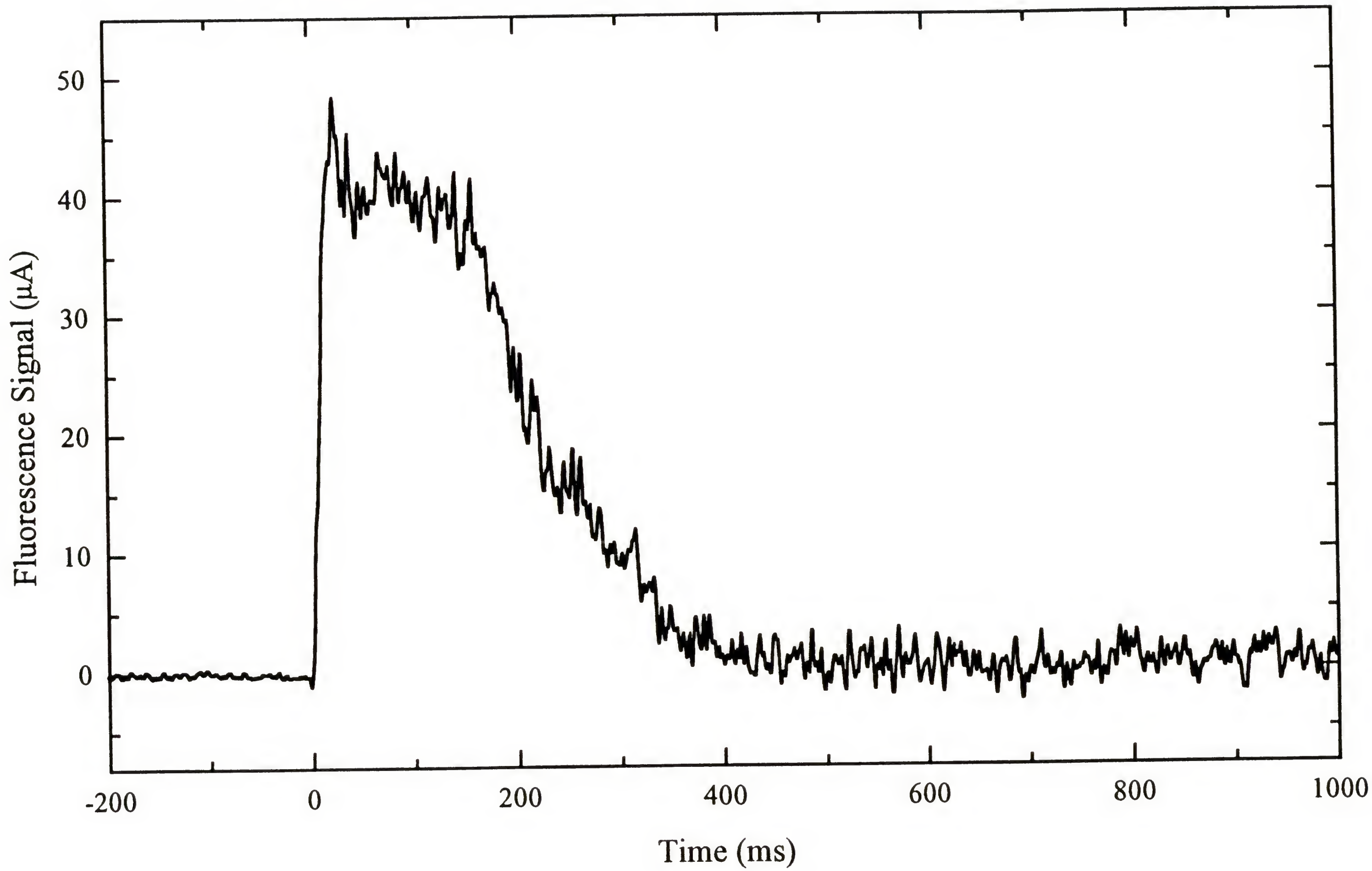

Figure 7-7. Temporal profile of 0.03 ng lead solution residue obtained under static conditions.

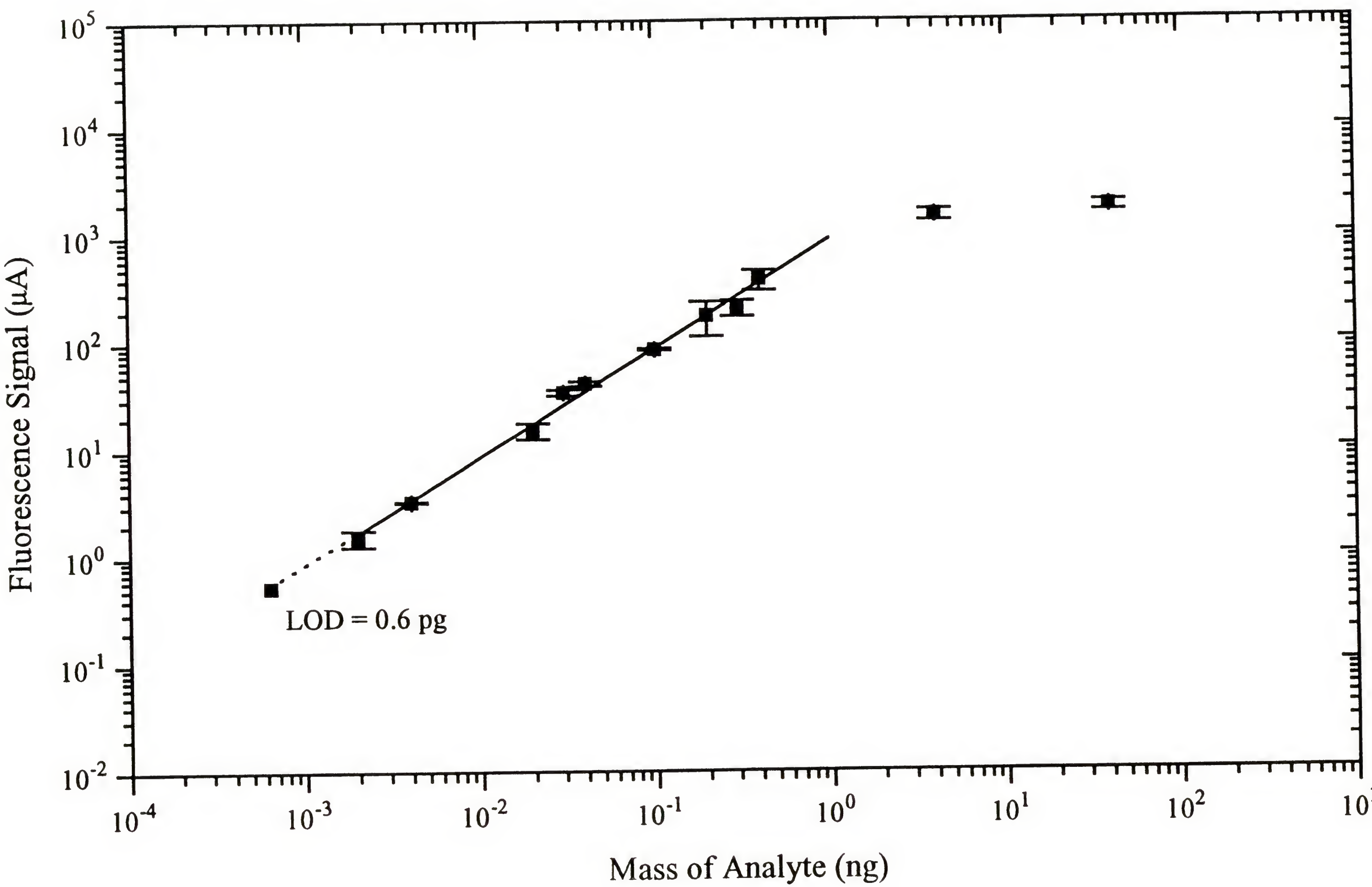

Figure 7-8. Calibration curve for lead solution residues based on peak detection.

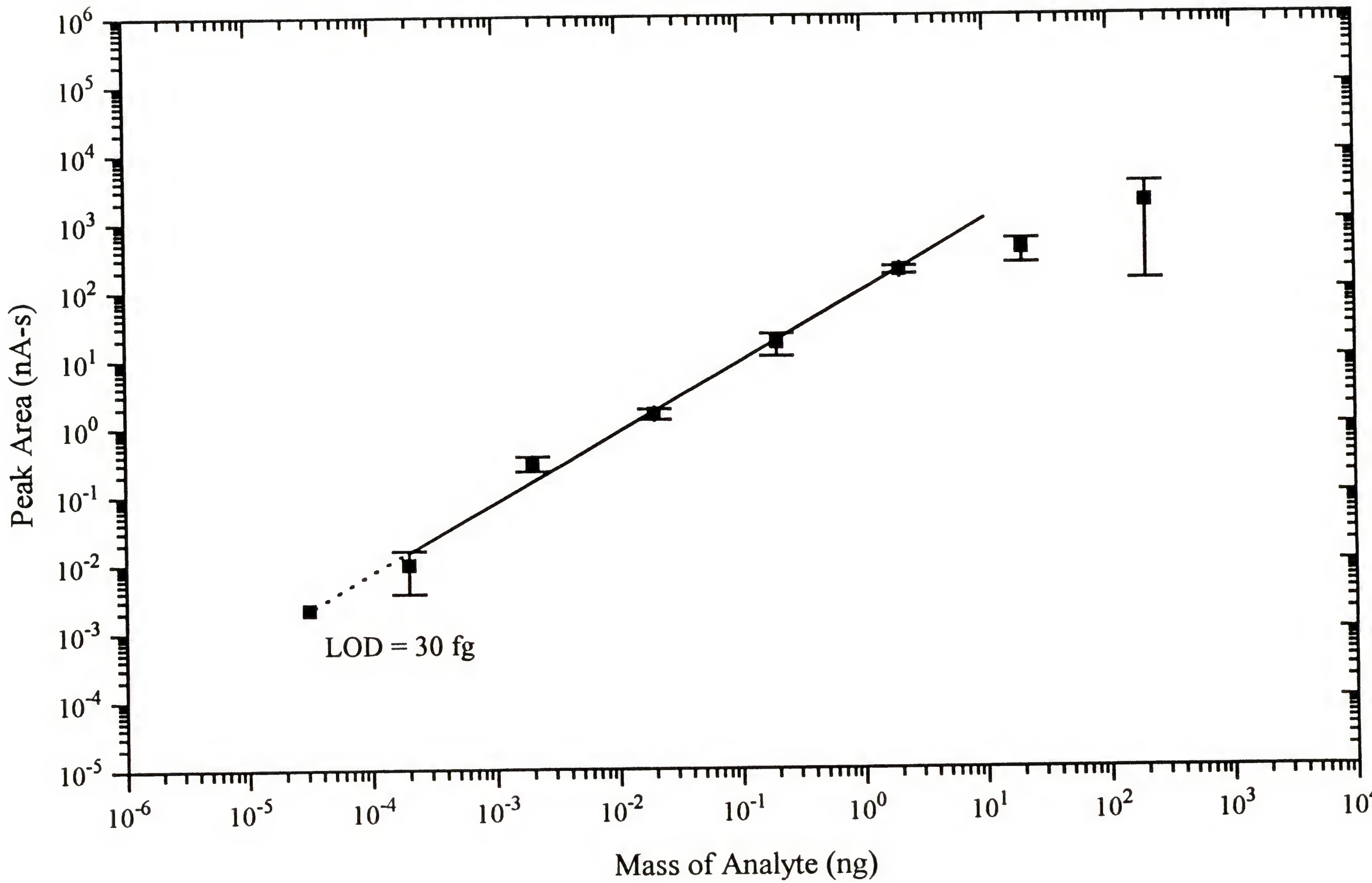

Figure 7-9. Calibration curve for lead solution residues based on gated peak integration.

was the same as that obtained with the quartz chamber. The absolute detection limit based on peak areas was somewhat better than that obtained with peak detection. The correlation coefficient of the linear regression analysis of the data depicted in Figure 7-9 was 0.99993 with the log-log slope being 1.032, indicating a linear dynamic range of 6 orders of magnitude. The average RSD was slightly higher at 25%. The detection limit of 30 fg was slightly higher than that anticipated considering the value obtained with the quartz chamber; however, the detection limit found with the larger chamber required extrapolation over several orders of magnitude, for no measurements were made near the calculated detection limit.

Analysis of Real Samples

On two separate occasions under both flowing and stop-flow operation, Standard Reference Material (SRM) 1643b, Trace Elements in Water, (National Bureau of Standards, Washington, DC) was measured for Pb content. The standard solution was certified at 24.1 $\pm$ 0.7 ppb for Pb. The measurements were performed in triplicate under the optimized conditions. Samples of 400 nL were analyzed. The equations of the lines representing the linear regression fit of the data composing the calibration curves recorded during these studies were utilized to determine the concentration of the standard. Under flowing conditions and with peak heights employed as the means of comparison, the standard was determined to contain 17.9 $\pm$ 4.6 ppb Pb, while under static conditions with peak areas used for comparison, the concentration was measured as 28.4 $\pm$ 6.8 ppb for Pb. These values are in agreement with the certified value, testifying to the applicability of this GD-LEAFS method of analysis.

Results and Discussion

The detection limits again compared favorably to that measured by Deavor *et al.* (76); however, there was no improvement over those obtained with the larger, quartz chamber. It would seem that the background noise and, possibly, the blank Pb content were limiting the measurements.

Intrinsic Detection Limit

The intrinsic limit of detection was once more determined. The efficiency of detection, $\varepsilon_d°$, at the intrinsic noise limit as defined by equation (5-1) was first calculated. Several parameters as presented in Chapter 5, such as g, A_{ul}, Δt_i, η_d and η_{el}, remained unchanged from the values determined for the quartz GD system; however, the collection efficiency of the fluorescence, η_{fl}, (equation (5-3)) and the number of laser pulses during the atom residence time, p, had slightly different values.

Substituting into equation (5-3) the values of 0.05 cm and 1.9 cm for the monochromator slit width and height, respectively, 0.05 sr for the solid angle of collected fluorescence, 0.03 cm^2 for the surface area of fluorescence and 0.8 for the transmittance of the optics, η_{fl} can be found to be 0.01. The residence time of the atoms decreased in the smaller chamber under flowing conditions to 25.0 ms. Multiplying this value by the laser pulse repetition rate of 10,000 s^{-1} gave the number of laser pulses during the residence time of 250.

With η_{fl} and p determined and the other parameters in equation (5-1) considered, $\varepsilon_d°$ was found to be 0.2. This is lower than the efficiency acquired with the larger chamber leading to an intrinsic limit of detection, N_L, as defined by equation (5-5) of

45 atoms. The limit of detection would be still lower for the system under static conditions since the atom residence time in the chamber was increased; however, due to the inherent problems with the current stop flow system, this value was not thought applicable and was not calculated.

Limiting Noises

The experimental detection limits of 1.8×10^9 atoms for peak detection and 9.0×10^7 atoms for peak integration are considerably higher than the calculated intrinsic limit of detection. As discussed in Chapter 5, background emission was determined to be the limiting noise in the case of peak detection while the peak area measurements were thought to be blank limited.

The exact source of the background noise had not yet been identified; in order to investigate this, a background emission spectrum covering the wavelength range of 220 nm to 570 nm was obtained by scanning the monochromator while the GD was ignited and a blank cathode was in place (Figure 7-10). The laser beam was blocked prior to the chamber, and the boxcar was not necessary. The output from the transimpedance amplifier was directly recorded.

Several emission lines were apparent in the spectrum, most being related to N_2. It was obvious that a vacuum leak was present; the integrity of the vacuum was not being maintained, for air was entering the chamber. The water and N_2 contained in the chamber were responsible for the high background noise level. Most importantly, a N_2 emission line was located at 405.9 nm, falling almost exactly at the Pb detection wavelength of 405.8 nm. This line is shown more clearly in Figure 7-11 which

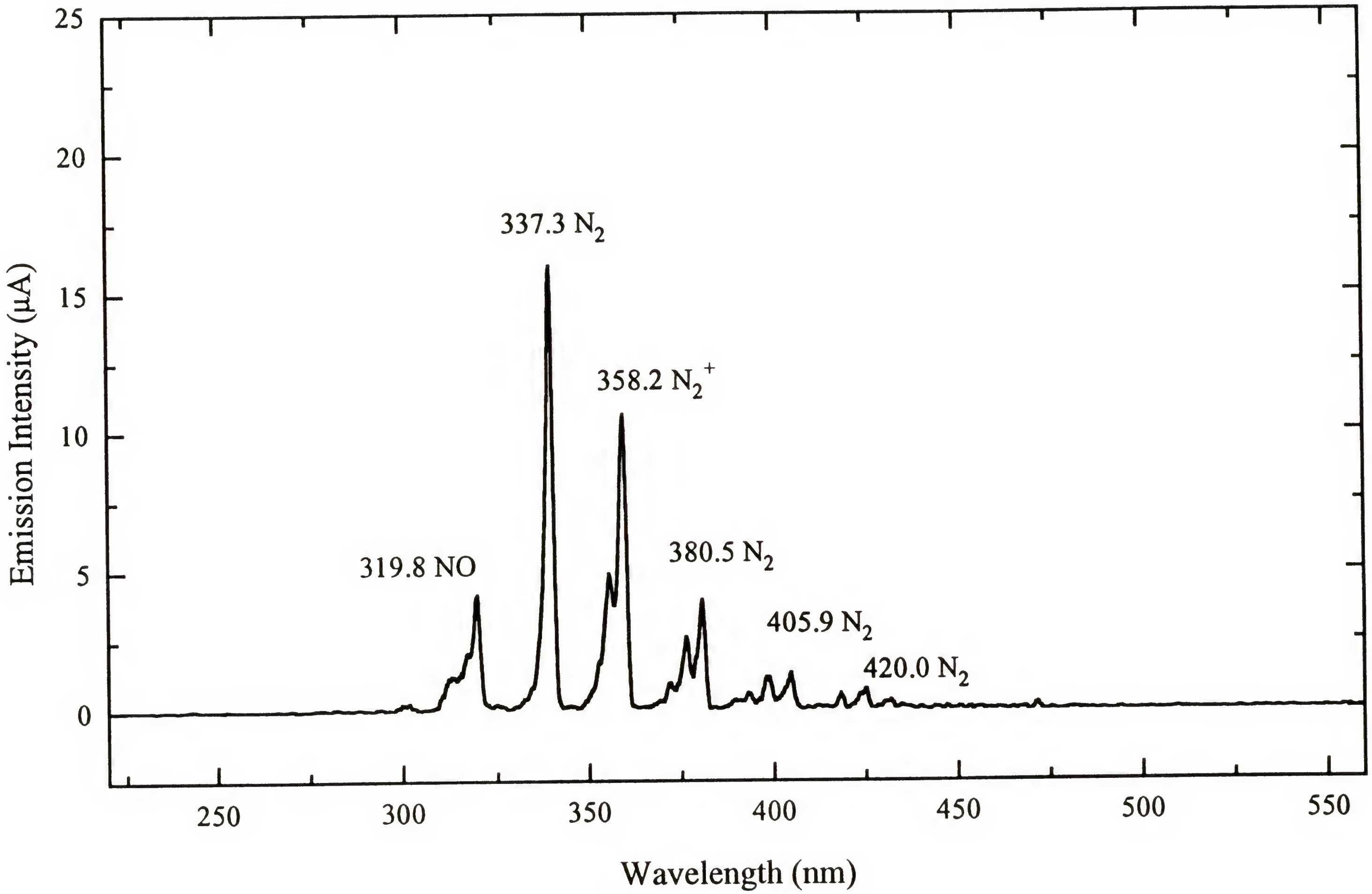

Figure 7-10. **Background emission spectrum.**

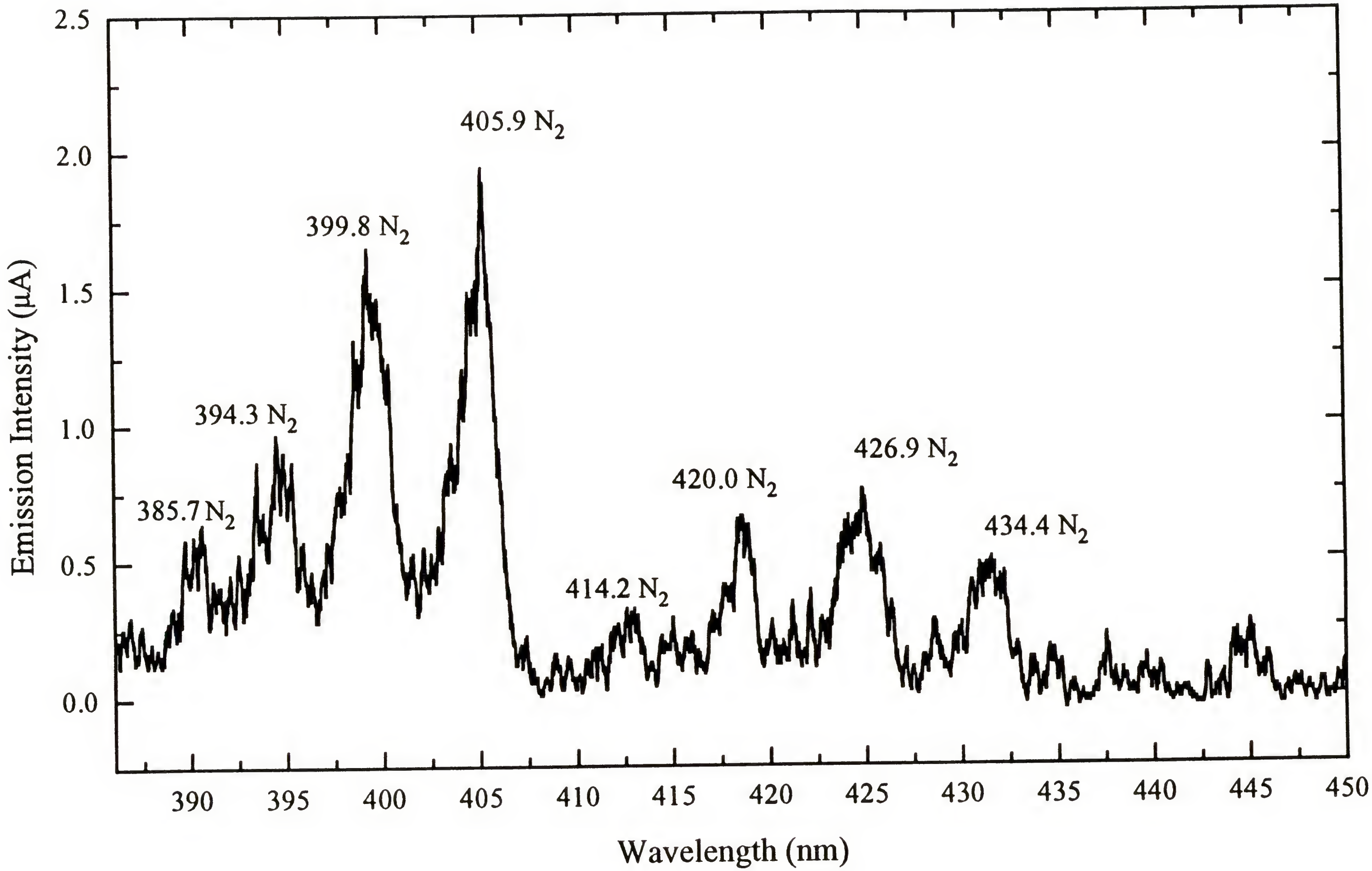

Figure 7-11. Background emission spectrum near 405.8 nm.

represents the emission occurring between 380 and 450 nm. The chamber would need to be redesigned so that a lower pressure could be reached in the GD, and all unwanted species could be removed from the chamber before sample measurement. An attempt was made to locate and seal the leaks, and some improvement was seen after a large leak was sealed (Figure 7-12).

Future Work

Considering the large emission background, the detection limits obtained for Pb were very respectable, and modification of the GD would be required in order to improve upon the results. It was thought, however, since the purpose of the GD-LEAFS system was not solely for the measurement of Pb that the system should not be changed and that other elements should be studied.

Elements with detection wavelengths falling in the quiet regions of the emission spectrum were to be measured. Several rare earth elements were found to have excitation and fluorescence detection schemes which were ideally suited for study with the present GD-LEAFS method. Six materials, Eu, Y, Tm, scandium (Sc), lutetium (Lu) and gadolinium (Gd), could possibly be measured with the system utilizing non-resonance fluorescence detection. Of these elements, Eu, Y and Tm were studied, and the results are reported in the following chapter.

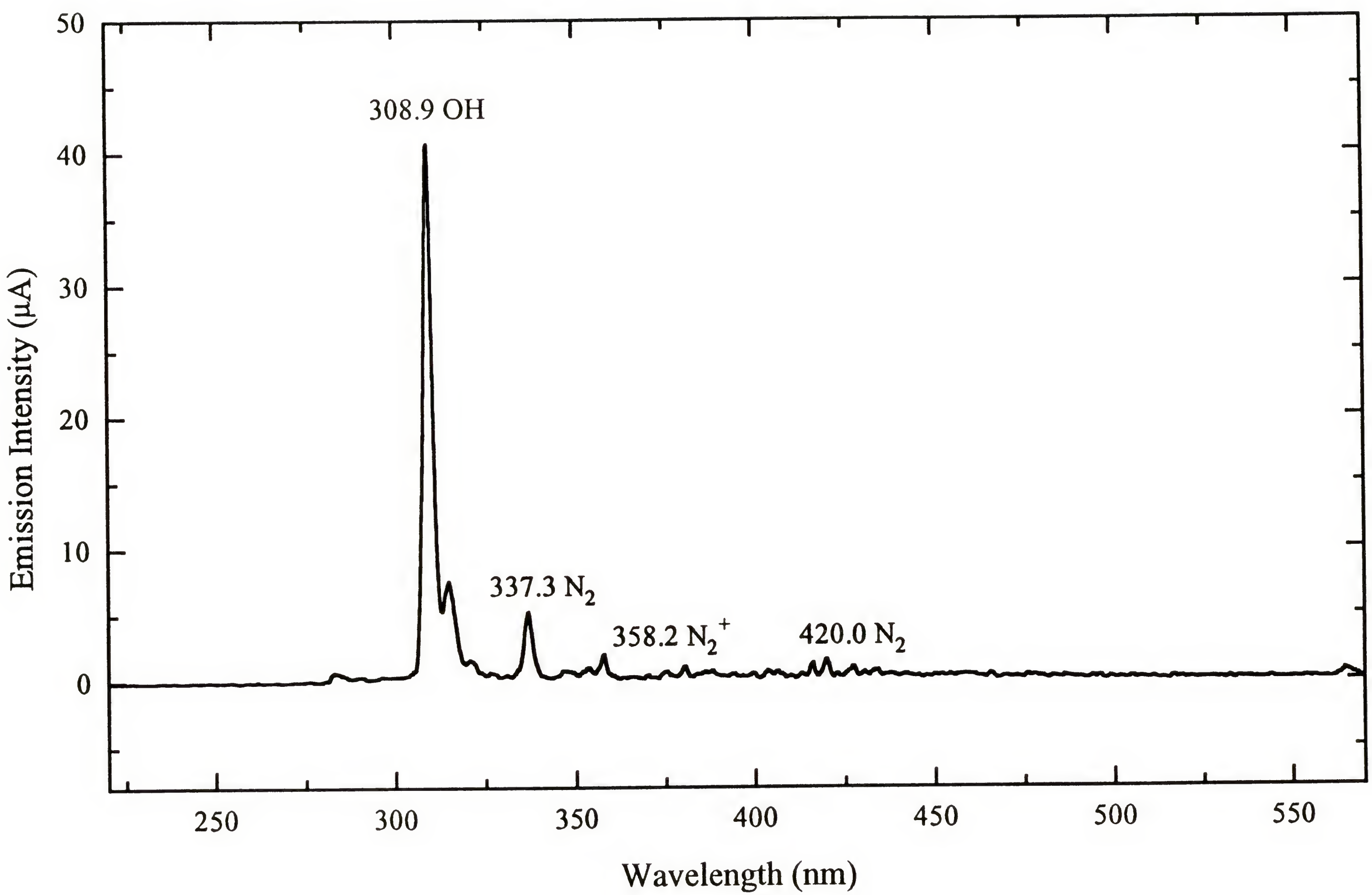

Figure 7-12. Emission spectrum following the sealing of a vacuum leak in the chamber.

CHAPTER 8
MEASUREMENT OF THE RARE EARTH ELEMENTS

Introduction

The rare earth elements have not been well characterized by spectroscopic methods. In fact, very few articles of analytical interest have been published regarding these materials. Partially due to this lack of information, the rare earth elements were chosen for study with the GD-LEAFS technique; in particular Eu, Y and Tm were measured.

The rare earth elements are known to have very rich spectra, for numerous atomic transitions have been documented. The excitation and fluorescence wavelength detection schemes that were chosen for these three materials are illustrated in Figures 8-1, 8-2 and 8-3. There were two possible detection wavelengths for Y; however, only the 543.8 nm line could be effectively isolated from the laser line by the sharp cut filter which was placed prior to the monochromator entrance slit. The laser energy per pulse varied from 500 nJ to 1 μJ, depending on the excitation wavelength; however, optical saturation was not achieved. The fluorescence signal was, as a result, linearly related to the energy of the laser. Although the maximum fluorescence signals could not be acquired, it was hoped that large S/N ratios would be obtained due to the decreased background noise levels. As noted previously, in each case the detection wavelength fell within a

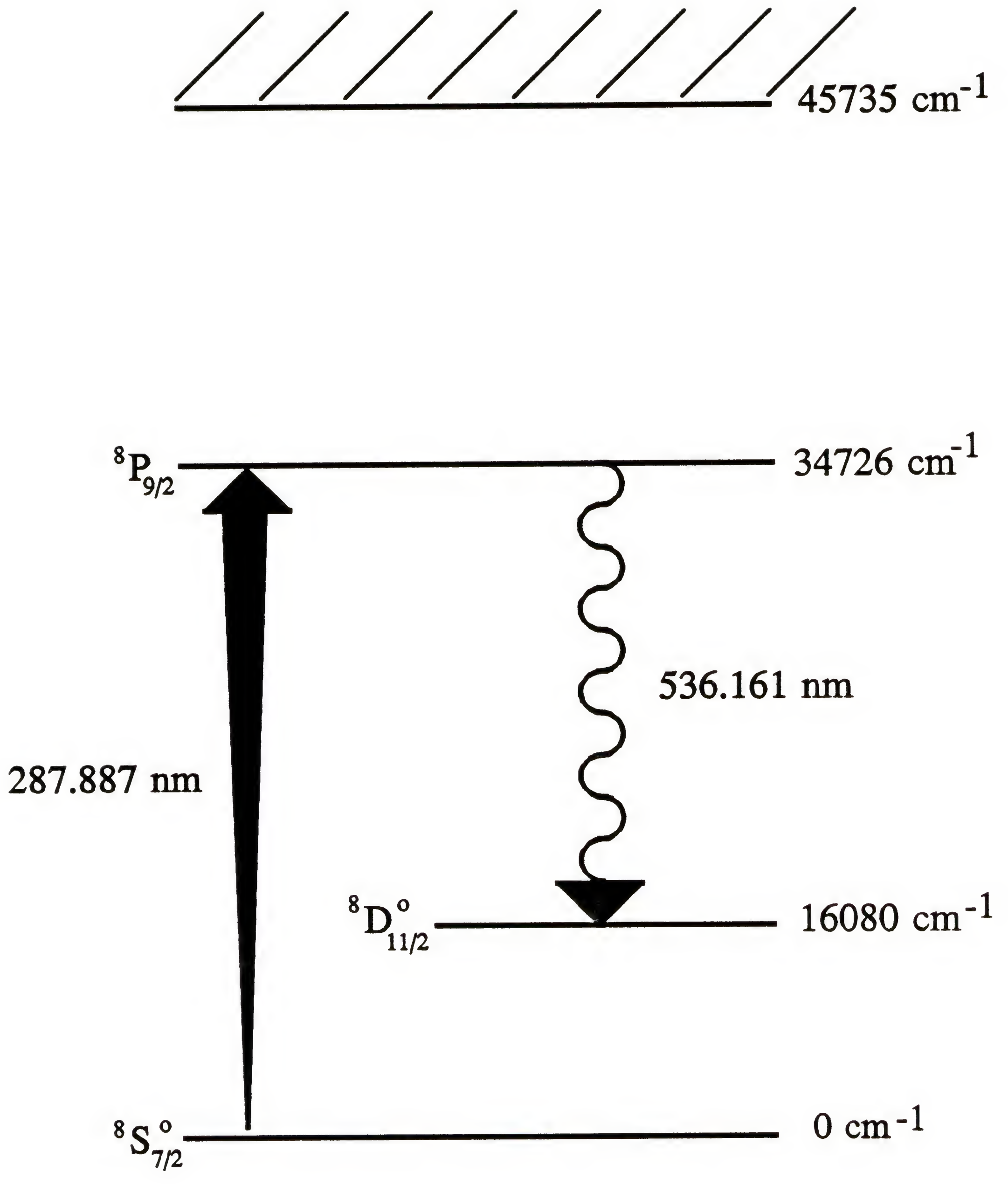

Figure 8-1. Partial Grotrian diagram for europium.

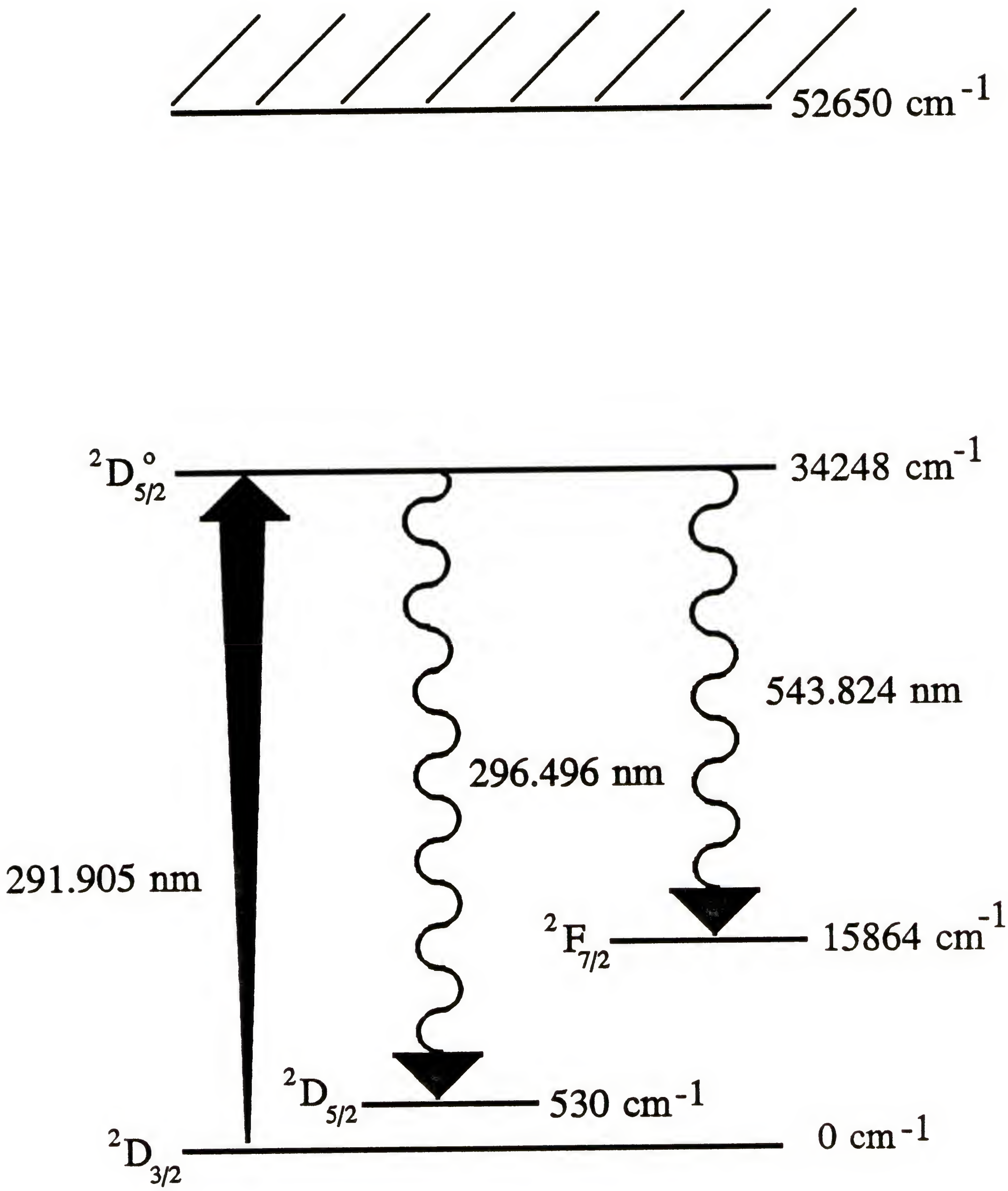

Figure 8-2. Partial Grotrian diagram for yttrium.

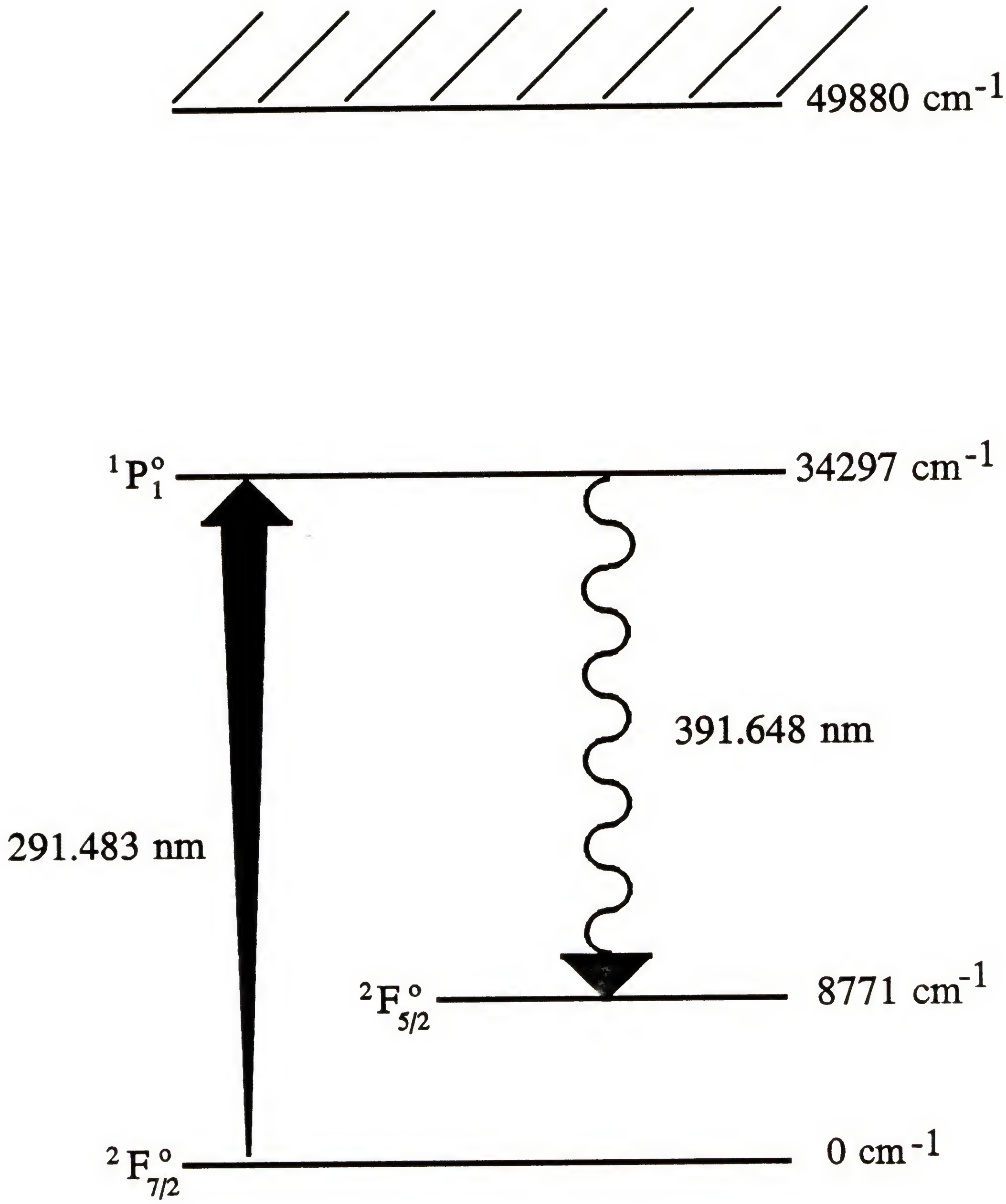

Figure 8-3. Partial Grotrian diagram for thulium.

relatively quiet region of the background emission spectrum (Figure 7-12) where few N_2 emission bands were found.

Experimental

Instrumentation

The instrumentation was identical to that described in Chapter 4 with the modifications noted in Chapter 6. There was one minor alteration; the second mirror employed to direct the laser beam back into the chamber was repositioned so that the reflected beam overlapped the principal beam. The fluorescence signal was effectively doubled. The gate of the boxcar was 360 ns in duration with a delay of 44.2 ns for all measurements.

Rhodamine 6G at a concentration of 0.46 g/L in optima grade methanol was utilized in the dye laser for the Eu measurements. A dye mixture consisting of 92% rhodamine 6G (0.46 g/L) and 8% kiton red 620 (1.5 g/L) in optima methanol was employed for the investigations involving Y and Tm. All laser dyes were supplied by the Exciton Corporation.

Sample Preparation and Procedure

The sample preparation and procedure were identical to those presented in Chapters 5 and 6. Research grade standard solutions of 10,000 ppm europium oxide in 10% hydrochloric acid (HCl), 1000 ppm yttrium oxide in 2% HCL (High-Purity Standards, Charleston, SC) and 1000 ppm thulium oxide in 2% HNO_3 (Spex Industries, Inc., Edison, NJ) were used in the serial dilutions.

Optimization of the Operating Conditions

Peak heights were used for comparison for the optimizations. A Ni rod served as the cathode once again, and the monochromator slit width was 0.5 mm. The laser pulse repetition rate remained at 10 kHz. The only parameters to be optimized were the chamber pressure and the current supplied to the cathode.

Response surfaces were recorded for each element. They are represented in Figures 8-4, 8-5 and 8-6. The signals produced by 2 μg, 20 ng or 200 ng solution residues of Eu, Y and Tm, respectively, were monitored with the corresponding background noise level. Each measurement was performed in triplicate. The optimal operating pressures for Eu, Y and Tm were 1, 2 and 3 torr, respectively. The ideal cathodic current for Eu and Y measurements was 10 mA, corresponding to a power of 3.5 W for Eu and 3.1 W for Y. The best S/N for the Tm measurements was obtained at 40 mA which corresponded to 12.8 W. Thulium had the most clearly defined optima, and a much greater cathodic current was required before sputtering became evident.

Temporal Profiles

The temporal profiles obtained for the three elements were quite similar and also resembled the profile of Pb shown in Figure 7-6. Figure 8-7 depicts the fluorescence signals obtained from a 200 ng residue of Eu, a 20 ng Y residue and a 0.2 ng residue of Tm. These profiles have been smoothed by the boxcar which was set to average 100 laser shots. Peak tailing was apparent in these profiles and was perhaps more pronounced than in the profile associated with Pb. It was decided that this phenomenon required more careful study at this time.

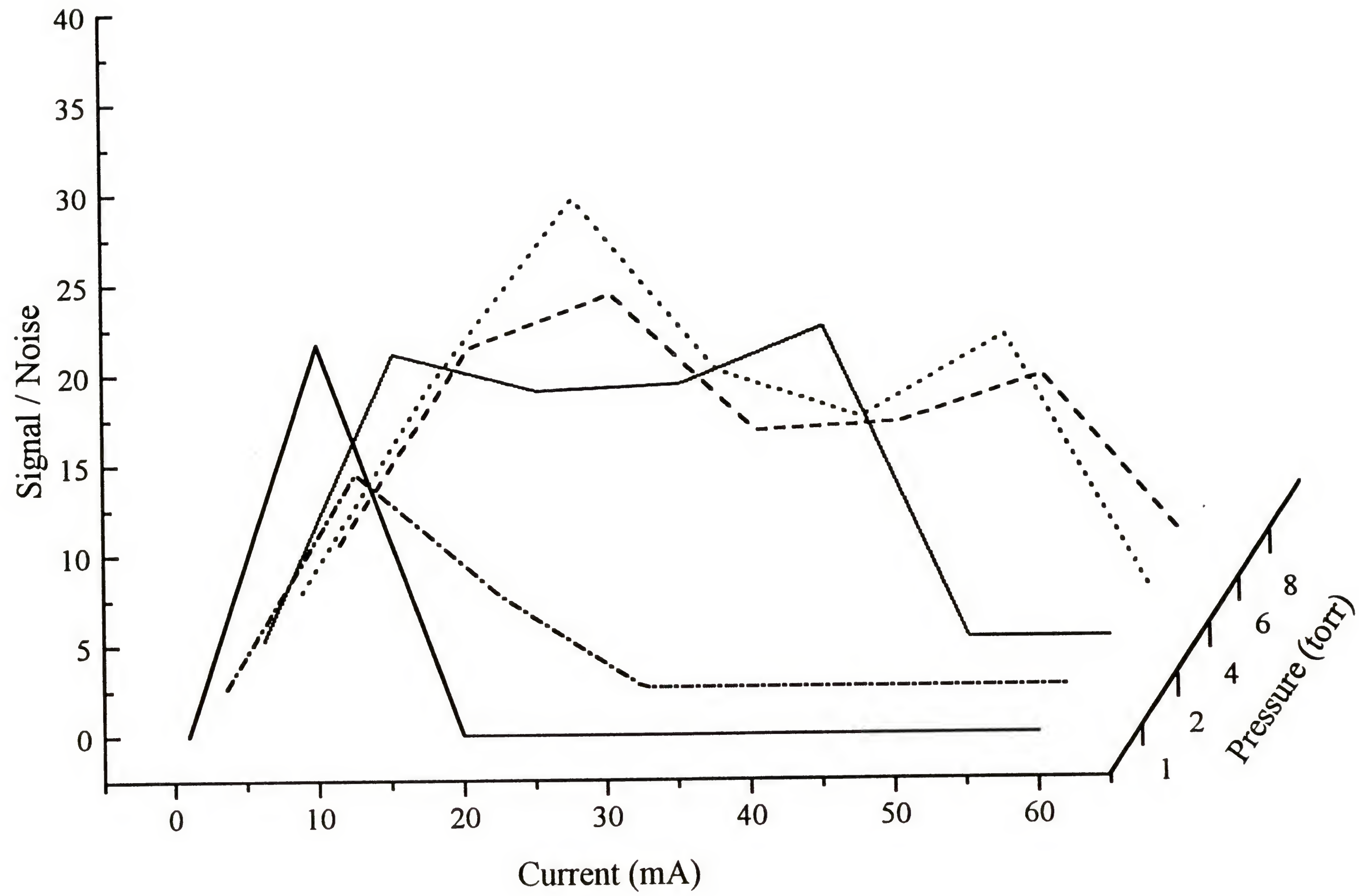

Figure 8-4. Response surface associated with the measurement of europium.

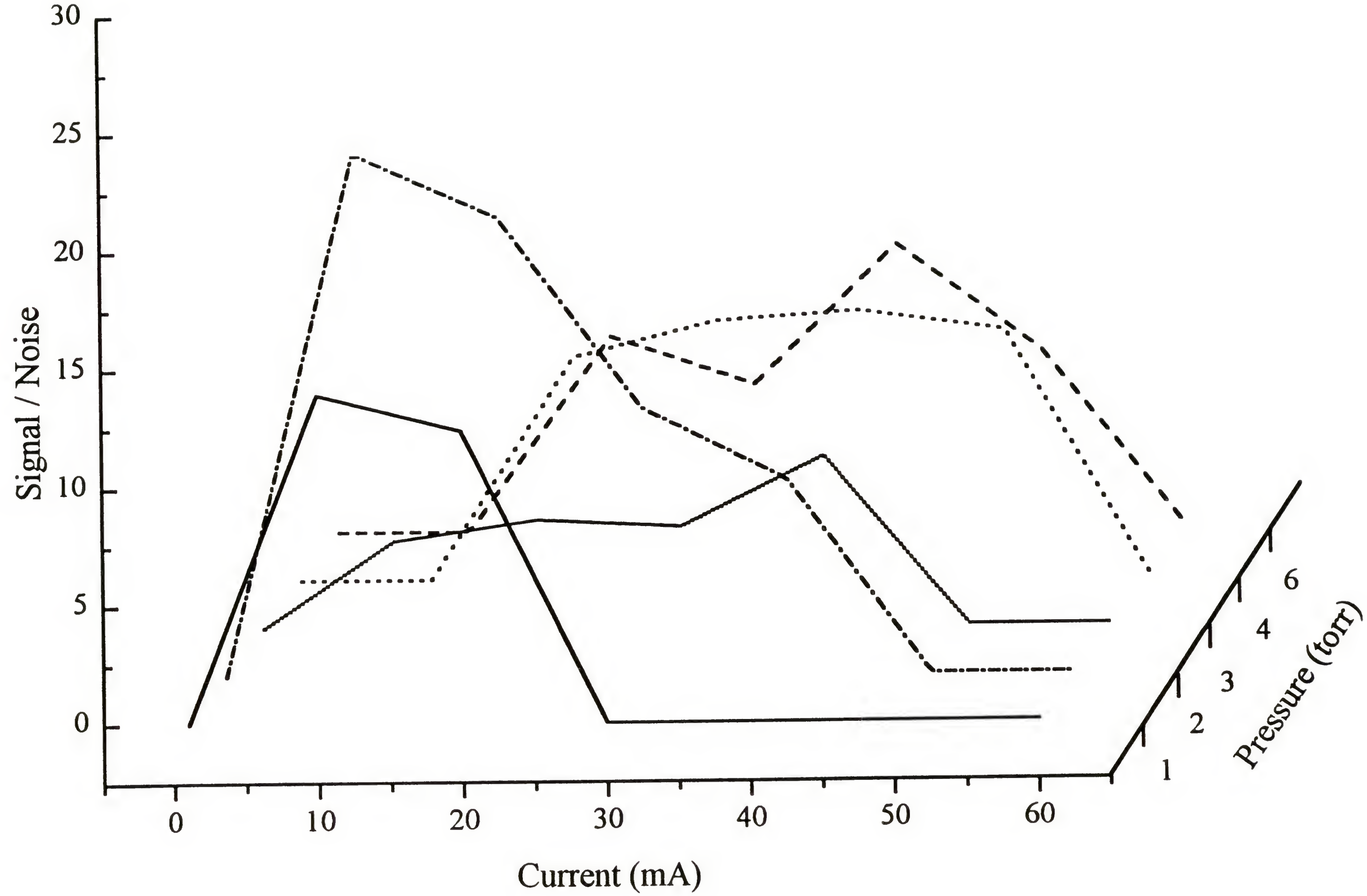

Figure 8-5. Response surface associated with the measurement of yttrium.

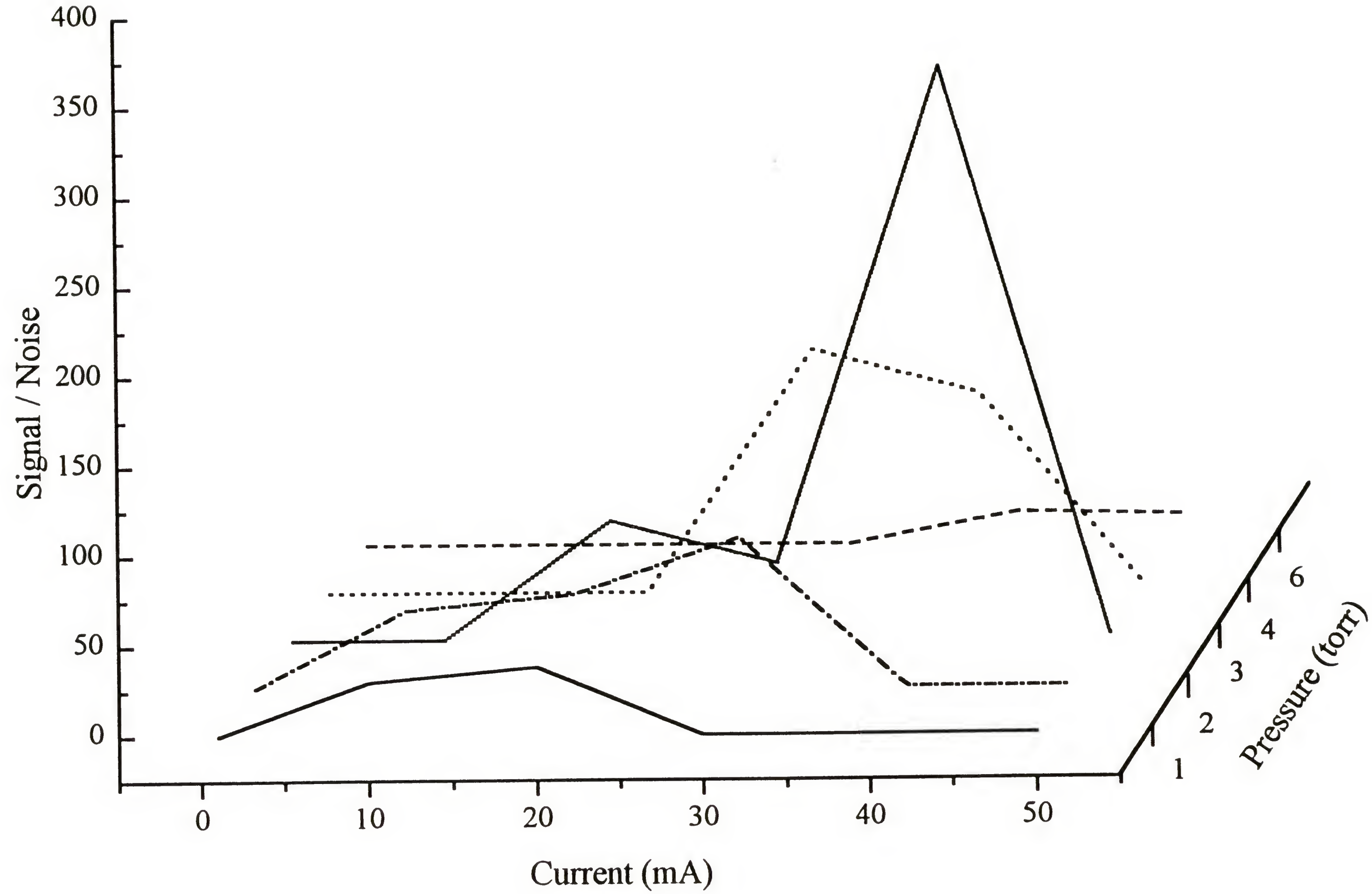

Figure 8-6. Response surface associated with the measurement of thulium.

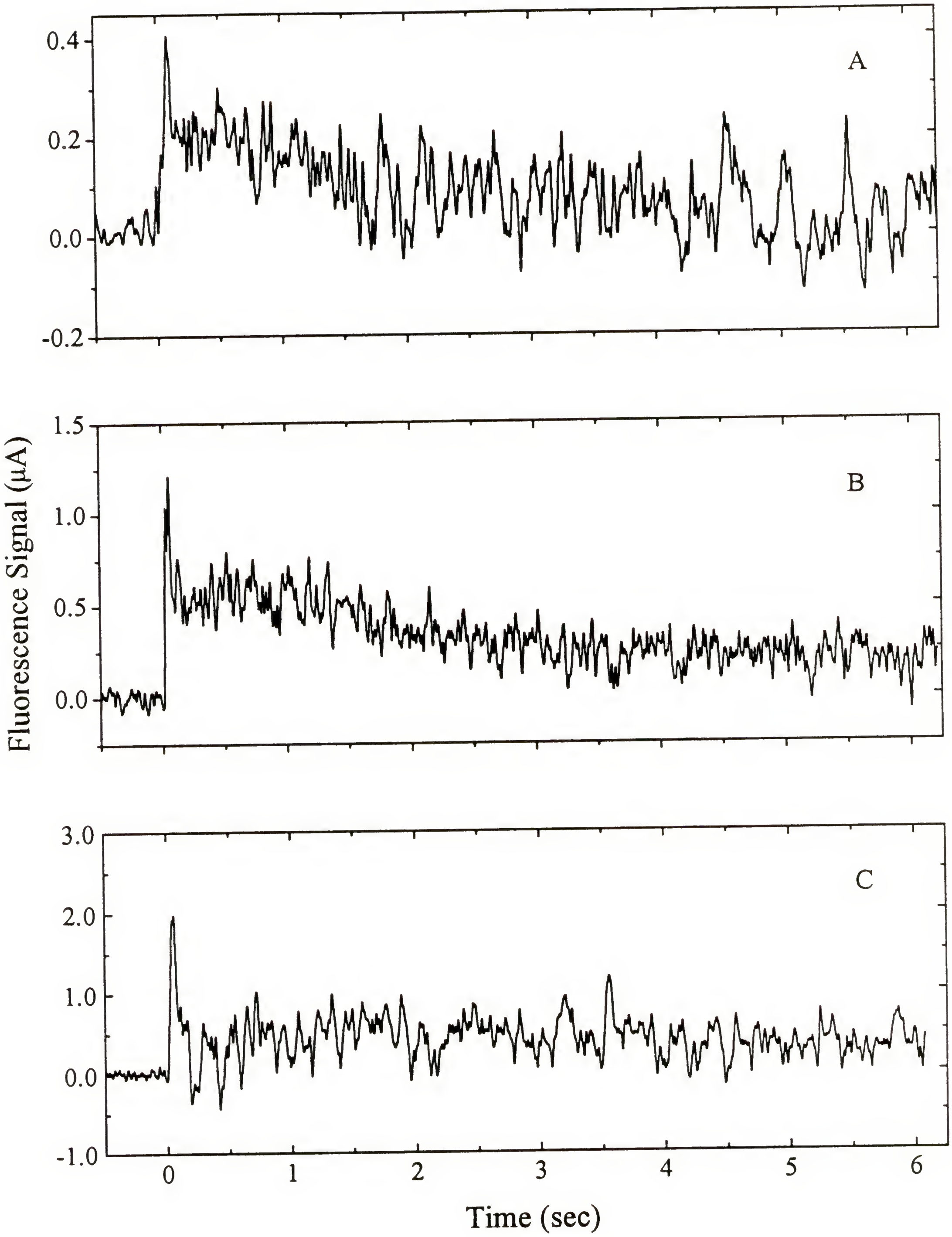

Figure 8-7. Temporal profiles of (A) a 200 ng europium residue, (B) a 20 ng yttrium residue and (C) a 0.2 ng thulium residue.

Investigation of the Peak Tailing Phenomenon

Whether or not this phenomenon was related to the atomic fluorescence of the analyte needed to be determined, for a chemical reaction or interaction, perhaps due to the presence of the laser, could have produced the tailing. The relationship of the peak tail to an atomic transition of the analyte could be confirmed by comparing the fluorescence profile to the atomic emission profile and the ionic emission profile. If these profiles were similar, it could be concluded that the tailing was definitely due to the presence of the analyte and that it was related to an excited state transition.

These emission profiles could be easily obtained with the present system. For these measurements, the GD was responsible for not only producing the atoms but for also causing those atoms to be excited. The laser beam was blocked prior to the GD reservoir, and the output of the transimpedance amplifier was directly recorded, bypassing the boxcar integrator and gated detector. Solution residues of 4 μg Eu were deposited as described before. The chamber pressure was held at 1 torr, and 10 mA of current were supplied to the cathode. A representative Eu atomic emission signal monitored at 466.2 nm is shown in Figure 8-8 along with a depiction of the ionic emission at 272.8 which was also measured. There was considerable background emission, for the baselines were above 0 μA when no analyte was present. However, the tailing was evident in both cases and was determined to be mainly due to the presence of the analyte and not simply to the background noise level. This result confirmed that the tail was due to an atomic transition of the analyte.

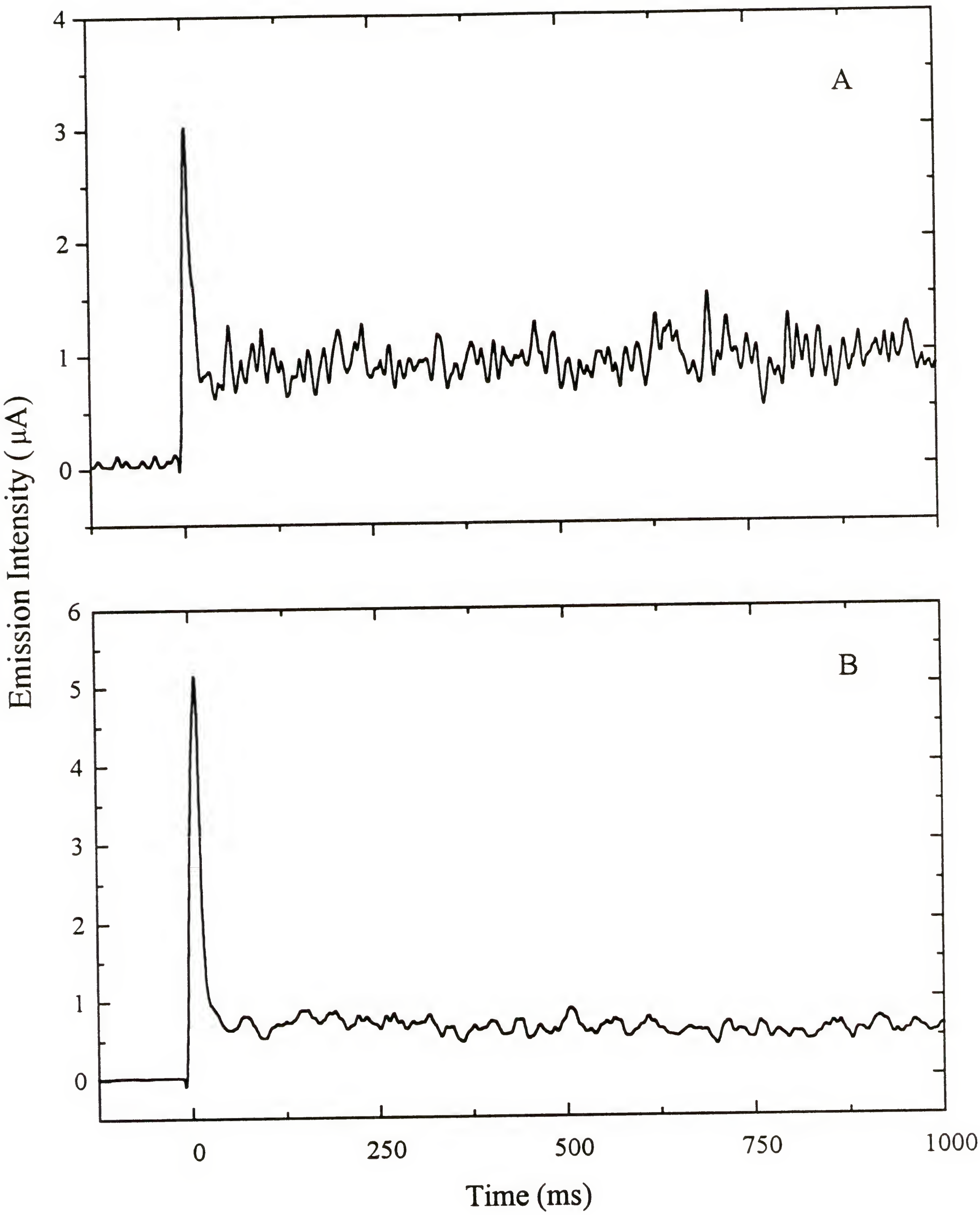

Figure 8-8. Temporal profiles associated with the emission of a 4 μg europium residue. Plot (A) depicts the Eu I emission at 466.2 nm, and (B) illustrates the Eu II emission at 272.8 nm.

Another means of verifying that the peak tailing was only due to an atomic transition of the analyte and not to a photodissociation process initiated by the laser was proposed. It could be checked by obtaining a fluorescence profile with the doubled beam of the laser attenuated prior to the chamber, so that its intensity was decreased by a factor of two, and then comparing this profile to one obtained with the laser at full power. If the process was due to some other type of interaction other than strictly atomic fluorescence of the analyte, the ratio of the initial peak height to the level of the tailing would not be linearly related to the laser power. In other words, if the profile represented only the fluorescence, the ratio would be exactly halved when the laser was attenuated. As can be seen in Figure 8-9, it was confirmed that the tailing was not due to any other process either than the fluorescence of the analyte, for the peak height and the level of the tail decreased proportionally when the laser energy was decreased.

At this point, it was confirmed beyond any doubt that the tailing of the signal peak was due to an atomic transition of the analyte. It was not known, however, if the tail was due to another form of the analyte other than the deposited salt. It had been suggested that the analyte could be forming the oxide and that the oxide could sputter more slowly from the surface of the cathode. If the oxide did have a lower sputtering efficiency, the prolonged, reduced fluorescence signal could be due to the presence of the oxide. In an earlier study, it was discovered that a crystalline residue remained on the surface of the cathode following the measurement of a Eu sample with a mass larger than 40 μg. The identification of this compound could confirm this theory. Since the residue consisted of very small crystals and only a limited amount was available, X-ray

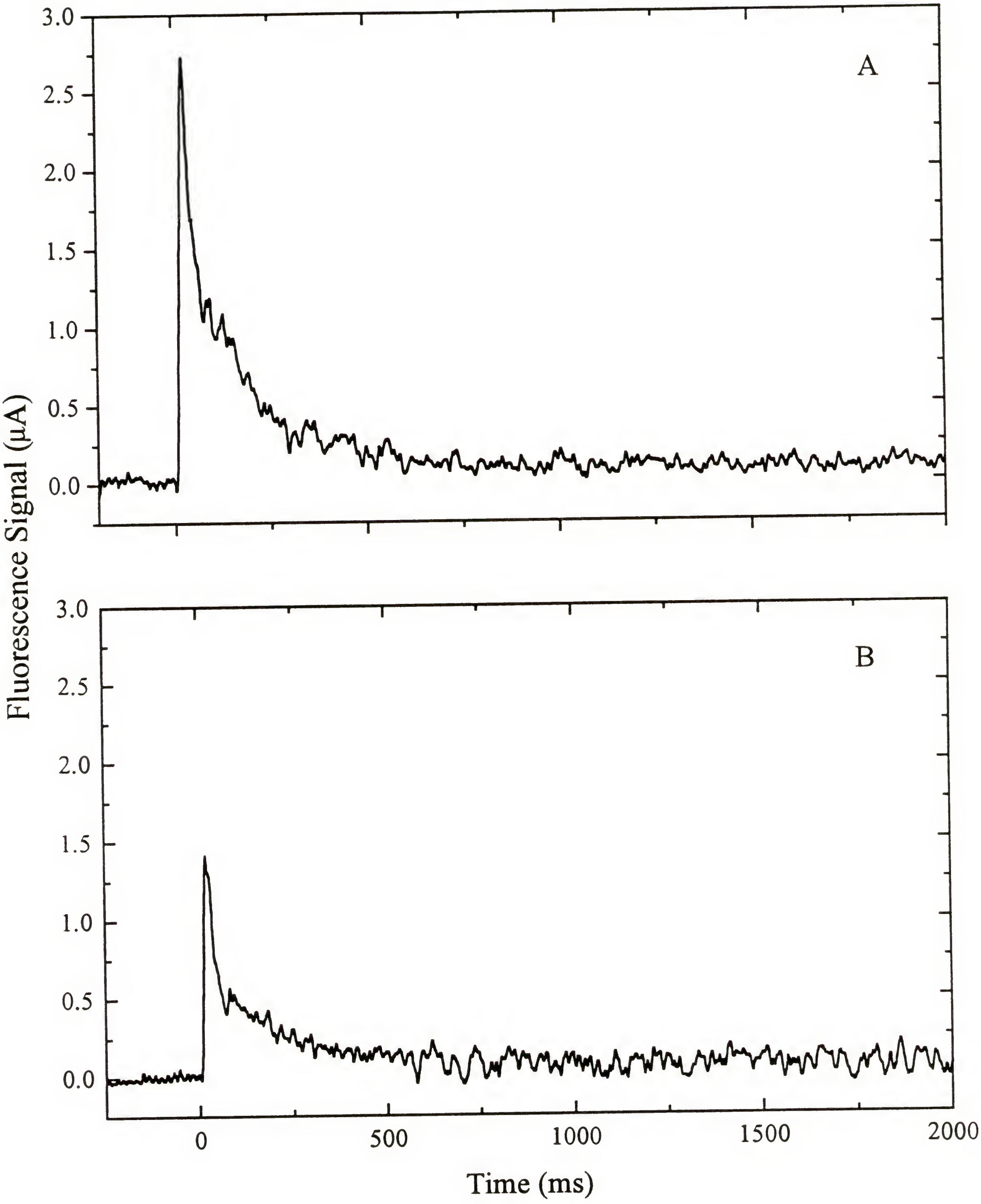

Figure 8-9. Temporal profiles of 1 μg solution residues of europium obtained with (A) the laser at full power and (B) the laser attenuated by 50%.

diffraction crystallography was not a feasible method of characterization. Fluorescence spectrometry could be utilized, and the instrumentation was available in the laboratory. A fluorescence spectrum of the unknown residue is shown in Figure 8-10.

This spectrum was obtained with a 0.85 m double grating spectrometer (Model 1403, Spex Industries, Inc., Edison, NJ) with entrance and exit slits of 1 mm and internal slits of 2 mm. An Ar ion laser (Series 2000, Spectra-Physics, Mountain View, CA) centered at 514.5 nm with a power of 300 mW was employed as the radiation source. A thermoelectrically cooled photomultiplier tube (Type R-1928, Hamamatsu) operating a photon counting system served as the detector. The data was processed and analyzed by a microcomputer equipped with DM 3000 version 2.41 software provided with the spectrometer. Sample preparation involved placing the residue into a quartz capillary tube. The tube was then positioned in the spectrometer sample holder.

A comparison between the unknown spectrum and the spectra obtained for solid, standard samples of europium chloride (99.9%, Alfa Products, Danvers, MA) and europium oxide (99.9%, Aldrich Chemical Co., Milwaukee, WI), which are also depicted in Figure 8-10, was made in an attempt to identify the residue. It was evident that the residue was indeed the chloride salt.

Determination of the Figures of Merit

Calibration curves were obtained for Eu, Y and Tm based on peak detection and gated peak integration over a 6 s time period with a 360 ns gate width. Three measurements of 400 nL volumes were made for each sample concentration. Error bars

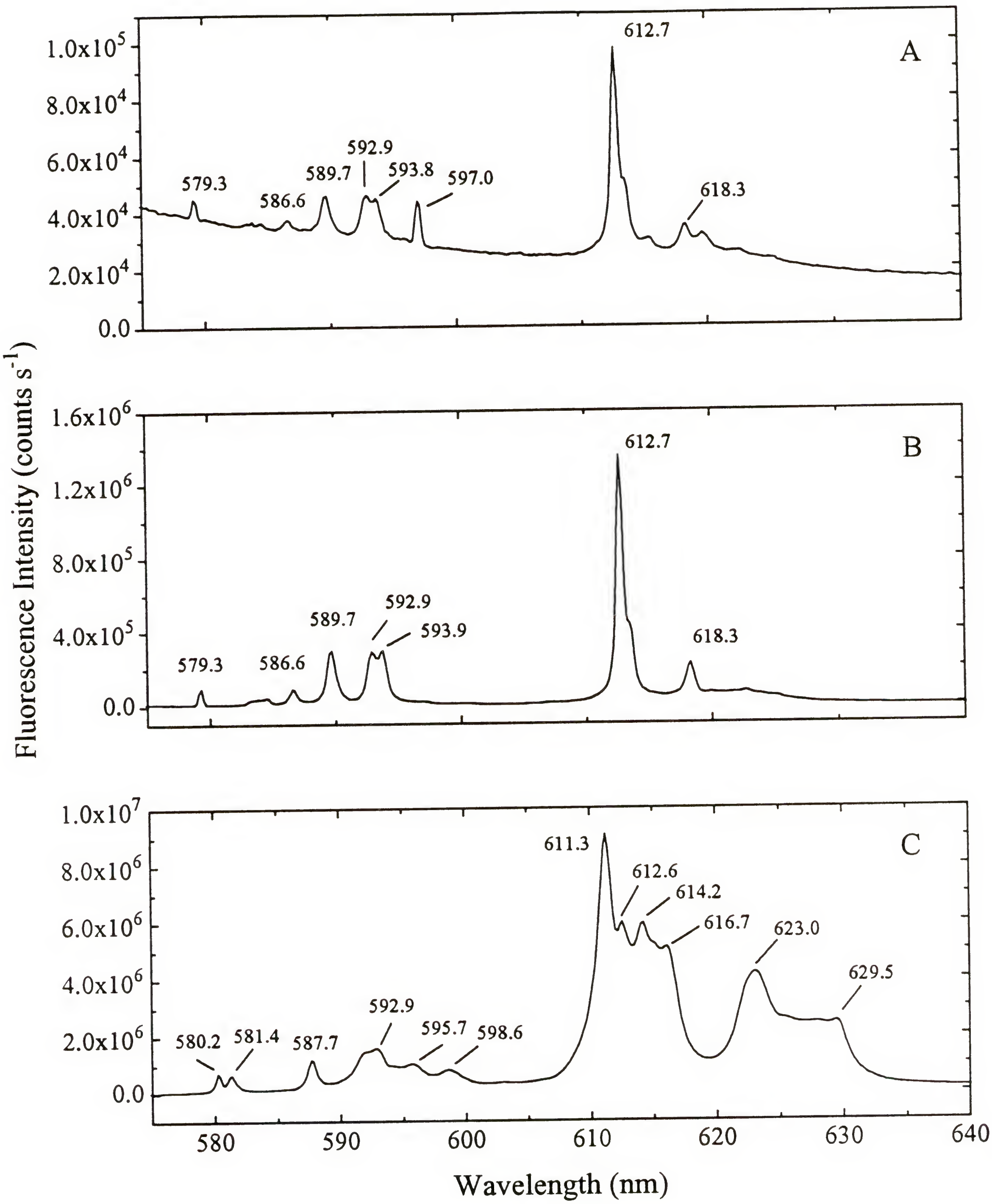

Figure 8-10. Fluorescence spectra of (A) the unknown residue, (B) europium chloride standard and (C) europium oxide standard.

on each plot represent one standard deviation from the mean value. Ten blank measurements were also performed in order to obtain a representation of the noise.

The calibration curves for Eu residues are shown in Figures 8-11 and 8-12 and represent two different data sets recorded on separate occasions. The correlation coefficients obtained from the linear regression analysis of the data were 0.9999 for peak detection and 0.99999 for peak area. The linear dynamic range covered 6 orders of magnitude. The slopes of the log-log plots were 0.8908 and 1.132 for peak height and peak area, respectively. Incomplete cleaning of the cathodes following each peak area determination at the higher concentrations could have led to the high value of the log-log slope. The absolute limits of detection based on 3σ were 5 ng for peak detection with an overall RSD of 7% and 9 fg for peak integration with an RSD of 38%. The high RSD for peak area measurements was not thought to be totally representative, for the precision improved to 10% at masses above 200 ng.

The calibration curves for Y are shown in Figures 8-13 and 8-14 with the same data set being represented in both. The correlation coefficients for peak height and peak area were 0.99811 and 0.99883, respectively, while the corresponding log-log slopes were 0.8934 and 1.227. Interestingly, the slopes followed the same pattern as the values recorded for Eu; however, the slope of the plot based on peak area was 1.015 over the lowest 5 orders of magnitude. It is highly probable that a memory effect produced this discrepancy. The limit of detection based on 3σ was 3 ng for peak detection and 100 fg for peak integration. The overall RSDs for peak detection and peak area were near 30%. The precision improved dramatically at higher concentrations so this overall RSD may not be an accurate indication of the system's reproducibility.

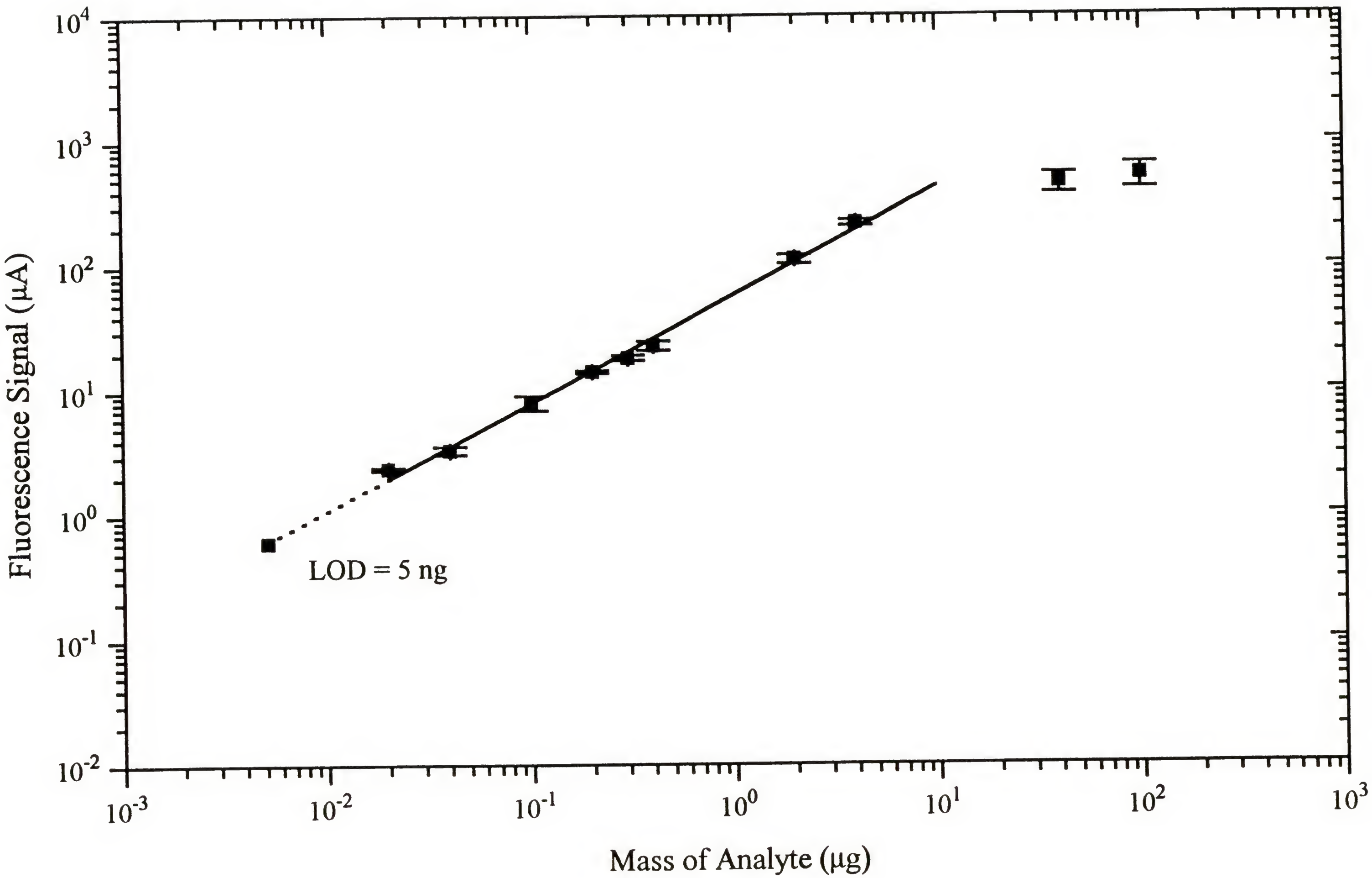

Figure 8-11. Calibration curve for europium solution residues based on peak detection.

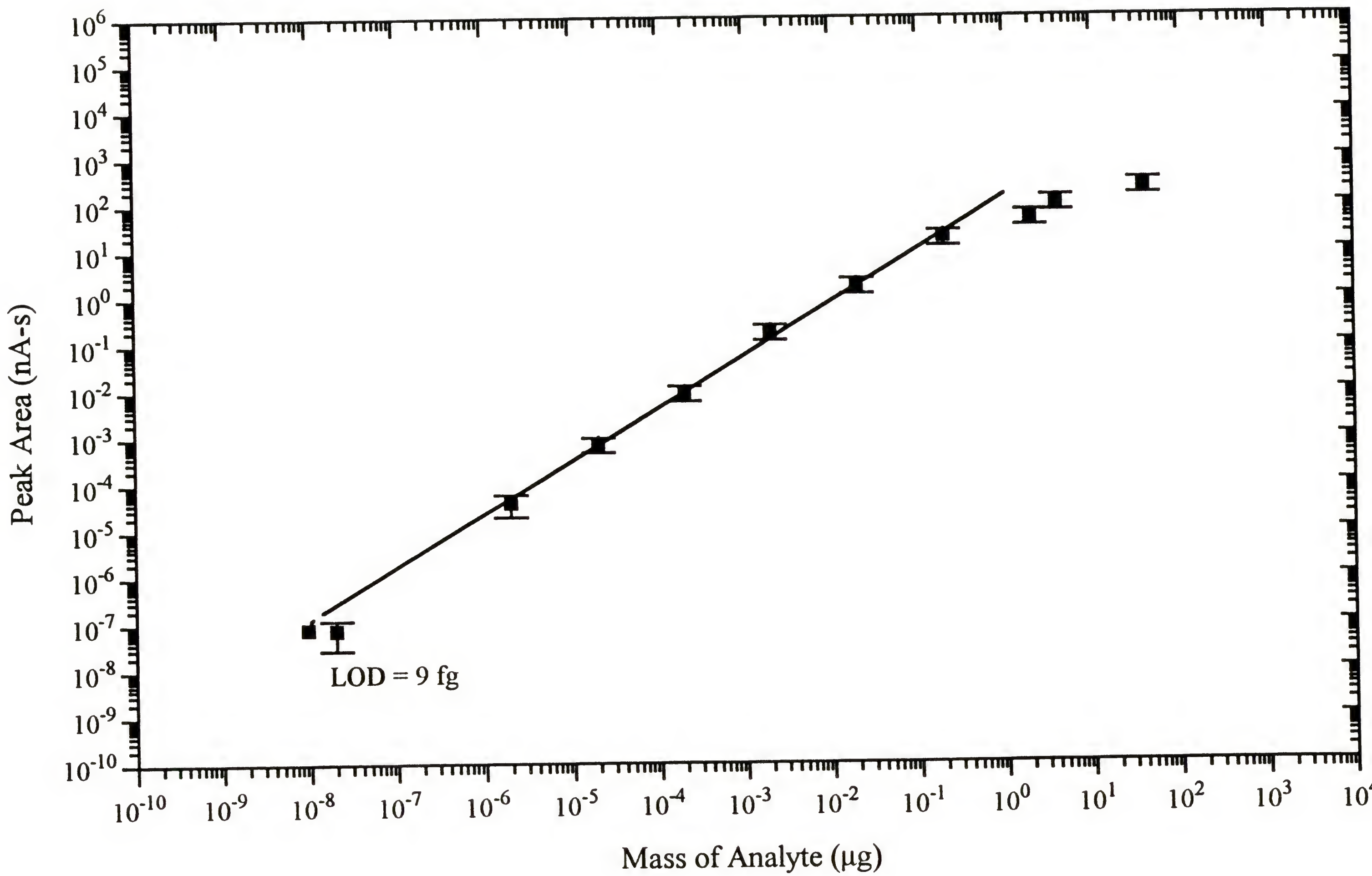

Figure 8-12. Calibration curve for europium solution residues based on peak integration.

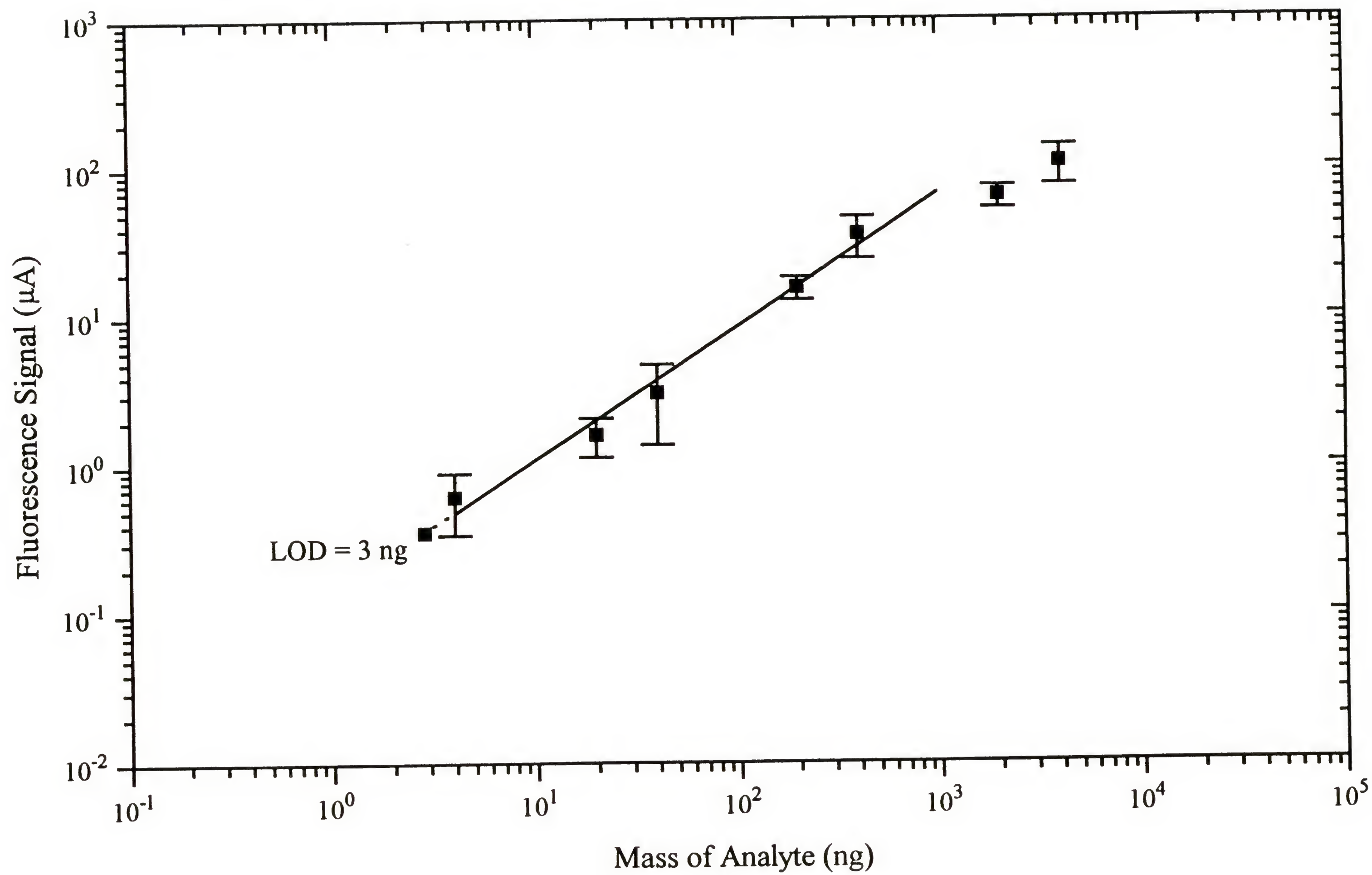

Figure 8-13. Calibration curve for yttrium solution residues based on peak detection.

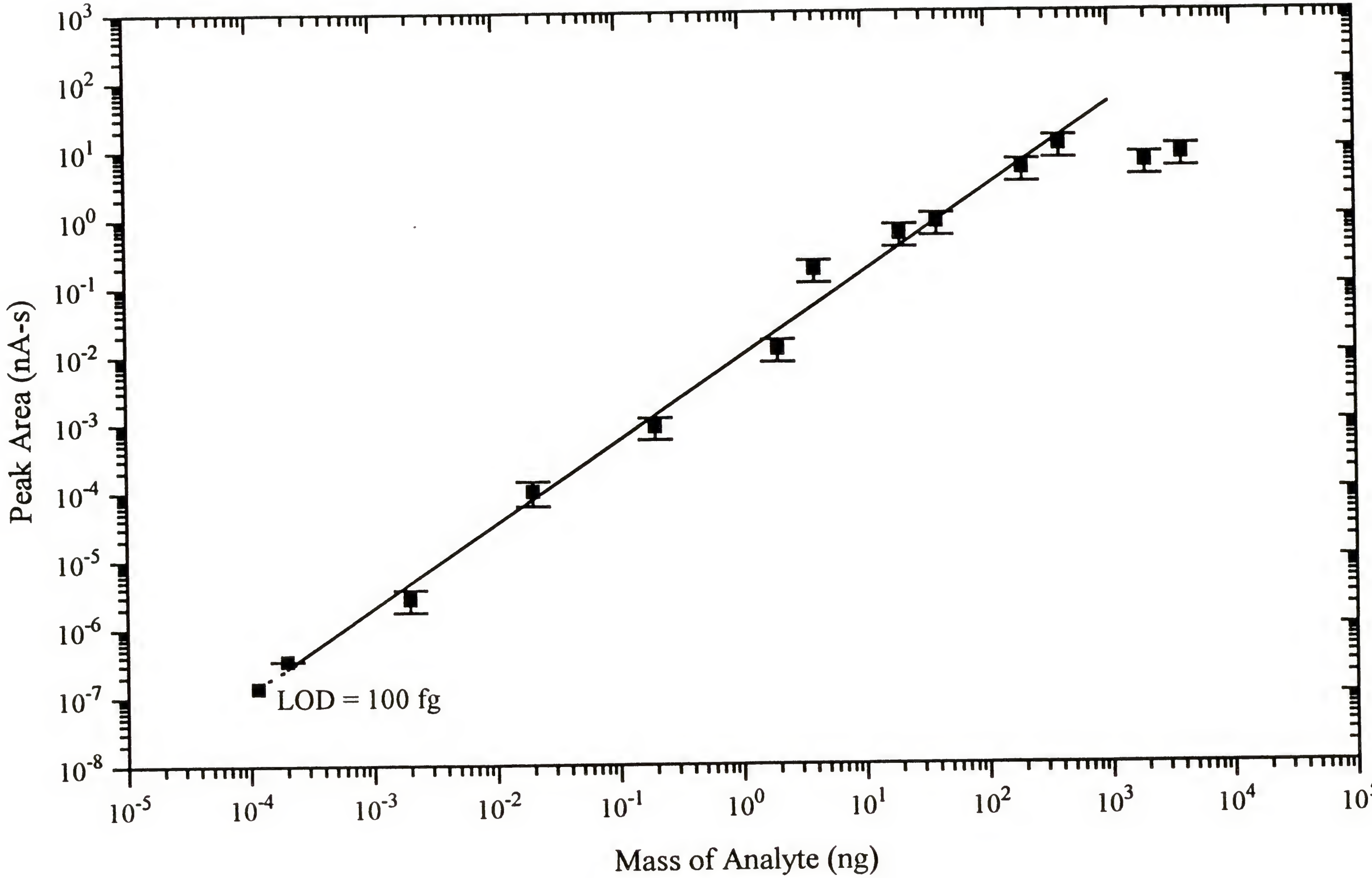

Figure 8-14. Calibration curve for yttrium solution residues based on peak integration.

Figures 8-15 and 8-16 depict the calibration curves obtained for Tm residues. Again, the same data set was depicted in both plots. The log-log slopes were nearer to the desired value of 1.00, likely due to scrupulous cleaning of the cathodes. The value obtained for peak detection was 0.93508, and for peak area, the slope was 1.009. The linear regression analyses of both plots yielded correlation coefficients of 0.9997 for peak height and 0.99911 for peak integration. The limits of detection were 60 pg for peak height with an overall RSD of 13% and 30 ag for peak integration with an overall RSD of 17%. The more thorough cleaning of the cathodes can probably be linked to the improved precisions as well.

Investigation of the Matrix Effects

As mentioned in the introductory chapters, one of the advantages of the GD atom reservoir is that the sputtering process is not affected by the elements present in the sample matrix. This is a particularly beneficial in real sample analysis, for samples usually consist of a complex and often unknown matrix. Since real sample analysis is the ultimate goal of this GD-LEAFS analytical technique, the effect of an element commonly found to be an interferant in other techniques on the fluorescence measurements was investigated. It is hoped that biological samples may be analyzed with this system, and since Na, a well-known interfering species, is present in large amount in biological fluids, it was selected for study. In addition, Na is present in natural waters, and this type of sample may also be suitable for analysis with the miniature GD-LEAFS system.

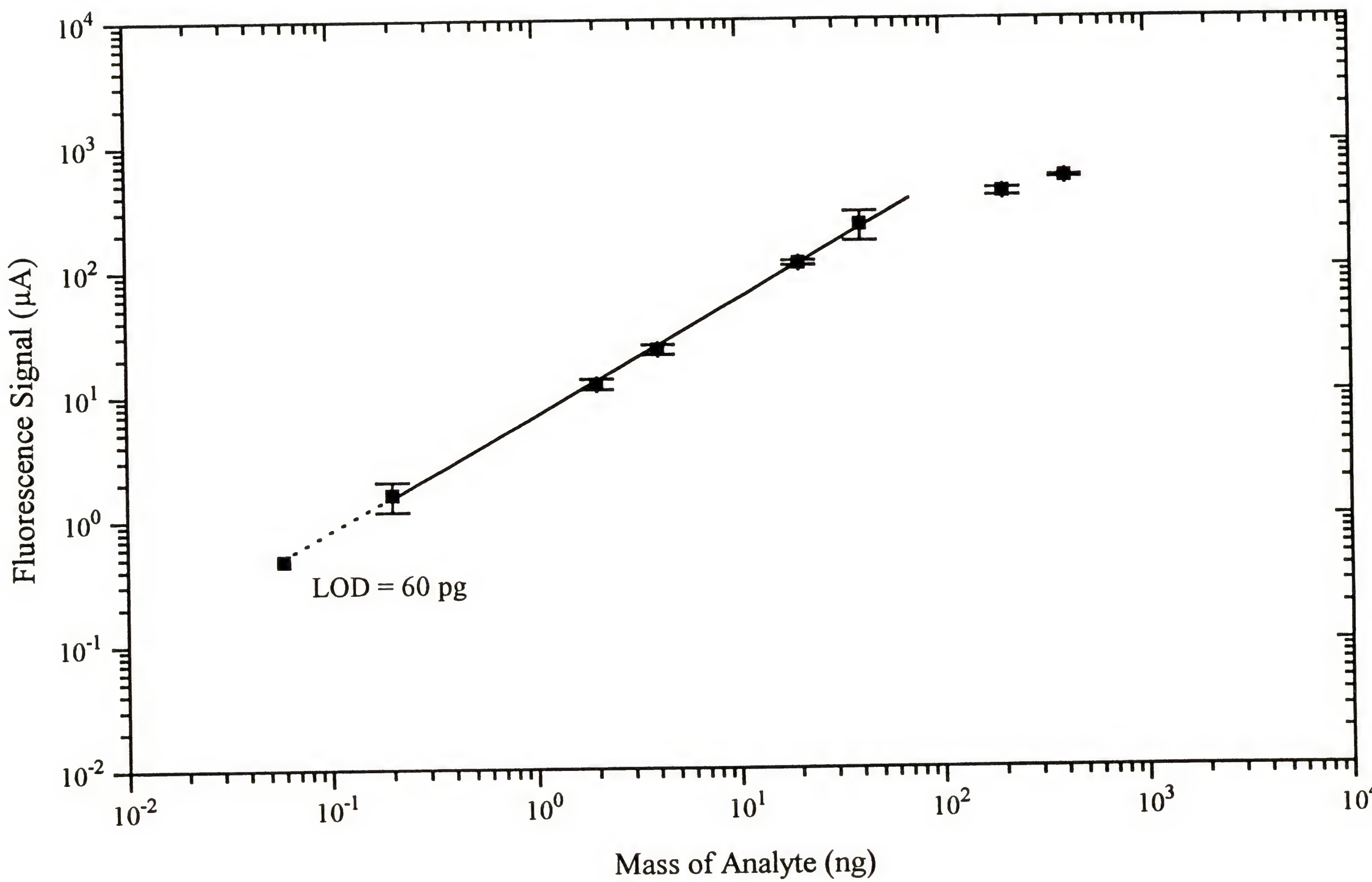

Figure 8-15. Calibration curve for thulium solution residues based on peak height.

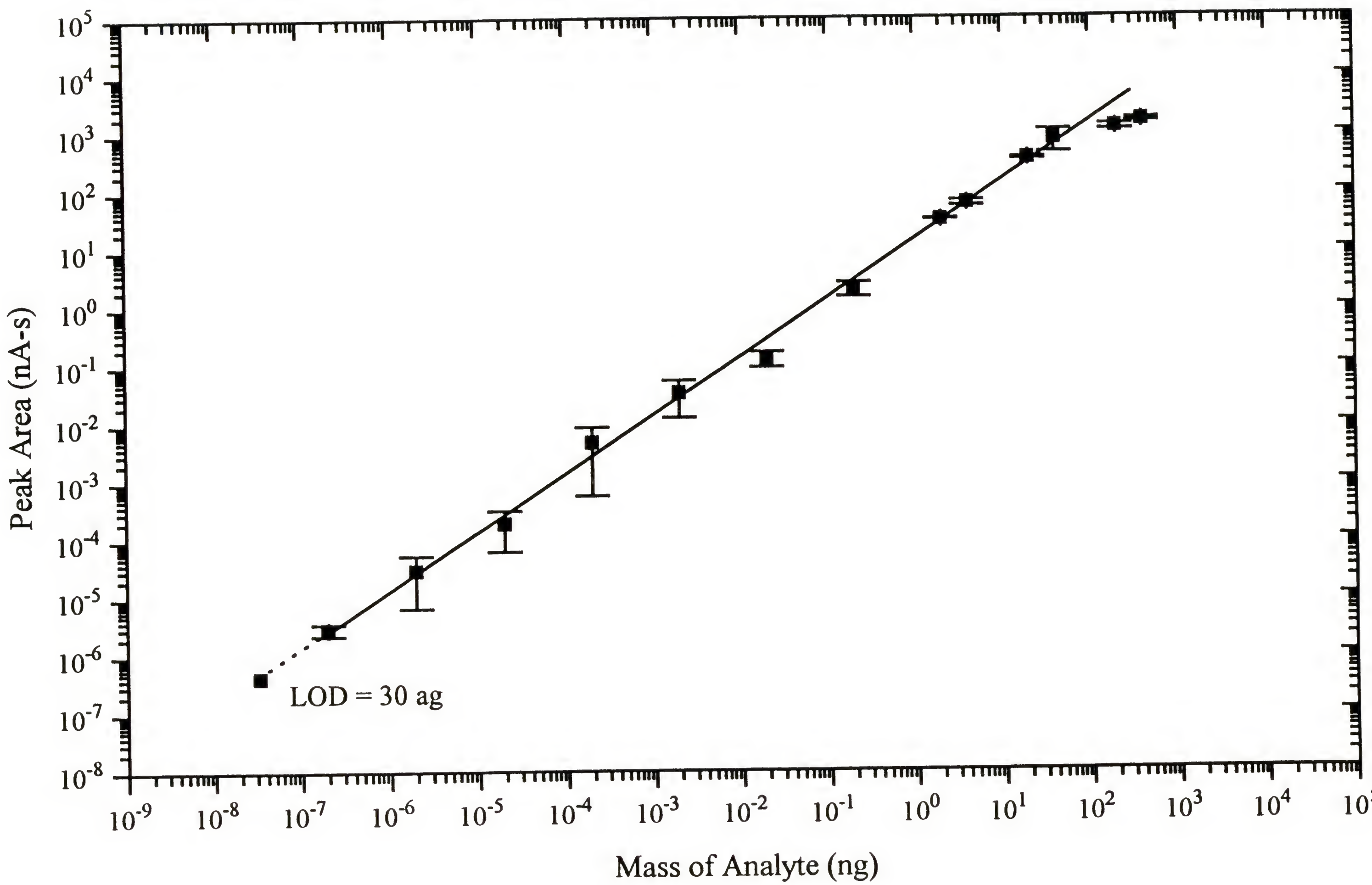

Figure 8-16. Calibration curve for thulium solution residues based on peak area.

Stock Na solutions of 1000 ppm and 5 ppm were prepared by dissolving NaCl crystals (Puratronic 99.999% metals basis, Johnson Matthey, Ward Hill, MA) in doubly deionized water. Solutions of varying Na concentrations were made by serial dilution of these standards, and each contained 500 ppb Eu. Measurements of the Eu fluorescence signal were made in triplicate at each Na concentration. Sample analysis followed the procedure previously used. Volumes of 400 nL were measured.

The temporal profiles acquired at the various concentrations indicated that the peak height of the Eu fluorescence differed little with the addition of Na up to a concentration of 40,000 ppm as was hoped. Peak area, however, was affected; the peak tailing noticeably decreased at higher Na concentrations. The matrix perhaps affected the redeposition process. The results of this study are summarized in Figure 8-17.

Results and Discussion

As stated earlier, little has been published concerning the measurement of the rare earth elements. Results obtained with a GD atom source for the rare earths have been reported by Broekeart (85, 86). Broekeart acquired detection limits for all of the rare earths, including Eu, Y and Tm, by an AES technique using a hollow cathode GD device. The concentration detection limits for Eu, Y and Tm were 400 ppb, 10 ppb and 500 ppb, respectively. Samples consisted of 1 mL volumes; therefore, the absolute detection limits were 400 ng for Eu, 10 ng for Y and 500 ng for Tm. The values obtained with the present GD-LEAFS technique were considerably better.

Once again, the detection limits obtained by measuring the peak area with the GD-LEAFS system were orders of magnitude lower than the limits of detection acquired

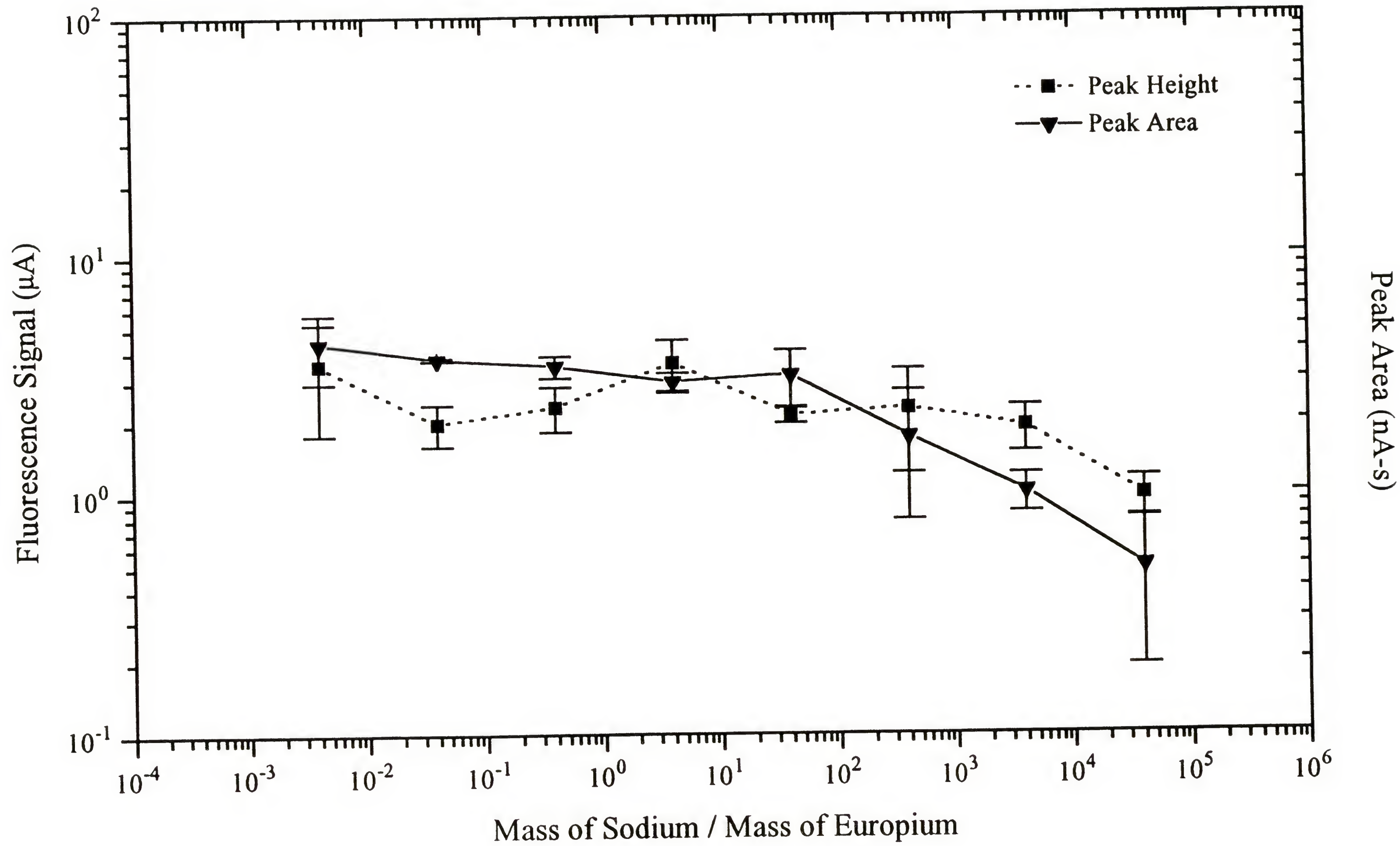

Figure 8-17. Effect of sodium addition on the europium fluorescence signal.

based on the fluorescence peak height. As mentioned in Chapter 5, most of the analytical information is not being considered when only the peak height is recorded.

Peak Tailing Effect

There are several explanations as to why peak tailing is evident; however, one theory seems to be the most probable, and it involves the redeposition of the analyte on the cathode surface. Bruhn and Harrison (51) have stated that at a pressure of 1 torr as much as 94% of the sputtered atoms may be redeposited on the cathode surface as a result of the collisional processes occurring in the gas phase. Westwood and Boyton (87) experimentally determined that approximately 50% of the sputtered material returned to the cathode surface at a pressure of 0.13 torr. This was demonstrated by monitoring the values of the deposition rates, R_m, compared to the discharge current, I, at discharge pressures between 2 and 35 torr. A tantalum cathode was sputtered for a measured period of time at each pressure. The mass of tantalum deposited on a quartz microbalance, which was placed in the discharge directly opposite to the cathode, was monitored. The deposition rate or sputtering rate was determined from this mass and the length of the deposition time. The R_m/I parameter should have remained constant as the pressure was increased, for the discharge pressure is directly related to the discharge current, which in turn determines the sputtering rate. However, the ratio was found to decrease as the pressure was increased. Back-diffusion was determined to be the cause of this decrease; the sputtered species were not reaching the quartz substrate but were returning to the cathode.

In terms of the present study, the fast, narrow peak seen in the temporal profiles may be resulting from the initial removal of the analyte from the cathode surface. The sputtered neutrals could then collide with other gaseous species, diffuse back toward the cathode and be redeposited on the cathode surface. The atoms on the surface could then be sputtered once more, and the process would be repeated. Not all of the atoms are redeposited, however; the system is a flowing system, and some of the analyte will be pumped away. Also, the analyte atoms would be mixing with the Ni matrix atoms, causing the analyte atoms to be diluted. This could explain why the signal level decays after the initial pulse of current. In effect, the atoms are sputtered and excited several times during the period of the measurement, thus explaining why peak integration yields considerably lower detection limits than peak detection. This technique could be easily capable of single atom detection if every atom was excited several times during one analytical measurement.

In order for redeposition to occur, the mean free path of the gaseous atoms must be short in relation to the scale of the experimental system. An estimate of the mean free path of the Ar atoms, the major constituent in the discharge, can be made. The Ar atom has a diameter of 0.65 Å, and it will collide with another atom if its center comes within 0.65 Å of that atom (18). The collision area therefore has a radius of 0.65 Å or an area of 1.3×10^{-16} cm^2, and this will displace a volume of gas as the atom moves. Considering Avogadro's law at a pressure of 1 torr and a temperature of 300 K, the atom density is 3.2×10^{16} cm^{-3} so that each atom occupies a volume of 3.1×10^{-17} cm^3. The average distance that the Ar atom must move to displace a volume of 3.1×10^{-17} cm^3 is

2 mm, the mean free path of the atom. This is a relatively low value for the mean free path, and the value obviously decreases at higher pressures.

A more precise estimate of the mean free path of an atom based on kinetic gas theory has been proposed by Westwood and Boyton (87). The simple expression which resulted from their derivation is given in equation (8-1) and states that

$$\lambda = [2 \times 10^{16} \sigma p]^{-1} \tag{8-1}$$

where λ is the mean free path of the atom (cm), σ is the cross section for atom collisions (cm^2), and p is the pressure in torr. For an Ar atom, the cross section, σ, has a value of 6.46×10^{-16} cm^2 (87). At a pressure of 1 torr, the mean free path, λ, would therefore be 0.077 cm or 0.77 mm which is still smaller than the value determined by the previous method. Considering these estimates of the mean free path, back-diffusion seems likely and is probably responsible for the peak tailing.

The peak tailing may be actually due to the poor sputtering efficiency of the solution residues. This is yet another explanation of the phenomenon. It seems more reasonable that the sputtering rate would be higher since the binding energy of the residue would be low; however, the opposite may be true. As the cathode is bombarded by the excited Ar atoms, energy is transferred to the atoms of the residue. A specific amount of energy is needed in order for the analyte to be sputtered from the surface. If this amount is not transferred to the residue, a low sputtering rate will result. When the GD is ignited, the initial peak might result from the high, transient, instantaneous pulse of current to the cathode. The sputtering could then reach almost a steady state condition as the discharge stabilizes, and the analyte is very slowly removed from the surface.

A third hypothesis has been proposed by Chakrabarti *et al.* (88). In their work involving transient atomization of solution residues by cathodic sputtering in a GD, the researchers recorded atomic absorption temporal profiles which were very similar to the atomic fluorescence profiles obtained in the work presented herein. They theorized that the peak tailing was actually due to a change in the atomization rate. In the early stages of atomization, the process proceeded rather slowly, and the reaction had a slow rate constant. This rate constant became considerably faster as the atomization continued. The researchers suggested that the solution residues initially formed a three-dimensional crystal structure on the cathode surface with the analyte atoms being strongly bonded to one another. This crystal structure was reduced to a two-dimensional monolayer during the atomization process. Since the bonding of the atoms in the monolayer was less strong than that in the crystal lattice, the atomization rate increased, and the rate constant increased. This explanation seems reasonable; however, in the present work, very low mass samples were deposited on the cathodes and, more feasibly, formed monolayers initially. As a result, redeposition most likely led to the peak tailing. In any case, whether or not the sputtering efficiency was very high and redeposition produced the tailing, or the efficiency was low and the analyte was slowly sputtered from the cathode at a variable rate, the tailing was due to the analyte and can be considered to be a part of the analytical signal when the figures of merit are determined for the system.

Theoretical Fluorescence Signal Levels

Intrinsic detection limits could not be easily determined since optical saturation of the excitation transitions was not achieved; however, assuming that the sputtering

process is steady state, the experimental signal levels at the tail of the temporal profiles can be compared to theoretical values. Dashin *et al.* (71, 72) derived the mathematical equations necessary to make such a comparison for a GD-LEAFS system which was similar to the miniature GD-LEAFS system. In their GD-LEAFS approach, only solid samples were measured, and the atom reservoir was considerably larger than the miniature chamber. The model which represented their system was modified by M.A. Bolshov to more accurately depict the miniature GD system which was designed for discrete sample analysis. The basis of the model is a geometric representation of the sputtering system. This depiction is illustrated in Figure 8-18.

The mathematical treatment involves first determining the number of fluorescent photons that are produced, considering the experimental conditions and the geometry of the experimental set up. The theoretical current from the photomultiplier tube, which is generated by the photons, is then correlated to the voltage output of the boxcar integrator and gated detector.

The number of fluorescent photons, n_p, within a laser pulse at the photomultiplier tube is given by

$$n_p = \bar{n}_a V \frac{\Omega}{4\pi} \eta \frac{U_v B_{13} \tau_L A_{32}}{g U_v B_{31} + A_{32} + A_{31}} \tag{8-1}$$

where $\bar{n}_a$ is the mean concentration of the analyte atoms (cm^{-3}) in the analytical volume, V (cm^3), Ω is the solid angle of collected fluorescence (sr), η is the fluorescence collection efficiency (dimensionless), A_{31} and A_{32} are the Einstein coefficients for spontaneous emission (s^{-1}) from the excited state to the ground state and from the excited

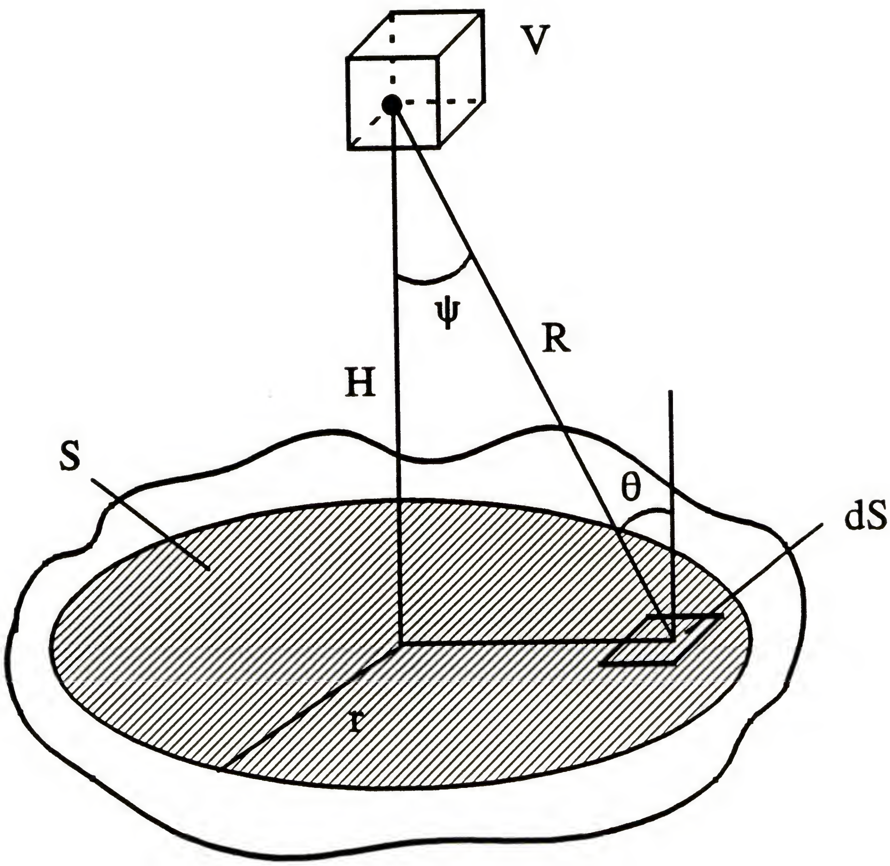

Figure 8-18. Sputtering geometry of the miniature glow discharge: H is the distance between the cathode surface and the center of the analytical volume, V; R is the distance between the element on the cathode surface, dS, and the center of the analytical zone; θ and ψ are the angles between the velocity vector of the sputtered atom and the normals to the cathode surface and the lower surface of the analytical zone, respectively; and r is the radius of the sputtered zone (72).

state to the intermediate energy level, respectively, U_ν is the spectral energy density (J Hz^{-1} m^{-3}), B_{13} and B_{31} are the Einstein coefficients of absorption and stimulated emission (m^3 s^{-1} J^{-1} Hz), respectively, τ_L is the duration of the laser pulse (s), and g represents the statistical distribution of the degeneracy (dimensionless).

The mean analyte atom concentration, $\bar{n}_a$, can be determined by considering the effective flux, j, of the sputtered atoms from the cathode surface. The effective flux, j, is defined as the difference between the flux of the analyte atoms from the surface and the flux of the backscattered atoms to the cathode surface. It can be expressed as

$$j = \frac{\alpha N}{S\tau_s} \tag{8-2}$$

where j has units of atoms cm^{-2} s^{-1}, α is a factor which accounts for the atoms that are lost in the fast, initial spike of the fluorescence temporal profile, N is the total number of atoms deposited on the cathode, S is the cathode surface area (cm^2), and τ_s is the duration of the sputtering process or the time required for all of the deposited analyte atoms to be completely sputtered from the surface (s).

The effective flux, j, is related to the flux of free analyte atoms, j_0, through the analytical volume, V, which can be defined as

$$j_0 = j \int_S \frac{\cos\theta\cos\psi}{2\pi R^2}\, dS \tag{8-3}$$

where θ and ψ, as shown in Figure 8-18, are the angles between the velocity vector of the sputtered atom and the normals to the cathode surface and the lower surface of the analytical volume, respectively, and R is the distance between the element on the cathode

surface, dS, and the center of the analytical volume. The integral accounts for the fact that the distance from the analytical volume to the surface of the cathode is directly related to the number of sputtered atoms that enter the volume.

The mean analyte concentration, $\bar{n}_a$, can be considered to be

$$\bar{n}_a = \frac{j_0}{<\upsilon>} \tag{8-4}$$

where $<\upsilon>$ is the mean velocity of the sputtered atoms (cm s^{-1}).

Combining equations (8-2), (8-3) and (8-4), the mean analyte concentration, $\bar{n}_a$, can be expressed as

$$\bar{n}_a = \frac{\alpha N}{S\tau_s <\upsilon>} \int_S \frac{\cos\theta \cos\psi}{2\pi R^2}\, dS \tag{8-5}.$$

The parameters α, $<\upsilon>$ and τ_s can be roughly estimated from the experimentally obtained, fluorescence temporal profiles. First, it is assumed that all of the atoms are removed in 100 s or τ_s. Signals were observed to last more than 70 s so this is a reasonable assumption. The mean velocity, $<\upsilon>$, is estimated to be near 100 cm s^{-1}. This value could not be easily measured; therefore, a relatively low value for this parameter was assumed, considering the relatively high pressure environment. The factor α can be determined with greater confidence by comparing the area of the fast peak, which had 25.0 ms FWHM for Eu, to the area of the tail, which is estimated to last 100 s. Assuming the maximum signal level or peak height is approximately two orders of magnitude higher than the mean signal level of the tail, the ratio of the transient peak area to the area of the tail is less than 2%. The contribution of the fast peak to the

total signal is therefore minimal, and α can be considered to be unity. The integral can be evaluated such that

$$\int_S \frac{\cos\theta\cos\psi}{2\pi R^2}\, dS = \frac{H^2 r^2}{2H^2(H^2 + r^2)} \tag{8-6}$$

where, as shown in Figure 8-18, H is the distance between the cathode surface and the center of the analytical volume (cm), and r is the radius of the sputtered zone (cm) (72). For the miniature GD-LEAFS system, H is equal to 0.8 cm, and r is equal to 0.1 cm so that the integral has a value of 7.7 x 10^{-3}, and the surface area, S, is 3.1 x 10^{-2} cm^2. Considering a 40 ng Eu sample, N would be 1.6 x 10^{14} atoms. Substituting these values into equation (8-5) with the estimates of τ_s, α and $<\upsilon>$, the mean analyte concentration, $\bar{n}_s$, is equal to 4.0 x 10^9 cm^{-3}.

The second term of equation (8-1) involves the analytical volume, V, which can be expressed as

$$V = hWd_L \tag{8-7}$$

where h and W are the monochromator slit height and width (cm), respectively, and d_L is the diameter of the laser beam (cm). For this system, the slit height was 1.9 cm, the width was 0.05 cm, and the laser beam diameter was approximately 0.1 cm; therefore, the analytical volume, V, is 9.5 x 10^{-3} cm^3.

The solid angle of collected fluorescence, Ω, and the monochromator transmittance or the fluorescence collection efficiency, η, are considered in the next two terms of equation (8-1). These values were determined in Chapter 5 to be equal to 0.05 sr and 0.8, respectively.

The last term of equation (8-1) concerns the fluorescence quantum yield and the spectral energy density, U_ν. Since the laser irradiance was experimentally found to be much below the saturation value,

$$\frac{U_v B_{13} \tau_L A_{32}}{g U_v B_{31} + A_{32} + A_{31}} \approx U_v B_{13} \tau_L \frac{A_{32}}{A_{32} + A_{31}} \tag{8-8}$$

with the ratio of the Einstein coefficients defined as the fluorescence quantum yield. Importantly, branching and electron impact collisions were not found to cause transitions other than the monitored 536.2 nm fluorescence transition for Eu. Since the rare earth elements have very rich spectra, numerous transitions were expected to result from the laser excitation; however, experimentally, the 536.2 nm line was the dominate feature of the fluorescence spectrum, which was obtained by scanning the monochromator with the excitation occurring at 287.9 nm. Considering this result and the values for the Einstein coefficients, 3.0 x 10^7 s^{-1} for A_{32} and 2.8 x 10^6 s^{-1} for A_{31}, the fluorescence quantum yield can be assumed to be unity, and relation (8-8) is also approximately equal to $U_\nu B_{13} \tau_L$.

The spectral energy density, U_ν, is directly related to the laser spectral irradiance, E_ν, and can be expressed as the laser spectral irradiance, E_ν, divided by the speed of light, c, as stated in equation (2-10). The laser spectral irradiance, E_ν, is defined as

$$E_v = \frac{P}{S_L \Delta v} \tag{8-9}$$

where P is the power of the laser (J s^{-1}), S_L is the cross sectional surface area of the laser beam (m^2), and $\Delta\nu$ is the half width of the laser (Hz). The power of the laser can be

expressed as

$$P = \frac{\varepsilon_L}{\tau_L} \tag{8-10}$$

where ε_L is the measured energy of the laser (J), and τ_L is again the laser pulse width (s). For the measurement of Eu, the laser energy was 7.5 x 10^{-7} J, and the laser pulse width was 5 x 10^{-9} s so that the power is equal to 150 J s^{-1}.

The cross sectional surface area of the laser, S_L, assuming a Gaussian shape, is given as

$$S_L = \frac{\pi r_L^2}{4} \tag{8-11}$$

where r_L is the radius of the laser beam. The surface area, S_L, is therefore equal to 7.9 x 10^{-7} m^2.

The laser spectral half width, $\Delta\nu$, can be expressed as

$$\Delta\nu = \frac{c\Delta\lambda}{\lambda^2} \tag{8-12}$$

where c is the speed of light (m s^{-1}), $\Delta\lambda$ is the half width of the laser (m), and λ is the laser wavelength (m). Substituting into equation (8-12) the half width of 4 x 10^{-11} m at 287.9 nm, $\Delta\nu$ is found to be 1.4 x 10^{11} Hz. With this value for $\Delta\nu$ and the values for P and S_L, equation (8-9) can be solved, and the laser spectral irradiance, E_ν, is found to be equal to 1.4 x 10^{-3} Hz^{-1} J s^{-1} m^{-2}. The spectral energy density, U_ν, is therefore equal to 4.7 x 10^{-12} J Hz^{-1} m^{-3}.

The Einstein coefficient of absorption, B_{13}, is defined as

$$B_{13} = \frac{A_{31}\lambda^3 g_3}{8\pi h g_1} \tag{8-13}$$

where g_3 and g_1 are the degeneracies (dimensionless) of the excited state and the ground state, respectively, and h is Planck's constant (J s). For the Eu system, g_1 is 8 and g_3 is 10 so that B_{13} is equal to 5.1×10^{18} m^3 Hz s^{-1} J^{-1}. Considering this value and the values for τ_L and U, calculated for Eu, the final term of equation (8-1) is equal to 0.12. Moreover, the number of fluorescent photons incident on the photomultiplier tube, n_p, for a 40 ng Eu residue, can now be determined by substituting all values into equation (8-1). This resulting value is 1.4×10^4.

The signal, s, that these photons will produce as a voltage at the output of the boxcar integrator and gated detector is given by

$$s = \frac{n_p G e R \eta_{pmt}}{\tau_g} \tag{8-14}$$

where s has units of V, G is the gain of the photomultiplier tube (dimensionless), e is the charge on an electron (C), R is the gain of the transimpedance amplifier (V A^{-1}), η_{pmt} is the quantum efficiency of the photomultiplier tube at 536.2 nm (dimensionless), and τ_g is the boxcar gate width (s). With the gain of the photomultiplier tube and the amplifier at 1×10^6 and 1×10^4 V A^{-1}, respectively, the gate width at 3.6×10^{-7} s, and the photomultiplier quantum efficiency of 0.15, the theoretical signal, s, for a 40 ng residue of Eu is 10 V. The experimentally determined value, however, was 0.03 V.

The experimental and theoretical values for Eu differ by two orders of magnitude. This discrepancy is likely due to the assumptions that were made, including the estimations of both $<\upsilon>$, the average velocity, and τ_s, the duration of the sputtering process, which may easily be off by an in order of magnitude. The necessary initial assumption that the sputtering process is steady state is also not completely valid, for the number of analyte atoms in the gas phase varies with time so that the atom concentration should be integrated over time. The calculation of the analytical volume, V, may be in error as well because the effective slit height might be less than 1.9 cm due to the collection efficiency of the optics.

The theoretical signal levels for 40 ng residues of Tm and Y can be similarly determined and were found to be 12 V and 40 V, respectively. The experimental signal for Tm of 1 V was one order of magnitude lower than the theoretical value. The experimental value for Y, however, was 3 x 10^{-3} V which differs from the theoretical value by four orders of magnitude. It is difficult to explain such a large discrepancy. The estimates of $<\upsilon>$ and τ_p might be invalid for Y, but it seems unlikely that the values should be altered by orders of magnitude. The largest error was most probably introduced in the calculation of equation (8-1), specifically in the final term. A fluorescence spectrum was not obtained for Y so it is not known whether or not there were other prominent transitions other than the monitored fluorescence transition at 543.8 nm. As shown in Figure 8-2, there are two possible detection wavelengths for Y, and in fact, the 296.5 nm transition has a higher transition probability than the 543.8 nm transition. The fluorescence quantum yield might be considerably less than unity.

Further experimental study would be required before a more reliable estimate of the quantum yield could be made. Also, the Einstein coefficients for Y were less certain, for they were obtained from a dated reference. More credible values are again needed.

Limiting Noises

Although excellent limits of detection were obtained with this system, the sensitivity of the measurements were nevertheless limited by the background emission levels. The representations of the noises associated with the measurement of Eu, Y and Tm are shown in Figure 8-19. Background fluorescence was a large source of noise for both Eu and Y, but the background emission was significant and was probably due to the presence of N_2.

Future Work

In order to improve upon the detection limits, the molecular species must be completely removed from the discharge. A new and improved chamber, one that is capable of reaching much lower pressures, is needed in order to accomplish this. The source of the background fluorescence should also be determined and minimized.

The applicability of this technique to the analysis of real samples could be illustrated with the measurement of several SRMs for either Eu, Y or Tm content. This is not a simple task, for there are no easily dissolved SRMs that are certified for these elements. There are two materials, estuarine sediment and coal fly ash, that have provisional Eu concentrations; however, the concentrations in the solids are near 1 ppm so that the resulting solutions would have Eu concentrations below the limit of quantitation.

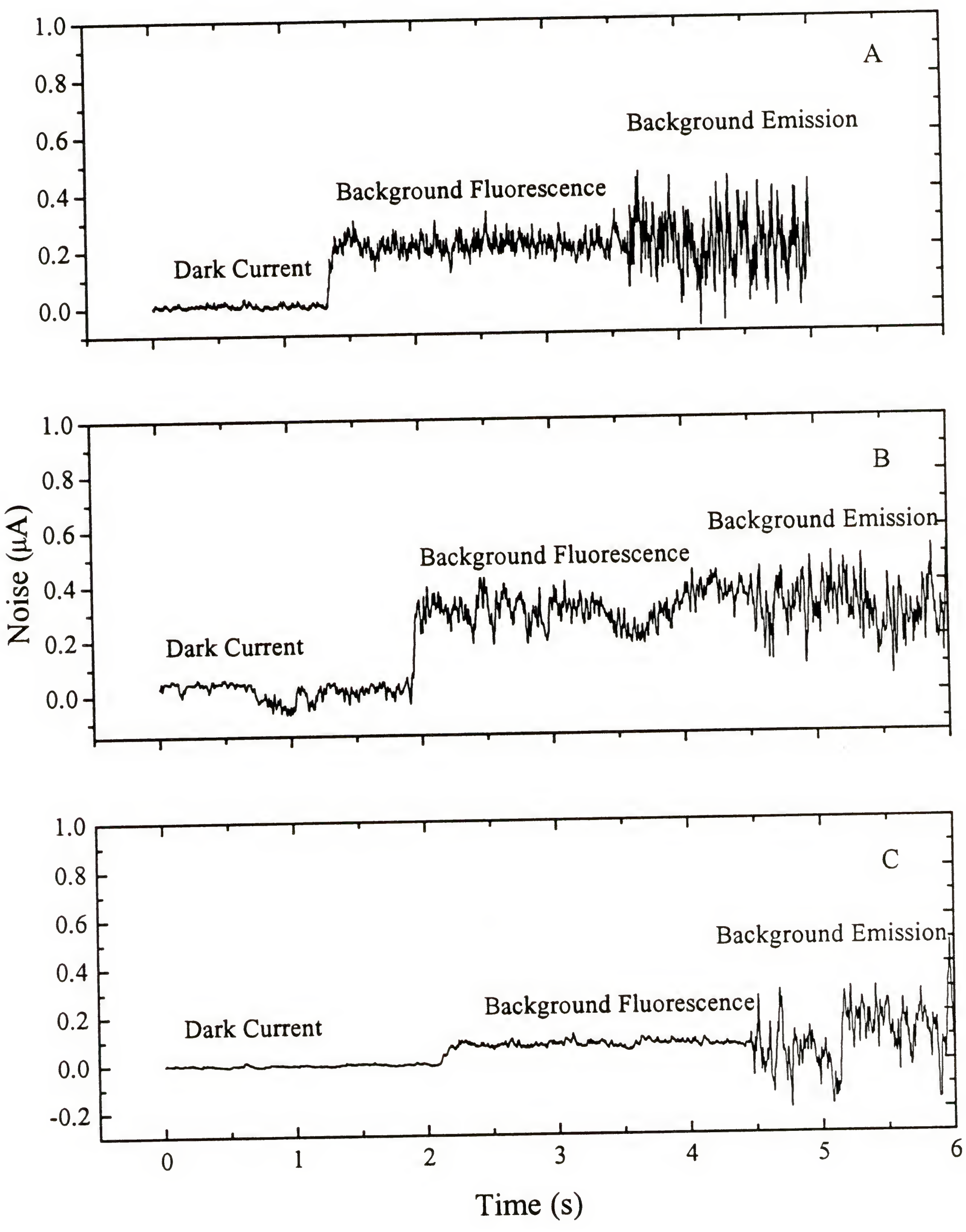

Figure 8-19. Representations of the noises associated with the measurement of (A) europium, (B) yttrium and (C) thulium.

CHAPTER 9
SUMMARY, CONCLUSIONS AND FUTURE WORK

This work has demonstrated that the miniature GD-LEAFS technique is capable of ultratrace analysis, providing detection limits in the femtogram range for aqueous solutions of Pb, Eu, Y and Tm. The system accurately measured the Pb content of SRM 1643b, indicating that real samples may be successfully analyzed. Table 9-1 summarizes the results of this study and compares these absolute detection limits to those obtained by other researchers employing a wide variety of methods. A good comparison can be made for the Pb measurements; however, as the rare earth elements are seldom studied, limited analytical information was available. This lack of information is partially due to the common difficulties associated with the measurement of the rare earths; for example, Y forms strong carbide compounds in the graphite furnace during electrothermal vaporization, decreasing the sensitivity of the technique.

Although the detection limits obtained with the present technique compare favorably with the reported literature values, there are disadvantages of the method. One of the more troublesome problems involves the poor precision of the measurements. The RSDs were typically between 10 and 30%, the range often quoted in the literature for GD techniques. Considering the small sample size and the variation in the laser energy from pulse to pulse, these values are respectable. It was found that careful cleaning of the cathodes prior to each measurement reduced the RSD of the measurements. A more thorough study of the cleaning technique should be made.

Table 9-1. Comparison of Absolute Detection Limits.

Technique	Lead (pg)	Europium (pg)	Yttrium (pg)	Thulium (pg)
Flame-LEAFS [89]	300			
ETA-LEAFS	0.0005 [30]	300 [14]		
ETA-AAS [33]	5	10		4
ICP-AES [90]	4500		400	
GD-AAS [91]	1600			
GD-AES	900 [92]	4×10^5 [85]	1×10^4 [85]	5×10^5 [85]
GD-LEAFS [69]	0.5			
This Work				
Quartz Chamber				
Peak Detection	0.6			
Peak Integration	0.002			
Miniature Chamber				
Peak Detection	0.6	5000	3000	60
Peak Integration	0.03	0.009	0.1	0.00003

As mentioned earlier, this analytical method is inherently a single element technique which can be a drawback since the instrumentation is costly. Multielement analysis is not feasible. Additional dye lasers could be added to the experimental set up so that their outputs could simultaneously excite several elements; however, the detection system would then require modification, for the bandpass of the monochromator is quite narrow and effectively monitors a single wavelength. A multielement GD-LEAFS technique would be far too complicated to be realistically implemented. The miniature GD-LEAFS system is already fairly intricate so that skilled operators would be required. The present technique does not seem suitable for routine analysis as it stands. Any further modifications would only add to the complexity.

The comparison between the experimental detection limits for Pb and the theoretical, intrinsic detection limits indicates that the system can be improved in order to increase the sensitivity of the system. First, the vacuum system should be redesigned. The taper joint must be removed from the chamber and be perhaps replaced by a Cajon fitting which would still allow for quick and easy cathode exchange. If the N_2 species were completely removed prior to measurement, the S/N might be dramatically improved. Stop-flow measurements could therefore be made, which may lead to still lower detection limits. In the new design, the two quartz windows that the laser beam passes through could be placed at an angle so that they are no longer parallel to one another. This may reduce the reflections off of their faces, which could in turn decrease the observed background fluorescence. A smaller chamber could also be constructed if a suitable fabrication material was found, and the photomultiplier tube could be cooled

in order to decrease the dark current levels. A more effective method of cooling the cathodes should also be considered.

In addition, future work should involve the measurement of many more elements so that the temporal fluorescence profiles could be compared to those previously recorded. The redeposition phenomenon should be thoroughly studied since it is not fully understood. An investigation of the effect of the cathodic current and chamber pressure of the shape of the temporal profiles should also be undertaken. Moreover, a more detailed mathematical model of the system could be employed to compare the theoretical signals based on both peak detection and peak integration in an effort to explain the discrepancy in the detection limits based on those parameters. The present model should also be studied further, for the discrepancy in the theoretical and experimental fluorescence signal levels warrants explanation.

REFERENCES

1. Ingle, J.D. Jr.; Crouch, S.R. *Spectrochemical Analysis*. Prentice-Hall: Englewood Cliffs, NJ, 1988.

2. van Loon, J.C. *Selected Methods of Trace Metal Analysis: Biological and Environmental Samples*. Wiley: New York, 1985.

3. Lajunen, L.H.J. *Spectrochemical Analysis by Atomic Absorption and Emission*. Royal Society of Chemistry: Cambridge, 1992.

4. Omenetto, N.; Smith, B.W.; Winefordner, J.D. *Spectrochim. Acta* **1988**, *43*, 1111.

5. Vera, J.A.; Leong, M.B.; Omenetto, N.; Smith, B.W.; Womack, B.; Winefordner, J.D. *Spectrochim. Acta* **1989**, *44B*, 939.

6. Jarvis, K.E.; Gray, A.L.; Houk, R.S. *Handbook of Inductively Coupled Mass Spectrometry*. Chapman and Hall: New York, 1992.

7. Hieftje, G.M. *J. Chem. Ed.* **1982**, *59*, 900.

8. Tölg, G. *Fresenius Z. Anal. Chem.* **1988**, *329*, 735.

9. Bowman, R.L.; Vurek, G.G. *Anal. Chem.* **1984**, *56*, 391A.

10. Ryu, J.Y.; Davis, R.L.; Williams, J.C.; Williams, J.C. Jr. *Appl. Spectrosc.* **1988**, *42*, 1379.

11. Little, C. "Microsample Analysis," in *Transport of Ions and Water in Animals*; Gupta, B.L.; Moreton, R.B.; Oschman, J.L.; Wall, B.J., Eds. Academic Press: London, 1977.

12. Roinel, N. *J. Microscopie Biol. Cell.* **1975**, *22*, 261.

13. Lechene, C. "Electron Probe Microanalysis of Picoliter Liquid Samples," in *Microprobe Analysis as Applied to Cells and Tissues*; Hall, T.; Hchlin, P.; Kaufmann, R., Eds. Academic Press: London, 1974.

14. Bolshov, M.A.; Zybin, A.V.; Smirenkina, I.I. *Spectrochim. Acta* **1981**, *36B*, 1143.

15. Dougherty, J.P.; Preli, F.R. Jr.; Michel, R.G. *J. Anal. At. Spectrom.* **1987**, *2*, 429.

16. Pagano, S.T. Doctoral Dissertation, Department of Chemistry, University of Florida, Gainesville, Fl, 1994.

17. Harrison, W.W.; Prakash, N.J. *Anal. Chim. Acta* **1970**, *49*, 151.

18. Chapman, B. *Glow Discharge Processes.* Wiley: New York, 1980.

19. Caroli, S.; Senofonte, O.; Femmine, P.D. *Analyst* **1983**, *108*, 196.

20. Chen, F.; Williams, J.C. *Anal. Chem.* **1990**, *62*, 489.

21. Morgan, C.A. Doctoral Dissertation, Department of Chemistry, University of Florida, Gainesville, Fl, 1994.

22. Deavor, J.P.; Becerra, E.; Smith, B.W.; Winefordner, J.D. *Can. J. Appl. Spectrosc.* **1993**, *38*, 7.

23. Winefordner, J.D.; Vickers, T.J. *Anal. Chem.* **1964**, *36*, 161.

24. Boutilier, G.D.; Blackburn, M.B.; Mermet, J.M.; Weeks, S.J.; Haragushi, H.J.; Winefordner, J.D.; Omenetto, N. *Appl. Opt.* **1978**, *18*, 1804.

25. Omenetto, N.; Winefordner, J.D. *Prog. Anal. At. Spectrosc.* **1979**, *2*, 1.

26. Winefordner, J.D.; Omenetto, N. "Laser-excited Atomic and Ionic Fluorescence in Flames and Plasmas," in *Analytical Applications of Lasers*; Piepmeier, E.H., Ed. Wiley Interscience: New York, 1986.

27. Alkemade, C.Th.J. *Appl. Spectrosc.* **1981**, *35*, 1.

28. Alkemade, C.Th.J. "Detection of Small Numbers of Atoms and Molecules," in *Analytical Applications of Lasers*; Piepmeier, E.H., Ed. Wiley Interscience: New York, 1986.

29. Winefordner, J.D.; Petrucci, G.A.; Stevenson, C.L.; Smith, B.W. *J. Anal. At. Spectrom.* **1994**, *9*, 131.

30. Omenetto, N. *Spectrochim. Acta* **1989**, *44B*, 131.

31. Butcher, D. *Spectrosc.* **1993**, *8(2)*, 14.

32. van Loon, J.C. *Anal. Chem.* **1981**, *53*, 332A.

33. Butcher, D.J.; Dougherty, J.P.; Preli, F.R.; Walton, A.P.; Wei, G.-T.; Irwin, R.L.; Michel, R.G. *J. Anal. At. Spectrosc.* **1988**, *3*, 1059.

34. Smith, B.W.; Womack, J.B.; Omenetto, N.; Winefordner, J.D. *Appl. Spectrosc.* **1989**, *43*, 873.

35. Fang, D.; Marcus, R.K. "Fundamental Plasma Processes," in *Glow Discharge Spectroscopies*; Marcus, R.K., Ed. Plenum Press: New York, 1993.

36. Llewellyn-Jones, F. *The Glow Discharge*. Wiley: New York, 1966.

37. Mavrodineanu, R. *J. Res. Nat. Bur. Stds.* **1984**, *89(2)*, 143.

38. Boumans, P.W.J.M. *Anal. Chem.* **1972**, *44*, 1219.

39. Penning, F.M. *Electrical Discharges in Gases*. Katwijk aan Zee: Netherlands, 1957.

40. van Straaten, M.; Gijbels, R.; Vertes, A. *Anal. Chem.* **1992**, *64*, 1855.

41. Caroli, S. *J. Anal. At. Spectrom.* **1987**, *2*, 661.

42. Hess, K.R.; Harrison, W.W. *Anal. Chem.* **1988**, *60*, 691.

43. Harrison, W.W.; Bentz, B.L. *Prog. Anal. Spectrosc.* **1988**, *11*, 53.

44. McHugh, J.A. *Methods of Surface Analysis, Volume I*. Czanderna, A.W., Ed. Elsevier: New York, 1975.

45. Hess, K.R.; Marcus, K.R. *Spectrosc.* **1987**, *2*, 24.

46. Coburn, J.W.; Harrison, W.W. *Appl. Spectrom. Rev.* **1981**, *17*, 95.

47. Sigmund, P. *Phys. Rev.* **1969**, *184*, 383.

48. Sigmund, P. *Phys. Rev.* **1969**, *187*, 768.

49. Laegreid, N.; Wehner, G.K. *J. Appl. Phys.* **1961**, *32*, 365.

50. Avni, R. *Applied Atomic Spectroscopy*. Grove, E.L., Ed. Plenum Press: New York, 1978.

51. Bruhn, C.G.; Harrison, W.W. *Anal. Chem.* **1978**, *50*, 16.

52. Coburn, J.W. *Rev. Sci. Instr.* **1970**, *41*, 1219.

53. Coburn, J.W.; Kay, E. *Appl. Phys. Lett.* **1971**, *18*, 435.

54. Oechsner, H.; Gerhard, W. *Surf. Sci.* **1974**, *44*, 480.

55. Oechsner, H. *Plasma Phys.* **1974**, *16*, 835.

56. Vieth, W.; Huneke, J.C. *Spectrochim. Acta* **1990**, *45B*, 941.

57. Gough, D.S.; Hannaford, P.; Walsh, A. *Spectrochim. Acta* **1973**, *28B*, 197.

58. Butler, L.R.P.; Kröger, K.; West, C.D. *Spectrochim. Acta* **1975**, *30B*, 489.

59. Human, H.G.C.; Ferreira, N.P.; Kruger, R.A.; Butler, L.R.P. *Analyst* **1978**, *103*, 469.

60. Bubert, H. *Spectrochim. Acta* **1984**, *39B*, 1377.

61. van Dijk, C.; Smith, B.W.; Winefordner, J.D. *Spectrochim. Acta* **1982**, *37B*, 759.

62. Hannaford, P.; Lowe, R.M. *Opt. Eng.* **1983**, *22*, 532.

63. Hannaford, P. *Aust. Phys.* **1986**, *23*, 36.

64. Hannaford, P.; Lowe, R.M. *Aust. J. Phys.* **1986**, *39*, 829.

65. Hannaford, P. "Laser Spectroscopy with Sputtered Atoms," in *Proceedings of the National Atomic and Molecular Physics Conference*, Bombay, India, December 1992.

66. Smith, B.W.; Omenetto, N.; Winefordner, J.D. *Spectrochim. Acta* **1984**, *39B*, 1389.

67. Patel, B.M.; Winefordner, J.D. *Spectrochim. Acta* **1986**, *41B*, 469.

68. Patel, B.M.; Winefordner, J.D. *Appl. Spectrosc.* **1986**, *40*, 667.

69. Glick, M.; Smith, B.W.; Winefordner, J.D. *Anal. Chem.* **1990**, *62*, 157.

70. Womack, J.B.; Gessler, E.M.; Winefordner, J.D. *Spectrochim. Acta* **1991**, *46B*, 301.

71. Dashin, S.A.; Karpov, Yu. A.; Kushlyansky, O.A.; Mayorov, I.A.; Bolshov, M.A. *Spectrochim. Acta* **1991**, *46B*, 467.

72. Dashin, S.A.; Mayorov, I.A.; Bolshov, M.A. *Spectrochim. Acta* **1993**, *48B*, 531.

73. Grazhulene, S.; Khvostikov, V.; Sorokin, M. *Spectrochim. Acta* **1991**, *46B*, 459.

74. Lunev, O.S.; Maksimov, D.E.; Oshemkov, S.V.; Rudnevskii, A.N. *Zh. Prik. Spek.* **1990**, 359.

75. Lunyov, O.S.; Oshemkov, S.V. *Spectrochim. Acta* **1992**, *47B*, 71.

76. Deavor, J.P.; Becerra, E.; Smith, B.W.; Winefordner, J.D. *Can. J. Spectrosc.* **1993**, *33*, 7.

77. Sasaki, K.; Kawata, S.; Minami, S. *Appl. Spectrosc.* **1986**, *40*, 185.

78. Synovec, R.E.; Yeung, E.S. *Anal. Chem.* **1985**, *57*, 2162.

79. Williams, R. *Appl. Spectrosc.* **1989**, *43*, 1409.

80. Bialkowski, S. *Appl. Spectrosc.* **1988**, *42*, 807.

81. Knoll, J.E. *J. Chrom. Sci.* **1985**, *23*, 422.

82. Laeven, J.M.; Smit, H.C. *Anal. Chim. Acta* **1985**, *176*, 77.

83. Foley, J.P.; Dorsey, J.G. *Chromatographia* **1984**, *9*, 503.

84. Voigtman, E. *Appl. Spectrosc.* **1991**, *45*, 237.

85. Broekart, J.A.C. *Bull. Soc. Chim. Belg.* **1976**, *85*, 261.

86. Broekart, J.A.C. *Bull. Soc. Chim. Belg.* **1976**, *85*, 471.

87. Westwood, W.D. *Prog. Surf. Sci.* **1976**, *7*, 71.

88. Chakrabarti, C.L.; Headrick, K.L.; Bertels, P.C.; Back, M.H. *J. Anal. At. Spectrom.* **1988**, *3*, 713.

89. Radziuk, B.; Tomassen, Y.; Butler, L.P.R.; van Loon, J.C. *Anal. Chim. Acta* **1979**, *108*, 31.

90. Akagi, I.; Haraguchi, H. *Anal. Chem.* **1990**, *62*, 81.

91. Chakrabarti, C.L.; Headrick, K.L.; Hutton, J.C.; Bicheng, Z.; Bertels, P.C.; Back, M.H. *Anal. Chem.* **1990**, *62*, 574.

92. Becerra, E. Doctoral Dissertation, Department of Chemistry, University of Florida, Gainesville, Fl, 1990.

BIOGRAPHICAL SKETCH

Cheryl Lynn Davis was born in Jacksonville, North Carolina, on January 22, 1967. Pursuing her love of dance, she began high school in 1982 at the North Carolina School of the Arts in Winston-Salem, North Carolina. She received her diploma with special emphasis in ballet in 1985. Following a year of performing and training in Atlanta, Georgia, she decided to continue her education by attending Mary Washington College in Fredericksburg, Virginia. She obtained her Bachelor of Science degree in 1990, earning high honors in chemistry. As the valedictorian of her class, she was awarded the Darden Award and the recognition of summa cum laude. Later that year, she entered the Graduate School of the University of Florida where she conducted research under Dr. James D. Winefordner.

I certify that I have read this study and that in my opinion it conforms to acceptable standards of scholarly presentation and is fully adequate, in scope and quality, as a dissertation for the degree of Doctor of Philosophy.

James D. Winefordner, Chair
Graduate Research Professor of Chemistry

I certify that I have read this study and that in my opinion it conforms to acceptable standards of scholarly presentation and is fully adequate, in scope and quality, as a dissertation for the degree of Doctor of Philosophy.

David H. Powell
Associate Research Scientist of Chemistry

I certify that I have read this study and that in my opinion it conforms to acceptable standards of scholarly presentation and is fully adequate, in scope and quality, as a dissertation for the degree of Doctor of Philosophy.

John R. Eyler
Professor of Chemistry

I certify that I have read this study and that in my opinion it conforms to acceptable standards of scholarly presentation and is fully adequate, in scope and quality, as a dissertation for the degree of Doctor of Philosophy.

Eric R. Allen
Professor of Environmental Engineering Sciences

I certify that I have read this study and that in my opinion it conforms to acceptable standards of scholarly presentation and is fully adequate, in scope and quality, as a dissertation for the degree of Doctor of Philosophy.

Paul A. Chadik
Assistant Professor of Environmental Engineering Sciences

This dissertation was submitted to the Graduate Faculty of the Department of Chemistry in the College of Liberal Arts and Sciences and to the Graduate School and was accepted as partial fulfillment of the requirements for the degree of Doctor of Philosophy.

December 1994

Dean, Graduate School